NOTICE

The quality of this microform is heavily dependent upon the quality of the original thesis submitted for microfilming. Every effort has been made to ensure the highest quality of reproduction possible.

If pages are missing, contact the university which granted the degree.

Some pages may have indistinct print especially if the original pages were typed with a poor typewriter ribbon or if the university sent us an inferior photocopy.

Reproduction in full or in part of this microform is governed by the Canadian Copyright Act, R.S.C. 1970, c. C-30, and subsequent amendments.

AVIS

La qualité de cette microforme dépend grandement de la qualité de la thèse soumise au microfilmage. Nous avons tout fait pour assurer une qualité supérieure de reproduction.

S'il manque des pages, veuillez communiquer avec l'université qui a conféré le grade.

La qualité d'impression de certaines pages peut laisser à désirer, surtout si les pages originales ont été dactylographiées à l'aide d'un ruban usé ou si l'université nous a fait parvenir une photocopie de qualité inférieure.

La reproduction, même partielle, de cette microforme est soumise à la Loi canadienne sur le droit d'auteur, SRC 1970, c. C-30, et ses amendements subséquents.

Rayleigh Spatial Spectral Estimation for Matched–Field Source Localization

Sami G. Khoury

A Thesis
in
The Department
of
Electrical and Computer Engineering

Presented in partial fulfillment of the Requirements
for the degree of Master of Applied Science at
Concordia University
Montreal, Quebec, Canada

October 1990

ISBN 0-315-64705-1

ABSTRACT

Rayleigh Spatial Spectral Estimation for Matched–Field Source Localization

Sami G. Khoury

This thesis addresses the problem of localizing underwater acoustic sources with a passive array. Source localization is commonly achieved by mapping field directionality or spatial spectrum. Spatial spectral estimation is analogous to temporal spectral analysis with the parameter of interest being the direction of arrival of the signal. A new family of spectral estimates, the Rayleigh family of power spectrum estimates, was recently introduced by Lagunas. It offers a range of resolution under control of the user.

In this work, the resolution of the Rayleigh estimate is analyzed and a closed–form expression is derived. As the order of the estimate increases, the asymptotic resolution also increases. However, if the assumed signal model is imprecise, mismatch occurs. An analytic expression describing the sensitivity to mismatch of the Rayleigh estimate is derived. The results here indicate that a degradation due to mismatch becomes more serious as the order of the estimator increases. This sensitivity is also apparent with an increase in signal to noise ratio. Simulation results are presented illustrating that as the order of the Rayleigh estimate is increased, higher spectral resolution is achieved at the cost of increased sensitivity to mismatch.

Matched–field processing is a localization technique which exploits complex propagation conditions to achieve three dimensional source localization. This approach generally requires numerical modeling of the ocean acoustic channel. However, performance is seriously degraded when knowledge about the environmental model is imprecise. In order to improve the robustness of matched–field processing, an incoherent approach which exploits only the structure rather than the coherent combination of multipath arrivals is presented. The performance of the conventional and incoherent processors in a complex numerical ocean model is examined. Results show that the incoherent method is considerably more robust than the conventional (coherent) approach under model mismatch conditions.

Acknowledgements

I would like to express my sincere gratitude to Dr. J. Krolik for introducing me to the exciting world of research. The continuous guidance, advice and encouragement were an asset throughout the span of this thesis. His dedication to the field of signal processing and his personal interest in my progress have given me the motivation to see this work to completion. He allowed me the freedom to develop my own ideas while providing me with ample comments and suggestions to keep me on the right track. His suggestions and constructive criticism were invaluable in the final stage of the preparation of this manuscript. I am grateful to have had him as my supervisor.

I wish to thank Dr. Arthur Newhall from the Woods Hole Oceanographic Institute, Woods Hole, Mass. for providing me with the Multiple–Profile Ray–Tracing Program. His cooperation in clarifying some of the complex issues involved in using the software is greatly appreciated. I would also like to acknowledge a useful discussion concerning this research held with Dr. Miguel Lagunas at the ICASSP-90 conference.

A final note of appreciation to the secretaries of the Electrical and Computer Engineering Department; Maureen, Monica, Kim, Elaine and Carleen for making it simpler to find our way in the big university maze. And to all my friends, thanks for your comments, encouragement and support.

Last but not least, I am forever in debt to my devoted parents and my dear brother for all their sacrifices. Their continuous moral support, encouragement and patience for the numerous hours I was unable to spend with them is sincerely cherished. UN GRAND MERCI POUR TOUT.

A MES CHERS
PARENTS

Contents

List of Figures

List of Tables

List of Key Symbols

BT	Blackman–Tukey
CSDM	Cross Spectral Density Matrix
FFT	Fast Fourier Transform
FIR	Finite Impulse Response
MFP	Matched Field Processing
MLM	Maximum Likelihood Method
MPP	Multiple Profile Program
MV	Minimum Variance (spectrum)
MVDR	Minimum Variance Distortionless Response
NMLM	Normalized Maximum Likelihood (spectrum)
PSD	Power spectral density
RE	Rayleigh estimate
$[.]^*$	Complex conjugate transpose
$[.]^T$	Transpose
$[.]^{-1}$	Inverse function
$\hat{[.]}$	Estimated version of the underlying quantity
$\perp$	Orthogonal vectors
$\parallel$	Parallel vectors
$\mathbf{a}, \mathbf{b}$	General vectors (Chapter 2)
$\mathbf{a}$	Vector of complex coherence between paths (MFP)
B	Effective bandwidth
c	Sound speed in the ocean
$\mathbf{d}$	True direction vector
$D(p, m)$	Propagation delay from p-th path at m-th sensor
e	Exponential operator
$\mathcal{E}$	Expectation operator
$\mathbf{h}$	Filter impulse response vector
$H(\omega)$	Filter transfer function
$\mathbf{I}$	Identity matrix
$\jmath$	Imaginary constant, $\sqrt{-1}$
ℓ	Sensor separation

L	Number of paths
M	Number of elements in the array
$n(t)$	noise component of the wave received at the array
N	Number of data samples
$N(\omega)$	Noise spectral function
$\mathbf{p}(\omega, \Phi)$	Direction vector in MFP
q	Order of Rayleigh estimate
$\mathbf{q}$	Noise vector
$\mathbf{Q}$	Noise cross-spectral density matrix
r_{xx}	Autocorrelation sequence
r	Range between source and receiver
$\mathbf{R}$	Correlation matrix
$\mathbf{R}_s, \mathbf{R}_n$	Signal and Noise correlation matrices
R_s, R_n	Signal and Noise autocorrelation functions
$s(t)$	signal component of the wave received at the array
$\mathbf{s}$	Hypothesized steering vector
S	Sound slowness, reciprocal of c
$S(\omega)$	Signal spectral function
S_o	Minimum sound slowness
S/N	Signal to noise ratio
t	Time quantity
T	Sampling rate
$\mathbf{u}_i$	i–th eigenvector
$\mathbf{V}(\Phi)$	Matrix of steering vectors
$\mathbf{w}$	Weight vector
w_m	m–th weight
$x(t)$	Random stationary process
$\mathcal{Z}(\omega)$	Output spectrum or spectral estimate
z	Depth of the water column (ocean)
z_o	Depth of minimum sound speed axis
ϕ	Azimuthal Bearing with respect to broadside
Φ	3D Position vector
δ	Delta function
λ_i	i–th eigenvalue
ω	Frequency band
ω_o	Frequency of interest or center frequency
ρ	Power ratio defined by Gingras
σ_n^2	Noise power
σ_s^2	Input signal power
τ_{lm}	Delay of the l–th path to the m–th sensor
θ	Elevation angle with respect to the ocean surface
$\varphi_l(\Phi)$	Delay of the l–th path through the array

Chapter 1

Introduction

An important application of digital signal processing is the estimation of the power spectrum of a random sequence. This need arises in various contexts such as the detection of signals embedded in noise. The physical situations often considered are those taking place in sonar [33], radar and seismology. A particular interest in the existence and nature of certain objects motivates the development in this area. For the underwater case, these bodies could be ships, marine life or unknown objects generating pressure waves.

The mathematical basis for modern spectral analysis has its roots in the 17th century work of the scientist Sir Isaac Newton. He observed that the sunlight was expanded into many colors when passed through a prism. He also discovered that each color represented a particular wavelength of light and that white sunlight contained all wavelengths. In 1671, Newton introduced the word *spectrum* to describe the band of light colors. Spectrum has its roots in the Latin language as *specter*, meaning image or ghostly apparition and the associated adjective is *spectral* [27]. Spectral estimation or spectral analysis is the name given to the collection of methods for applying imperfect answers to the question: 'What is the frequency content of this signal?' [39,19,27].

The nature of the processing will depend on the data or signal under consideration and the purpose for which they are intended. The use of numerical or digital algorithms adds versatility to the processing. Through various computational techniques, the pertinent parameters for the application at hand can be extracted from the available time varying signal. A common processing approach is to first transform the signal into its equivalent frequency domain representation; in many cases this version of the signal is easier to interpret and characterize. Systems designed to receive these propagating signals often encounter

the presence of other signals, which corrupt the main signal of interest. These signals are referred to as noise and are of less concern. Different types of noise exist: self noise generated by the measuring device, interferences from objects similar to the one of interest, and background or ambient noise.

Signal processing can be accomplished in the temporal or spatial domain [47, 4]. If the signal of interest and the interferer occupy the same temporal frequency band, discrimination on the basis of frequency components is difficult to achieve and temporal processing cannot be applied. However, usually the signal and interference originate from different spatial locations and spatial processing can be used to separate the signal from the interferer. Spatial processing is analogous to spectral analysis or filtering with the element of interest, being the direction of arrival of the signal. This direction is also known as the bearing of the source. Sonars, radars and communication systems are areas where spatial processing is applied.

An array of sensors is often used in the detection and estimation process. Its operation is analogous to that of an Finite Impulse Response (FIR) filter. The array combines the spatially sampled time series from each sensor to obtain a scalar output time series, whereas the FIR filter linearly combines temporal sampled data. The discriminating capability depends on the physical size of the aperture. As the size increases, discrimination improves. Spatial processing is also versatile in real time applications where it is necessary to modify the spatial filtering function. Implementation of the change is easily achieved by changing the approach used to combine the sensor data. The goal of the array processor is to act on the measured data originating at the sensors, in order to make decisions about the nature of the target [28]. This is usually followed by the evaluation of several parameters such as the range, depth, bearing, and temporal frequency content.

Underwater propagating acoustic signals at long distances operate at frequencies ranging from a few hertz to several thousand hertz. Uncertainty must be included in the characterization of the response due to the corrupting signals present and the random nature of the target signals themselves. Statistics play an important role in spectral analysis. Since the exact attributes of the signal of interest are unknown *a priori*, only an *estimate* of the signal spectrum can be obtained.

Classical spectral estimation techniques are robust methods that employ the Fast–Fourier Transform (FFT) algorithm and are used on an unrestricted number of signals and noise classes. The periodogram and the correllogram are examples of such estimators. The

resolution of the classical methods is directly related to the length of the data records or observation intervals and often in real time applications, short data segments are forced. For all these methods, the user is faced with many trade–offs in an attempt to produce a statistically reliable estimate of the highest possible resolution with a finite amount of data samples.

Modern methods are concerned with an improved performance with short data segments or observation interval; an increase in resolution, and more robust statistical properties. Recently, there has been a proliferation of eigenstructure spectral estimation methods [37,6,25,24,33]. These methods exploit the eigenvalue–eigenvector structure of the Cross Spectral Density Matrix (CSDM). The use of the modal decomposition for spectral analysis has evolved from nonparametric and adaptive array processing schemes to applications such as high resolution spectral estimation [6,33,4]. These methods are based on the notion of separability of the signal and noise processes into orthogonal vector subspaces. When the data consist of known signals in background noise of known covariance, these methods are important because they perform well. The Pisarenko approach [37] and the Multiple Signal Characterization (MUSIC) [40] algorithm are included in this class of eigenvector–based frequency estimators.

In this work, a new family of spectral estimators, the *Rayleigh family*, originally proposed by Lagunas [24] is investigated. This new approach is based on previous work undertaken by Pisarenko, where he proposed the use of non–linear functions of the covariance matrix to form different spectral estimates. It represents a family of *true* power spectral density estimates with resolution under user control. An introduction to array signal processing with application to a sensor array is given in Chapter 2. The basic estimator is presented followed by important issues affecting the selection of a particular analysis approach. Two estimators are then derived: the Capon estimator [6] and the Normalized Maximum Likelihood method of Lagunas [25]. A comparison of their respective properties will follow. An overview of the previous work by Pisarenko will serve as an introduction to the development and presentation of the properties of the Rayleigh family.

Chapter 3 is concerned with the study of the properties of this new family of spectral estimates [20]. A common notation and model are first developed for consistency reasons and to maintain a common frame of reference with other works, mainly Cox [9], Lacoss [22] and Gingras [12]. Since the new proposed estimators form a *family*, the analysis will be conducted in such a way as to generalize previously derived results for any order

or member of this family. The investigation reported in this work deals with the single source or single target case. Although limited in nature, it could serve as the basis for the development of the multiple signal case to be considered for future work. Cox considered the case of 2 sources for which he presents closed form expressions [9]. In most instances, the noise is assumed white and uncorrelated with the signal. This assumption leads to a considerable simplification of the derivation of the different expressions and offers the possibility for comparison with existing results. In some cases, expressions for an unknown noise environment are also presented.

The output spectrum response of the Rayleigh family is first investigated in Chapter 3. A general expression is derived and results are presented for the first few members. The system response is then categorized into two types, the *matched* and the *not matched* response. Each case is investigated individually and bounds for the output spectrum level are derived. A measure of resolution presented by Lacoss [22] and expressed as the width of the main peak at the -3dB point is then used as a basis for the analysis of the resolution property of the Rayleigh family. A closed form expression is derived to predict the bandwidth of any member of this family of spectral estimates. Numerical results are used for comparison purposes and to support the derived expressions. The analysis of the sensitivity to mismatch of the Rayleigh family then follows. This measure is an indication of the variability of the peak value at the true location when a mismatch occurs. Based on a definition presented by Gingras [12], a general expression for the sensitivity of the Rayleigh family is then derived. This expression represents the percentage drop in the peak value for a given mismatch. The result is compared with Gingras' work and further extended to the general case.

In the remaining part of this chapter, other properties and concepts related to the family of spectral estimates are presented. In most of the analysis, the observation interval over which the data was collected, is assumed infinite. However, any real application requires working with finite or limited data segments or observation intervals. The effect of the reduced amount of available data on the overall performance of the estimate is investigated through Monte–Carlo simulations. The mean and variance of various Rayleigh estimates for different data segment lengths are calculated. The simulation approach was used rather than the development of a general statistical model, since the complexity involved in the latter approach was considered beyond the scope of this work [7,17]. The asymptotic convergence of the spectrum as the observation interval grows to infinity, and

the minimum and maximum bounds of the resulting spectrum are then presented [24].

Conventional bearing estimation procedures use plane wave steering vectors as replicas of the true signal field and seek to resolve the different sources by maximizing a power function representing the correlation between the hypothesized and actual steering vectors. This approach is effective in signal detection if the received signal consists of a few plane waves. However, in a inhomogeneous medium, the signal fields are quite complex and a more general scheme may be more effective in detecting and localizing the target. This non-plane modelling approach is called Matched Field Processing (MFP) [3,38,1,34].

Matched Field Processing uses the same traditional spectral estimators such as the Bartlett [38,12,1], the Capon's Minimum Variance [1,15,12,21] or the Rayleigh [21] except that the hypothesized steering vector is replaced by a hypothesized vector derived from a full wave propagation model comprised of wave arrival structure and delay information. Also, the '*look direction*' is replaced by a '*look position*'. Similarly, the Cross Spectral Density Matrix is compared to that of the target at the assumed position. When the processor relies on the full–wave model, it is known as the Coherent MFP [21]. The performance of such a method is strongly affected by the uncertainty in the environmental model as will be shown in Chapter 5 [21,10]. In practice, if the assumed environmental model does not agree with the real ocean model, discrepancy and mismatch will result, leading to a degradation of the system performance.

Chapter 4 presents an introduction to the underwater acoustic field [2,32,43]. The nature and properties of sound propagation in the ocean are discussed. Sound propagation in the ocean and the underlying ocean environment can be modeled using different approaches. Three alternatives ranging from the simplest to the most complete are considered in this work: the Isovelocity model [44,5], the Munk and Wunsch Linear and Quadratic models [30] and the Multiple–Profile Ray–Tracing Program (MPP) provided courtesy of the Woods Hole Oceanographic Institute (WHOI) [31]. Sample ray traces of sound propagation in a given environment along with a comparison of the three approaches will follow. Issues involved in the modeling of the ocean are also discussed.

With the high sensitivity to model mismatch inherent in coherent matched–field processing, a new approach was presented by Krolik *et al* [21]. This new method, the incoherent MFP relies only on the arrival structure of the rays. Combining a reduced wave model with a higher resolution estimator, using the Lacoss definition, results in a processor more robust to model mismatch. Thus a trade–off between the completeness of the wave

model and the resolution of the processor can be selected. In case of a mismatch, the coherent processor relying on the full wave model will be more affected than the incoherent processor that relied only on a robust subset of the pressure field model. In Chapter 5, the basics of Matched-Field Processing are outlined [3,1]. The development of the full pressure field model is presented. Coherent MFP is presented followed by the incoherent approach. A comparison of the performance of both processors when operating in a real ocean environment then follows [38,34,36]. The ocean profile for the Bay of Monterey, CA, is used. The matched case response, i.e. when the assumed ocean model is equivalent to the true one, is first considered. The sound speed profile is then modified to introduce a small mismatch and the same experiment is repeated. The sensitivity and performance of the different estimators are presented. Chapter 6 serves as a conclusion and briefly discusses the different results obtained. Some possible directions for future work along related lines are also outlined.

Sections in the body of the thesis will be referred by section numbers (e.g. 3.3.1) and equations will bear the number of the section in which they appear followed by another identifier (e.g. 3.12). References are made numerically to the alphabetized bibliography at the end of the thesis and are enclosed in square brackets (e.g. [12]). Upper case bold letters denote matrices (e.g. $\mathbf{R}, \mathbf{I}$) and lower case bold letters denote vectors (e.g. $\mathbf{s}, \mathbf{d}$). Programs used to generate and process the different data files are not included in order to keep the present work concise. However, they are available upon request from the author.

Chapter 2

High Resolution Estimators

2.1 Array Signal Processing

The primary objective of performing array signal processing is to estimate the temporal and spatial characteristics of the received signal. Often an array is divided into two or more subarrays. The beams on each subarray are formed first. to allow for the pre-processing of the data received from various directions. Signal and data processing is then performed across the beams. Similar processing is performed for the data available at other arrays and the results is combined to develop a common picture as seen by all the arrays. The block diagram of a general array configuration with the interconnections between the different functions is shown in Fig. 2.1 [14].

Spatial processing is accomplished when the array is set to receive signals from a given direction and to a certain degree reject signals from all other directions. Each hydrophone in the array receives a combination of signal and noise, assumed Gaussian for the purpose of this discussion. The signal processing task can be thought of as the localization of energy in time, frequency, direction or some other variable. Source localization systems make use of the received signals time delays and their variation in time to estimate the location. These systems process data spatially and temporally. The received data is processed spatially across the different elements of the array and temporally during sequential observation intervals spread out in time. The overall system performance depends on both the spatial and temporal characteristics. Spatial gain is influenced by such factors as the size of the array, the number of elements and their configuration in space. It is inversely proportinal to the effective linear dimension of the array, the longer the array and the higher

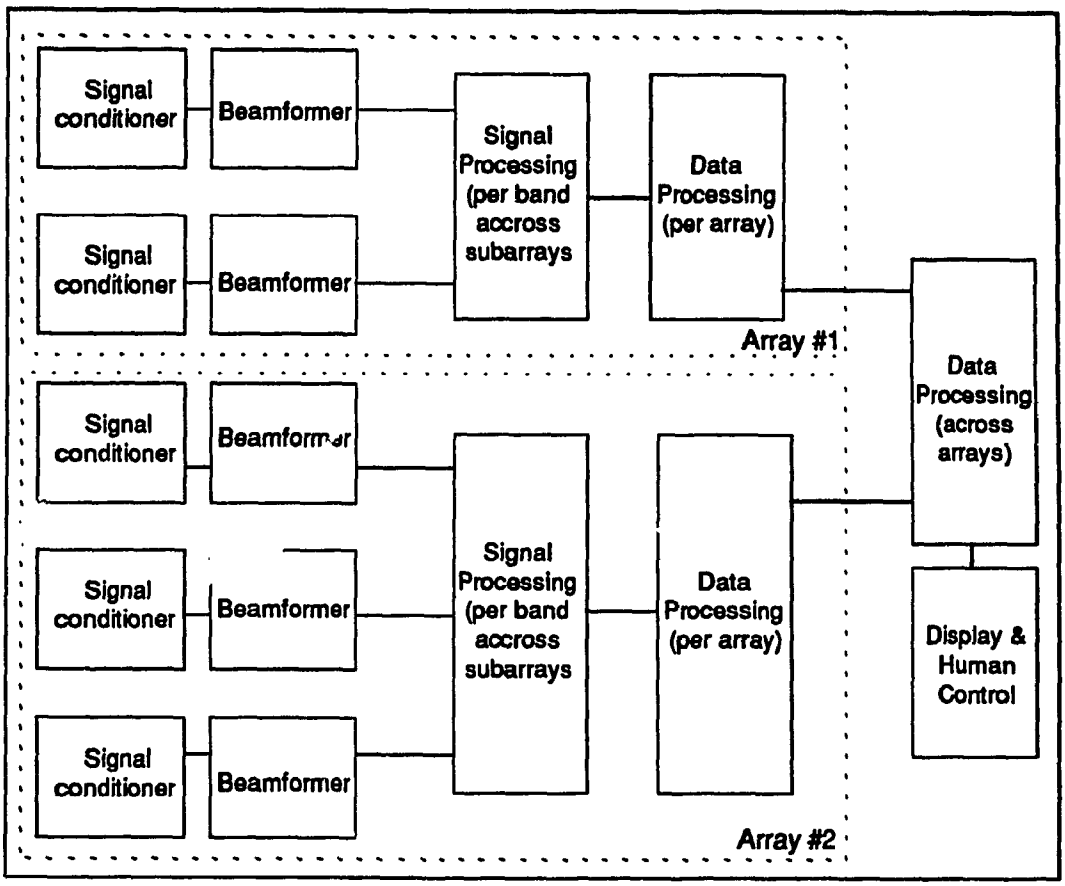

Figure 2.1: Generalized partitioning and interconnection of functions

the signal frequency, the sharper is the resolution. Temporal performance or resolution is inversely proportianal to the observer response bandwidth [14]. For an optimum system performance, optimization in both domains is desirable. However, practical considerations such as cost and dimension of the array, and the measurement accuracy in the presence of noise limit the achievable gain.

Beamforming is a term associated with the process of forming beams in order to receive a signal from a specific direction and attenuate those from other locations [47]. The processor that performs the spatial filtering is called a beamformer. In delay–and–sum beamforming, delays are used to align the signals from a desired direction before they are summed. This causes signal components to add coherently, resulting in a large output when the array is steered in the direction of the source, whereas the noise components are added incoherently. A weighting operation is applied on the resulting delays to emphasize the peak and reduce the sidelobe levels.

Similar beamforming is possible in the frequency domain. Blocks or segments of data from each hydrophone are formed first. Each block is transformed using a Fast Fourier Transform to the frequency domain. For a given direction of interest, a beam is formed by multiplying the transformed block by an appropriate complex phase–shift factor. This is equivalent to *steering* the beam to the angle ϕ. A filtering operation will be applied to each beam before finally being summed over the hydrophones.

Spectral decomposition is accomplished when the time signal from a given beam is represented in terms of amplitude and phase as a function of frequency [14,19]. Application of spectral estimation include:

- Classification of signatures and identification of their source.
- Doppler tracking and estimation of the source speed.
- Digital filter design.
- Spectral smoothing

In this chapter, the fundamental mathematical relations will be presented. They serve as the basis for the development of the Rayleigh family in the remaining of this work. The analogy between spectral analysis and the spatial spectrum will be outlined. Important issues in the selection of a particular approach will be presented and the model used throughout this

work as it relates to the source localization with a line array, will be derived. Two spectral estimation methods, the Minimum Variance and the Normalized Maximum Likelihood Method are presented in order to better appreciate the Rayleigh family and its properties, discussed in the next chapter. Comparative results between the two estimators are also included. Finally the work by Pisarenko that lead to the formulation by Lagunas of the Rayleigh family is introduced.

2.2 Spectral Relations

In the context of an underwater localization problem, the object is to detect a distant source using a line array. An array of M sensors is present in the medium and positioned in a horizontal way parallel to the surface of the ocean, with each sensor recording the acoustic field at its position. The first sensor is taken as a reference point. Furthermore, the following basic assumptions are made:

- Signal and noise are stationary Gaussian processes.
- The signal comes from a source sufficiently remote so that its wavefront can be regarded as planar over the dimensions of the array.
- The noise waveshapes received by different hydrophones are statistically independent of each other and of the signal.
- Their energy is contained within a frequency band centered around ω_o.
- The receiving array is linear.
- The ocean's propagation speed is constant and equal to c.

The propagating wave field emanating from the source and having reached the array is expressed at the outputs of the M hydrophones, as M random processes $x_k(t)$, each observed for a period of T seconds:

$$\mathbf{x}(t) = [x_0(t), x_1(t), \ldots, x_{M-1}(t)]$$

Rewriting this output in terms of the Fourier coefficients results in

$$X(\omega_k) = \sum \mathbf{x}(t) e^{-j\omega_k t} \tag{2.1}$$

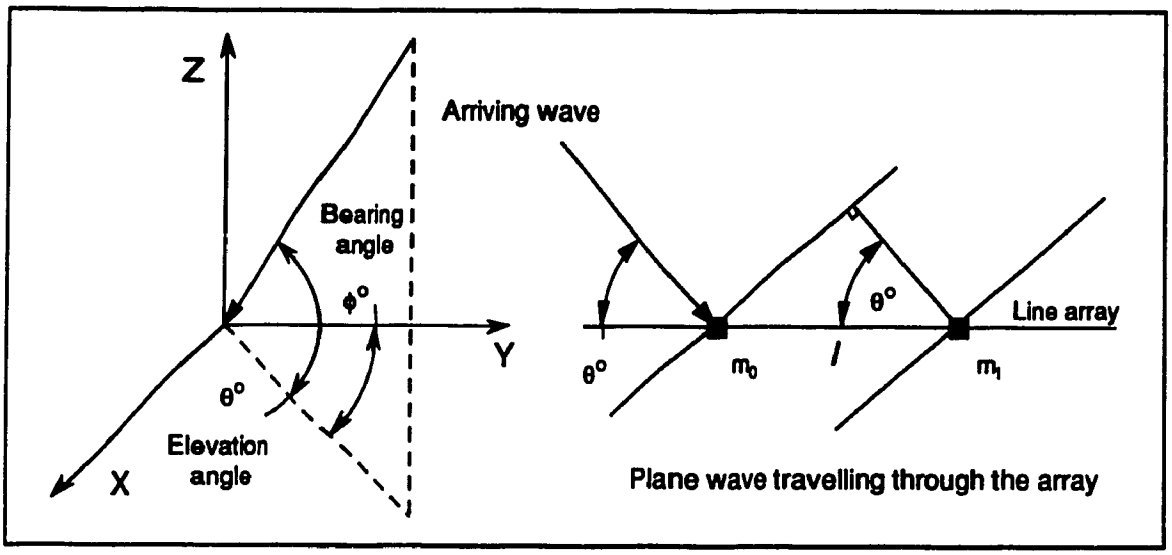

Figure 2.2: Ray arrival at the array

where

$$\omega_k = \frac{2\pi k}{T} \tag{2.2}$$

The cross-spectral density matrix (CSDM) or moment matrix [26] $\mathbf{R}$ is defined as

$$\mathbf{R} = \mathcal{E}\{XX^*\} \tag{2.3}$$

where $\mathcal{E}$ denotes the expectation operator or mean and the individual elements of $\mathbf{R}$ are given by

$$\mathbf{R} = \mathcal{E}\{X_i(\omega_l)X_j(\omega_n)^*\} \tag{2.4}$$

$$= \int_{-T/2}^{T/2}\int_{-T/2}^{T/2} e^{\jmath(\omega_l t - \omega_n u)}\mathcal{E}\{x_i(t,\phi)x_j^*(u,\phi)\}\,du\,dt \tag{2.5}$$

The superscript symbol $*$ in $x_j^*(u,\phi)$ is used to denote complex conjugate transpose.

Prior to further development of the CSDM matrix, insight into the ray arrivals and the relative delay is needed. Figure 2.2 depicts the ray arrival at the first sensor of a horizontal line array. From the figure, the propagation delay introduced between two adjacent sensors separated by distance ℓ along the y axis, for a plane wave, is expressed as

$$\frac{\ell \sin\phi\cos\theta}{c} \tag{2.6}$$

where θ is the elevation angle, ϕ is the azimuthal bearing angle with respect to the array broadside and c is the sound speed. Consequently, the total delay at a given sensor m with

respect to the first sensor in a linear equi-spaced array is

$$\tau_m = \frac{m\ell \sin\phi \cos\theta}{c} \qquad 0 < m < M-1 \tag{2.7}$$

The waveform measured at time t at the m–th sensor relative to the reference, is given by

$$x_m(t) = s_m(t-\tau_m) + n_m(t) \tag{2.8}$$

where $s_m(t)$ is the assumed propagating wave, τ_m is the delay between the first and m–th sensor and $n_m(t)$ is the additive noise. For narrowband signals, let $x(t)$ be modeled as being a narrowband gaussian processes centered around a single frequency ω_o. Using the complex signal representation results in:

$$s(t) = a(t)e^{j\omega_o t} \tag{2.9}$$

where $a(t)$ is the complex signal envelope and ω_o is the carrier frequency. The delayed version of the signal at the m–th sensor relative to the origin is written as

$$s_m(t-\tau_m) = a_m(t-\tau_m)\, e^{j\omega_o(t-\tau_m)} \tag{2.10}$$

If the signal is narrowband and the signal wavefront travels across the array in a time small compared to the observation interval or the reciprocal of the signal bandwidth, such that

$$\tau_m \ll T \qquad \forall m\,\ell, \phi \tag{2.11}$$

the following approximation can be used [35]

$$a_m(t-\tau_m) \cong a_m(t) \tag{2.12}$$

The worst–case maximum interelement delay for a linear array, called endfire condition, is for the direction of propagation of the ray to be parallel to the array axis (i.e. $\phi = 90°$). Similarly, for the direction of propagation to be perpendicular, called broadside condition, the delay is zero. Under the worst condition, the maximum delay between the first and last sensor is:

$$\tau_{\max} = \frac{(M-1)\ell}{c} \tag{2.13}$$

A sufficient condition for 2.12 to hold is

$$\frac{(M-1)\ell}{c} \ll T \tag{2.14}$$

Substituting the above expression in (2.5) and using the assumption of the noise independent from sensor to sensor as well as between signal and noise, we obtain

$$\mathcal{E}\{X_i(\omega_l)X_j(\omega_n)^*\} = \int_{-T/2}^{T/2}\int_{-T/2}^{T/2} e^{\jmath(\omega_l t-\omega_n u)} \times [R_s(t-u+\tau_j-\tau_i)+R_n(t-u)\delta_{ij}]\,du\,dt \quad (2.15)$$

where $R_s(\tau)$ and $R_n(\tau)$ represent the signal and noise autocorrelation function and δ_{ij} is the Kroneker delta function defined as

$$\delta_{ij} = \begin{cases} 1 & i=j \\ 0 & i\neq j \end{cases} \quad (2.16)$$

For a single stationary process, there exist no correlation of Fourier coefficients associated with different frequencies. The signal and noise autocorrelation functions can be defined in terms of the corresponding spectral function such as

$$R_s(\tau) = \frac{1}{2\pi}\int_{-\infty}^{\infty} S(\omega)e^{\jmath\omega\tau}\,d\omega \quad (2.17)$$

$$R_n(\tau) = \frac{1}{2\pi}\int_{-\infty}^{\infty} N(\omega)e^{\jmath\omega\tau}\,d\omega \quad (2.18)$$

Introducing 2.17 and 2.18 in 2.15 and evaluating the outer integral between $-T/2$ and $T/2$ results in the following [26]

$$\mathcal{E}\{X_i(\omega_l)X_j(\omega_n)^*\} = \quad (2.19)$$
$$\frac{T^2}{2\pi}\int_{-\infty}^{\infty} [S(\omega)+N(\omega)\delta_{ij}]e^{\jmath\omega(\tau_j-\tau_i)}\,d\omega \left[\frac{\sin(\omega+\omega_l)T/2}{(\omega+\omega_l)T/2}\right]\left[\frac{\sin(\omega+\omega_n)T/2}{(\omega+\omega_n)T/2}\right]$$

Over a small interval of ω equal to $1/T$, the two final terms are essentially non-zero. Similarily, over the same interval, if the signal and noise correlation time are short and the wavefronts sweeps accross the array in a short time, compared to T, then using the orthogonality of the last two terms [26]

$$\mathcal{E}\{X_i(\omega_l)X_j(\omega_n)^*\} = \begin{cases} 0 & l\neq n \\ T[S(\omega_n)+N(\omega_n)\delta_{ij}]e^{\jmath\omega_n(\tau_j-\tau_i)} & l=n \end{cases} \quad (2.20)$$

The result is a correlation matrix $\mathbf{R}$ of size $M\times M$ that can be expressed as the sum of the signal and of the noise components; an important property that will be used to develop the model used throughout this work.

2.3 Beamforming and Spatial Filtering

In this section, beamforming and spatial filtering are discussed. An analogy will be drawn between beamforming in the spatial domain and FIR filtering in the temporal domain. It will be shown that there exist a close resemblance between the two operations where the estimation of a frequency in the time domain is analogous to the estimation of a position in the spatial domain.

The frequency response of a finite impulse response filter with M tap weights w_m^* such that $0 \leq m \leq M-1$ and a tap delay line of T seconds is

$$Y(\omega) = \sum_m w_m^* e^{-\jmath\omega T m} \tag{2.21}$$

The response of the filter to a complex sinusoid at frequency ω can be expressed as the product of two vectors such that

$$Y(\omega) = \mathbf{w}^* \mathbf{d}(\omega) \tag{2.22}$$

where $\mathbf{w} = [w_0, w_1, \ldots, w_{M-1}]$ is the vector of the individual weights and $\mathbf{d}(\omega)$ describes the phase at each tap of the filter such that $\mathbf{d}(\omega) = [1, e^{\jmath\omega T}, \ldots, e^{\jmath(M-1)\omega T}]$.

Similarly, beamforming is used to represent the amplitude and phase of complex plane waves as a function of spatial frequency and location. The location is usually a three dimension quantity expressing the position of the source of interest as a function of range, depth and bearing. In the analysis to follow, one of the parameters, the direction of arrival or bearing is of interest. The simplest approach for determining the bearing of a source at ϕ_o is beamforming where the outputs of the sensors are summed with weights and delays in order to align their propagation delays. This will result in a reinforcement of the signal.

The data consists of M random processes $[x_0(t), x_1(t), \ldots, x_{M-1}(t)]$, the outputs of the M hydrophones, each observed for a period of T seconds. Expressing this output in terms of the Fourier coefficients results in

$$X_m(\omega_k) = \int_{-T/2}^{T/2} x_m(t)\, e^{-\jmath\omega_k/Tt}\, dt \tag{2.23}$$

replacing $x_m(t)$ by Eq. 2.8 when there is *no noise*

$$X_m(\omega_k) = \int_{-T/2}^{T/2} s(t-\tau_m)\, e^{-\jmath\omega_k t}\, dt \tag{2.24}$$

For the case where each sensor output consists of a single propagating signal represented by a plane wave, the elevation angle equals zero ($\theta = 0°$) and the term $\cos\theta$ can

be neglected (since $\cos\theta = 1$) from the propagation delay expression. For a given frequency ω and bearing ϕ of interest, beams can be formed by summing the output of the different sensors. the Fourier transform of a beam is given by

$$Y(\omega,\phi) = \sum_m w_m e^{-\jmath(\omega/c)m\ell\sin\phi} X_m(\omega) \tag{2.25}$$

where $X_m(\omega)$, the Fourier transform of the signal with its corresponding delay at sensor m, is expressed as:

$$X_m(\omega) = S(\omega)e^{\jmath(\omega/c)m\ell\sin\phi_o} \tag{2.26}$$

Combining 2.25 and 2.26 results in

$$Y(\omega,\phi) = S(\omega)\sum_m w_n e^{-\jmath(\omega/c)m\ell(\sin\phi-\sin\phi_o)} \tag{2.27}$$

The spatial frequency or wavenumber component is therefore $(\omega/c)\sin\phi$. As $c = \frac{\omega\lambda}{2\pi}$, this variable can be written as $\frac{\sin\phi}{\lambda}$ and the beamformer output is

$$Y(\omega,\phi) = S(\omega)\sum_m w_n e^{-\jmath 2\pi\frac{m\ell}{\lambda}(\sin\phi-\sin\phi_o)} \tag{2.28}$$

Since expression 2.27 represents the Fourier transform of a sequence, and the Fourier transform is a periodic function with a period of 2π, then the spatial spectrum $Y(\omega,\phi)$ is also periodic with a period of 2π. For the linear array with sensor separation ℓ, this period is:

$$\frac{\ell}{\lambda/2} \tag{2.29}$$

If the wavelength of the source is such that the above expression is greater than 1, aliasing will occur. In the opposite case where the quantity is less than 1, the Fourier transform which assumes a periodicity of 2π will evaluate frequencies for non–physical arrival angles.

The previous results can be formulated in matrix notation by expressing the spatial spectrum in terms of two vectors $\mathbf{w}$, the weights vector and $\mathbf{x}$ defined as the sum of the plane wave signals and noise components such that:

$$\mathbf{w}_m = w_m^* e^{\jmath(\omega/c)m\ell\sin\phi} \tag{2.30}$$

$$\mathbf{x} = \sigma_s\mathbf{d}(\omega,\phi_o) + \sigma_n\mathbf{q} \tag{2.31}$$

where $\mathbf{q}$ is the noise component assumed statistically independent from the signal. The vector $\mathbf{d}(\omega,\phi_o)$ represents an ideal plane wave signal propagating from the direction of

$\sin\phi_o$ and is known as the true direction vector of the wave and σ_s is the total expected signal power. The two vectors $\mathbf{w}$ and $\mathbf{d}(\omega,\phi_o)$ are represented in vector form as follow:

$$\mathbf{d}(\omega,\phi_o) = \left\{ \begin{array}{l} 1 \\ \exp\{\jmath(\omega/c)\ell\sin\phi_o\} \\ \exp\{\jmath 2(\omega/c)\ell\sin\phi_o\} \\ \vdots \\ \exp\{\jmath(M-1)(\omega/c)\ell\sin\phi_o\} \end{array} \right\} \tag{2.32}$$

$$\mathbf{w} = \left\{ \begin{array}{l} 1 \\ \exp\{\jmath(\omega/c)\ell\sin\phi\} \\ \exp\{\jmath 2(\omega/c)\ell\sin\phi\} \\ \vdots \\ \exp\{\jmath(M-1)(\omega/c)\ell\sin\phi\} \end{array} \right\} \tag{2.33}$$

The output $Y(\omega,\phi)$ of the beamformer is then given by the inner product of the two vectors defined in 2.30 and 2.31:

$$Y(\omega,\phi) = \mathbf{w}^*\mathbf{x} \tag{2.34}$$

Assuming that all the sensors are equally weighted (i.e $w_m^* = 1$) and considering the ideal case with no noise, then

$$\mathbf{w}_m = e^{\jmath m(\omega\ell/c)\sin\phi}$$

and $Y(\omega,\phi)$ is

$$Y(\omega,\phi) = \mathbf{w}^*\mathbf{d}(\omega,\phi_o) \tag{2.35}$$

The weight vector $\mathbf{w}$ and the array response vector $\mathbf{d}(\omega,\phi_o)$ are vectors in an M dimensional space. The angles between the two vectors $\mathbf{w}$ and $\mathbf{d}(\omega,\phi_o)$ determine the response of the system. If for some angle ϕ, $\mathbf{w}$ is orthogonal to $\mathbf{d}(\omega,\phi_o)$, the resulting system response will be zero. However if the angle is close to 0°, such that $\mathbf{w}$ is aligned with $\mathbf{d}(\omega,\phi_c)$ then the magnitude response will be large, thus indicating the presence of a source. Typically, several values of ϕ are used to steer the array and the output is examined for maxima.

Comparison of 2.22 and 2.35 reveals a close resemblance between FIR filtering and beamforming when the beamformer operates at a single temporal frequency ω_o. This relationship between temporal frequency ω in $\mathbf{d}(\omega)$ (FIR filter) and direction ϕ in $\mathbf{d}(\omega_o,\phi_o)$ (beamformer) is defined as

$$\omega = \omega_o(\ell/c)\sin\phi_o$$

Therefore, the temporal frequency in a finite impulse response filter corresponds to the sine of direction in a narrowband beamformer with equally spaced sensors. Hence, the discriminating capabilities of the array are dependent on the sine of the angle. The narrowband decomposition is often prefered since one can ignore the temporal frequency component. In the remaining of this work, the spatial domain along with spatial frequencies is used.

The energy in the beam as a function of spatial frequency ω and look direction ϕ is evaluated by computing $\int |Y(\omega,\phi)|^2 \, d\omega$, where $Y(\omega,\phi)$ is given by Eq. 2.34.

$$\begin{aligned} \mathcal{Z}(\omega,\phi) &= \mathcal{E}\left\{|Y(\omega,\phi)|^2\right\} && (2.36) \\ &= \mathcal{E}\{\mathbf{w}^*\mathbf{x}\mathbf{x}^*\mathbf{w}\} \\ &= \mathbf{w}^*\mathcal{E}\{\mathbf{x}\mathbf{x}^*\}\mathbf{w} \\ &= \mathbf{w}^*\mathbf{R}\mathbf{w} && (2.37) \end{aligned}$$

$\mathcal{Z}(\omega,\phi)$ will be know as the output spectrum or spectral estimate and $\mathbf{R}$ in the above result is a Hermitian Toeplitz matrix of autocorrelation estimates. Expression 2.37 describes the fundamental relation in spectral estimation, that of the output power spectrum in the beam. It will be used as the basis for the derivation of the various spectral estimators presented in this work. By introducing different weight vectors, a number of estimators can be formulated as will be demonstrated later in this chapter. Figure 2.3 represents a general array system configuration based on a frequency domain implementation [33]. It illustrates the different signal transformations required for the data analysis. Following the data collection, the various beams are aligned through delays of phase shifts. The weighting operation is then applied and finally the data is summed resulting in the beamformer output $Y(\omega,\phi)$.

The true autocorrelation sequence is not usually available and must therefore be estimated from the available data. Power Spectral Density (PSD) estimation approach based on forming first correlation estimates from the data are called correlogram methods of spectral estimation. These methods substitute a finite sequence of autocorrelation estimates for the infinite sequence of true autocorrelation values. Prior to presenting different approaches for computing the correlation sequence, important issues of concern when considering the quality and performance of a given estimator are first presented [39].

Positivity is the property of a given approach to always result in non–negative spectral estimates. The periodogram approach, where PSD estimates based on direct transformation of the data followed by averaging, is always non negative.

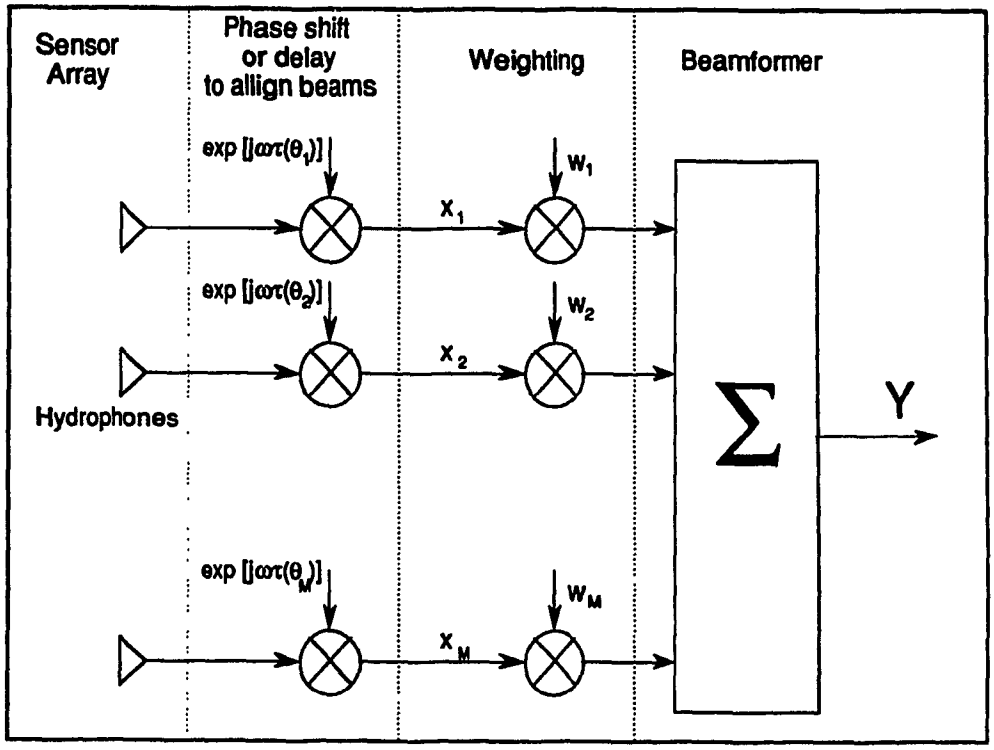

Figure 2.3: General array system configuration

Bias Ideally, the estimate $\hat{\mathcal{Z}}(\omega)$ of $\mathcal{Z}(\omega)$, the output spectrum, should be close, in some sense, to the true value of $\mathcal{Z}(\omega)$. An estimate is *biased* if its expected value differs from the true value. This discrepancy or difference between the two values is called Bias. In power spectrum estimate, the bias is a function of frequency and expressed as:

$$\text{Bias}(\omega) = \mathcal{E}\{\hat{\mathcal{Z}}(\omega)\} - \mathcal{Z}(\omega) \tag{2.38}$$

Variance Similar to the bias, the variance of an estimator can be expressed as a function of frequency and is given by

$$\sigma^2(\omega) = \mathcal{E}\left\{\hat{\mathcal{Z}}(\omega) - \mathcal{E}\{\hat{\mathcal{Z}}(\omega)\}\right\}^2 \tag{2.39}$$

This criterion is often used to indicate the statistical variability of a given approach.

Consistency An estimator is consistent if it will faithfully reproduce the true spectrum, when given an infinite amount of data. Let N be the length of the data segments and $\hat{\mathcal{Z}}_N(\omega)$ represent a sequence of estimates, generated as the data is accumulated, the estimator is said to be *asymptotically unbiased* if

$$\lim_{N\to\infty} \text{Bias}_N(\omega) \equiv 0 \tag{2.40}$$

and *consistent* in a mean square sense if

$$\lim_{N\to\infty} [\text{Bias}_N(\omega)]^2 + \sigma_N^2(\omega) \equiv 0 \tag{2.41}$$

One such approach to increasing the length of the data record is achieved by using larger array. It will be demonstraded later that as the number of elements in the array M increases and goes to infinity, higher resolution estimates result.

Stability The issue of stability, not to be confused with *statistical stability*, arises in the analysis/synthesis approach to spectral estimation. If the model is highly sensitive to the input parameters, the resulting power spectral estimate will be inappropriate. It is important that the inverse of the whitening filter be stable.

Computation It is of importance that the expense incurred in generating an estimate is minimized. This expense is expressed as a function of the computational complexity of the estimator. If two estimators are roughly equivalent, the easiest to compute is preferred.

The estimate of the autocorrelation sequence, plays an important role in the power spectral density estimator. Caution should be exercised in the procedure used to obtain the estimated autocorrelation sequence to avoid any bias in the resulting estimator. Several approaches are described by Marple to reduce the bias and variance of the estimate [27]. Averaging and smoothing through convolution with a selected window are two such approaches.

2.4 Correlation Matrix

From the previous section and more specifically Eq. 2.20, the correlation matrix (**R**) was found to be expressed as the sum of a signal and noise component. The parameter of interest corresponds to the incident plane wave originating from the source. This plane wave will contribute in **R** the following term

$$\sigma_s^2 \mathbf{d}(\omega, \phi_o)\mathbf{d}^*(\omega, \phi_o) \tag{2.42}$$

where $\mathbf{d}(\omega, \phi_o)$ is the unit norm $M \times 1$ direction vector for a signal wavefront and σ_s^2 is the total expected signal power at the array at frequency ω_o. The product $\mathbf{d}(\omega, \phi_o)\mathbf{d}^*(\omega, \phi_o)$ is the rank one matrix of the signal cross–spectral density. Noise is the second component affecting the correlation matrix. The most random and unpredictable sequence is called white noise. This signal is defined by the Discrete Fourier Transform (DFT) [39]

$$r_k = \sigma^2 \delta_k \overset{DFT}{\longleftrightarrow} \mathcal{Z}(\omega) = \sigma^2$$

Such a signal cannot be predicted using any linear filter with a prediction error variance any less than σ^2. The name white noise refers to the fact that $\mathcal{Z}(\omega)$ has power uniformly distributed among all frequencies and since its spectral density function is constant. It is a good model for many physical processes and is usually artificially generated with a pseudo-random number generator [39]. If the noise model is unknown, the noise cross–spectral density matrix is denoted by **Q** and the noise contributes in **R** the following term:

$$\sigma_n^2 \mathbf{Q} \tag{2.43}$$

where σ_n^2 is the total expected noise power at the array. However, when the noise is assumed white, the matrix **Q** is replaced by the matrix **I**, the identity matrix. Combining the signal and the noise contribution to **R**, the complete correlation matrix is expressed as

$$\mathbf{R} = \sigma_n^2 \mathbf{Q} + \sigma_s^2 \mathbf{d}(\omega, \phi_o)\mathbf{d}^*(\omega, \phi_o) \tag{2.44}$$

where the outer product $\mathbf{d}(\omega,\phi_o)\mathbf{d}^*(\omega,\phi_o)$ and the matrix $\mathbf{Q}$ are both normalized to have their trace equal to the number of sensors M.

In most instances, the true direction vector of the contact defined earlier as $\mathbf{d}(\omega,\phi_o)$ is unknown or the information concerning its characteristics is imprecise. A new vector which represents the assumed true direction vector must be defined. This new vector will be known as the hypothesized steering vector $\mathbf{s}(\omega,\phi)$. It is expressed as:

$$\mathbf{s}(\omega,\phi) = \left\{ \begin{array}{l} 1 \\ \exp\{\jmath(\omega\ell/c)\sin(\phi)\} \\ \exp\{2\jmath(\omega\ell/c)\sin(\phi)\} \\ \vdots \\ \exp\{(M-1)\jmath(\omega\ell/c)\sin(\phi)\} \end{array} \right\} \tag{2.45}$$

A mismatch at the array processor output will occur when $\mathbf{s}(\omega,\phi) \neq \mathbf{d}(\omega,\phi_o)$ or more specifically when $\sin\phi \neq \sin\phi_0$. This mismatch can result from imprecise knowledge of the ocean medium, phase or position errors in the sensors or signal and noise levels. The steering vector will usually correspond to a set of directions where some source of interest might be located. When steering the array close to the true direction of the contact, a peak will result in the array output response. These maxima of energy as a function of the look direction are assumed to correspond to an acoustic source, while the bearings correspond to the location of these maxima.

When the steering vector $\mathbf{w}$ is set equal to $\mathbf{s}$, where $\mathbf{s}$ is given by 2.45, the Blackman–Tukey estimate results. This estimate is expressed as

$$P_{BT} = \mathbf{s}^*\mathbf{R}\mathbf{s} \tag{2.46}$$

In the remainder of this work a narrowband representation of the signal is assumed and unless needed, the dependence of the various quantities on ω and ϕ will not be shown explicitly.

2.5 The Minimum Variance Method

The Minimum Variance spectral estimator was originally proposed by Capon [6] for use in multi–dimensional seismic array frequency wavenumber analysis. Lacoss reformulated the original space–time analysis for applications to one dimensional time–series analysis and

renamed it the *Maximum Likelihood Method* (MLM) [22]. This method is also known as the constrained Minimum Variance Distortionless Response (MVDR) beamformer is closely related to the MLM of Capon [33]. It is based on two constraints whereby the response is distortionless (unit) and the signal space is of known dimension with uniform independent noise. The approach results from a linearly constrained quadratic minimization problem formulation. The beamformer is derived as an optimum linear processor with unity gain and minimum variance. The frequency domain approach is used to reflect a trend in the implementation in passive and narrowband active sonars [33]. It is typical in modern passive systems to transform immediately the time sampled sensor data to the discrete frequency domain by means of a Fourier transform operation.

The objective of the proposed method is the minimization of the output variance of the estimator; this is expressed as

$$\sigma^2_{MV} = \mathcal{E}\left\{|Y|^2\right\} \tag{2.47}$$

$$= \mathbf{w}^*\mathbf{R}\mathbf{w} \tag{2.48}$$

With $\mathbf{R}$ the $M \times M$ Toeplitz autocorrelation matrix. The coefficients or weights are to be selected such that at the spatial frequency of interest (where it is assumed that a target is present), the response results in unity gain. The constrained minimization problem is stated as:

$$\textbf{minimize} \quad \sigma^2_{MV} = \mathbf{w}^*\mathbf{R}\mathbf{w} \tag{2.49}$$

$$\textbf{subject to} \quad \mathbf{w}^*\mathbf{s} = 1 \tag{2.50}$$

where $\mathbf{s}$ is the previously defined hypothesized $M \times 1$ direction vector. The constraint imposed is such that the signals of interest are passed while the effect of all other unwanted signals is minimized. The effect of the selection of the optimum weight vector is to preserve the desired signal and at the same time minimize the effect at the output of any interfering signals or noise arriving from directions not of interest. Using the Lagrange multiplier method, the solution of the optimum weights vector was found to be [28]

$$\mathbf{w}_{opt} = \frac{\mathbf{R}^{-1}\mathbf{s}}{\mathbf{s}^*\mathbf{R}^{-1}\mathbf{s}} \tag{2.51}$$

Substituting 2.51 in 2.48 results in the Minimum Variance output power given by

$$P_{MV} = \frac{1}{\mathbf{s}^*\mathbf{R}^{-1}\mathbf{s}} \tag{2.52}$$

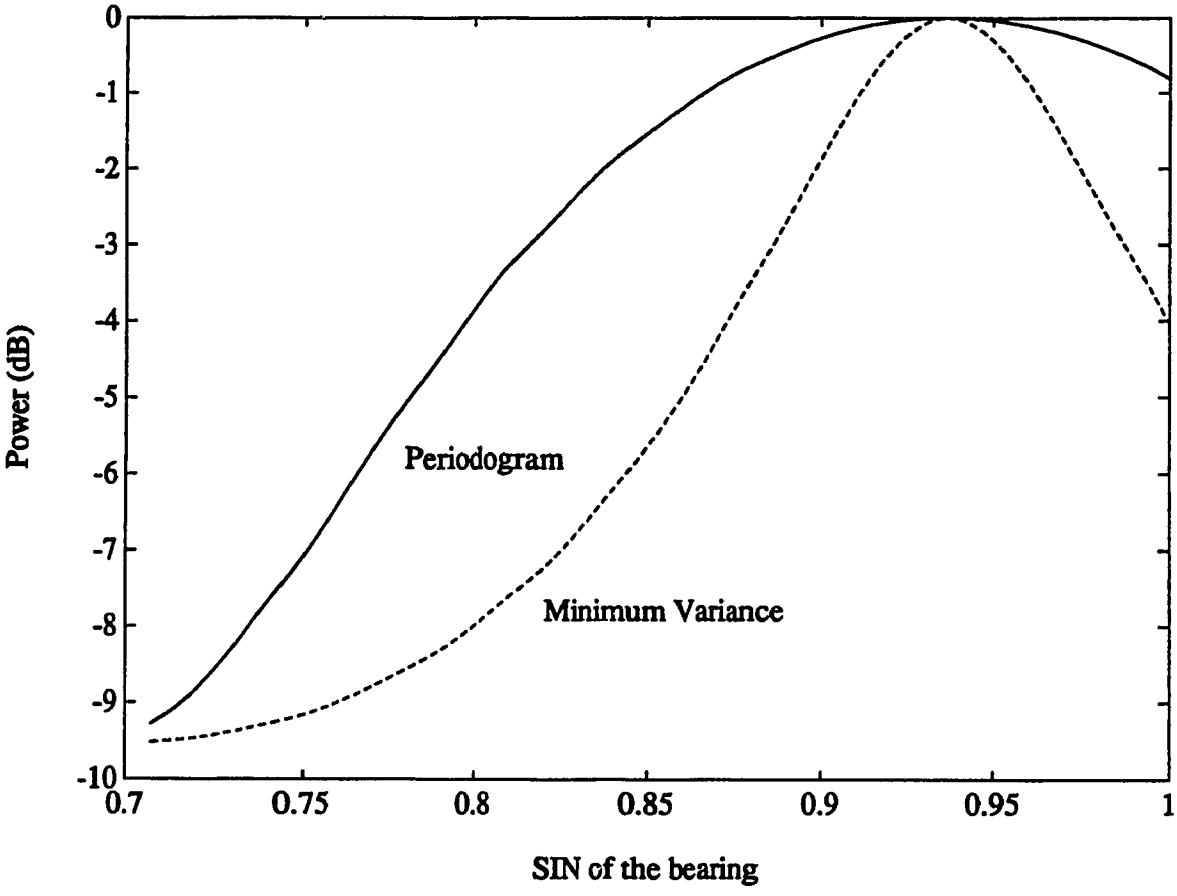

Figure 2.4: Comparison of the output spectrum of the MV and BT

A sample spectrum is presented in Fig. 2.4 where the Minimum Variance estimator is compared to the conventional Blackman–Tukey given by

$$P_{BT} = \mathbf{s}^* \mathbf{R} \mathbf{s} \tag{2.53}$$

An 8 sensors line array, with infinite observation interval, was used to localize a 0dB source inserted at 110.4884°. From the figure, The Capon approach offers an increase in the *resolution* as demonstrated by the sharper peaks at the location of the source. It is appropriate to mention that the minimum variance method does not result in true power spectral density estimate [27]. The area under the estimate does not represent the total power in the process. It describes the relative components' strength over a wide range of frequencies and the peak heights are linearly proportional to the power of the sinusoids present in the signal.

2.6 The Normalized Maximum Likelihood Method

Based on the Minimum Variance estimator developed by Capon, Lagunas introduced a modification to obtain an estimate of the spectral density from its output [23,25]. This new estimation method, the Normalized Maximum Likelihood Method (NMLM), will address the possibility of measuring power spectral density, rather than power levels, with a maximum likelihood (ML) filter. Since this approach to spectral estimation is based on the minimum variance method normalized by its effective bandwidth, as will be shown, it should more appropriately be labelled as the Normalized Minimum Variance estimator. However, since this section is used to report the work by Lagunas [25], the original name of this approach will be maintained for consistency with referenced literature.

The spectral density of the signal of interest can be decomposed in terms of its signal and noise components, as shown in Fig. 2.5 and described below.

$$Z(\omega) = S(\omega) + N(\omega) \tag{2.54}$$

where $S(\omega)$ and $N(\omega)$ represent the spectral density of the region of interest around ω_o and that of the interference. The object is to minimize the output due to $N(\omega)$ without affecting $S(\omega)$. The average power of the signal in the neighborhood of ω_o can be expressed as

$$P_o = \frac{1}{2\pi} \int_{\omega_o - \epsilon}^{\omega_o + \epsilon} S(\omega)\, d\omega \tag{2.55}$$

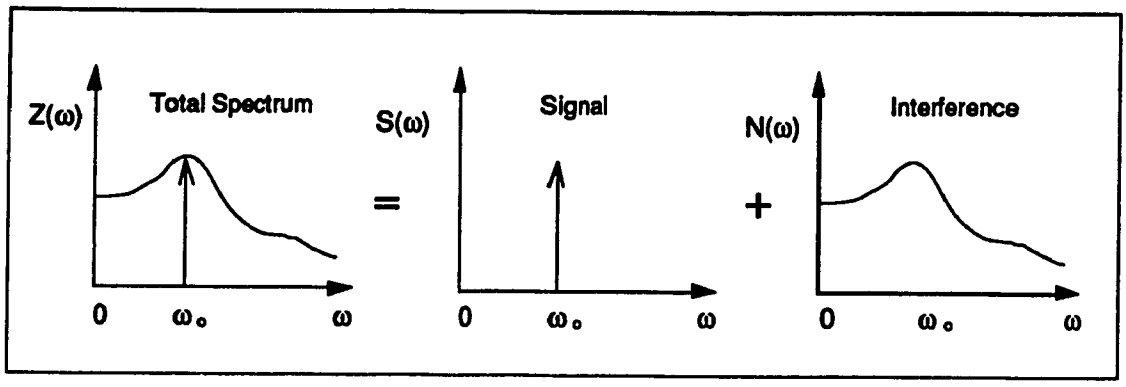

Figure 2.5: Spectrum decomposition of the signal

Using this property, the total input spectrum can be approximated by a spectral line centered around ω_o plus the added spectrum of the interference. Eq. 2.54 is rewritten as:

$$\mathcal{Z}(\omega) = P_o\,\delta(\omega - \omega_o) + N(\omega) \tag{2.56}$$

It is desired to constraint the signal output power to P_o and to minimize that of the interference. Let $\mathbf{h}$ represent the impulse response of the filter $h(n)$ presented in Fig. 2.6, where $n = 0, \ldots, M-1$ such that

$$\mathbf{h}^* = [h(0), h(1), h(2), \ldots, h(M-1)] \tag{2.57}$$

The objective is to design $H(\omega)$ in order to have at its output the spectral content of the input signal in a given band around the central frequency of the filter. In beamforming applications, this spatial frequency is referred to as the steering angle. $H(\omega)$ provides as its output the spectral content of the input signal in the neighborhood of the frequency band of interest. The selection and design of the filter must be in such a way that any interference or leakage from other frequencies in the input spectrum are avoided.

When the filter is steered at ω_o, its power output representing the estimate of $P(\omega_o)$ is expressed as

$$\hat{P}(\omega_o) = \frac{1}{2\pi}\int_{-\pi}^{\pi} \mathcal{Z}(\omega)|H(\omega)|^2\,d\omega \tag{2.58}$$

substituting $\mathcal{Z}(\omega)$ by 2.56 and rewritting the above equation

$$\hat{P}(\omega_o) = \frac{1}{2\pi}\int_{-\pi}^{\pi} N(\omega)|H(\omega)|^2\,d\omega + P(\omega_o)\delta(\omega - \omega_o)|H(\omega_o)|^2 \tag{2.59}$$

The filter impulse response $H(\omega)$ should therefore be selected as follow

$$\textbf{minimize} \quad \frac{1}{2\pi}\int_{-\pi}^{\pi} N(\omega)\,|H(\omega)|^2\,d\omega$$

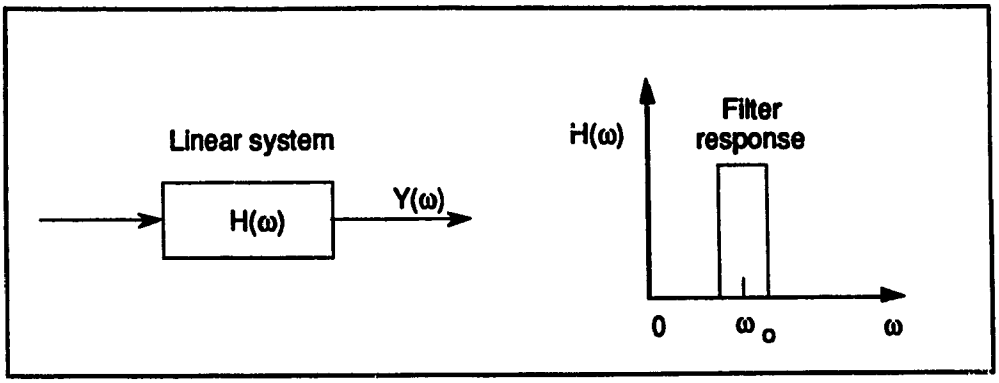

Figure 2.6: System representation of the filter response

$$\textbf{subject to} \quad H(\omega_o) = 1$$

In vector notation, this minimization problem is stated as

$$\begin{aligned} &\textbf{minimize} && \mathbf{h}^*\mathbf{R}\mathbf{h} \\ &\textbf{subject to} && \mathbf{h}^*\mathbf{s} = 1 \end{aligned}$$

where $\mathbf{s}$ is the previously defined hypothesized steering vector. The optimum weight vector that satisfies the constraint condition is [28]:

$$\mathbf{h}_{opt} = \mathbf{R}^{-1}\mathbf{s}(\mathbf{s}^*\mathbf{R}^{-1}\mathbf{s})^{-1} \tag{2.60}$$

The power level estimate around ω_o is now obtained by substituting 2.60 in the quadratic form which was to be minimized, resulting in

$$\hat{P}(\omega_o) = \frac{1}{\mathbf{s}^*\mathbf{R}^{-1}\mathbf{s}} \tag{2.61}$$

The above result represents the output power level estimate of the process in the neighborhood of ω_o and not the spectral density estimate. To derive the corresponding spectral estimate, the analysis of the effective bandwidth is needed. The power level at the output of the filter $\mathbf{h}$ with frequency response $H(\omega)$, and steered at ω_o, is given by

$$\hat{P}(\omega_o) = \frac{1}{2\pi}\int_{-\pi}^{\pi} \mathcal{Z}(\omega)|H(\omega)|^2\, d\omega \tag{2.62}$$

With the filter bandwidth denoted by B and considering that in the range of frequencies $[\omega_o - \pi B$ to $\omega_o + \pi B]$ the power density $\mathcal{Z}(\omega)$ is continuous, flat and equal to the central

value of $\mathcal{Z}(\omega_o)$, then 2.62 can be rewritten as

$$\hat{P}(\omega_o) = \frac{1}{2\pi}\int_{-\pi}^{\pi} \mathcal{Z}(\omega_o)|H(\omega_o)|^2\, d\omega \tag{2.63}$$

$$= \mathcal{Z}(\omega_o)B|H(\omega_o)|^2 \tag{2.64}$$

However, due to the constraint imposed ($H(\omega_o) = 1$), the above expression is rearranged as a function of the spectral density

$$\mathcal{Z}(\omega_o) = \frac{\hat{P}(\omega_o)}{B} \tag{2.65}$$

The energy in a signal is defined as the area under the curve. Given an ideal filter with frequency response equal to that of $H(\omega)$ and its bandwidth is the effective bandwidth B of $H(\omega)$. For the two filters to be equivalent, the equivalent-area constraint implies that B has to verify [23]

$$\frac{1}{2\pi}\int_{-\pi}^{\pi} |H(\omega)|^2\, d\omega = B\,|H(\omega_o)|^2 \tag{2.66}$$

The solution for B is found by introducing the previously defined constraint and applying Parseval's theorem, where the energy in a signal is $1/2\pi$ the area under the square of the magnitude of the Fourier transform of the signal [11], such that

$$B = \frac{1}{2\pi}\int_{-\pi}^{\pi} |H(\omega)|^2\, d\omega \tag{2.67}$$

$$= \mathbf{h}^*\mathbf{h} \tag{2.68}$$

Substituting $\mathbf{h}$ by the optimum vector in 2.60 results in the following bandwidh expression

$$B = \frac{\mathbf{s}^*\mathbf{R}^{-2}\mathbf{s}}{(\mathbf{s}^*\mathbf{R}^{-1}\mathbf{s})^2} \tag{2.69}$$

Accordingly, the power spectral density estimate of the normalized maximum likelihood method is derived by substituting the above expression for B in Eq. 2.65, resulting in

$$\hat{\mathcal{Z}}(\omega) = \frac{\mathbf{s}^*\mathbf{R}^{-1}\mathbf{s}}{\mathbf{s}^*\mathbf{R}^{-2}\mathbf{s}} \tag{2.70}$$

The power spectral density of the signal can be viewed as as the estimate of the power around ω_o normalized by the effective bandwidth of the filter. When processing in the spatial domain is desired, the vector $\mathbf{s}$ in the above expression is the hypothesized steering vector defined in 2.45. Fig. 2.7 shows the plotted output response of the Normalized Maximum Likelihood Method versus that of the Capon Minimum Variance and the conventional

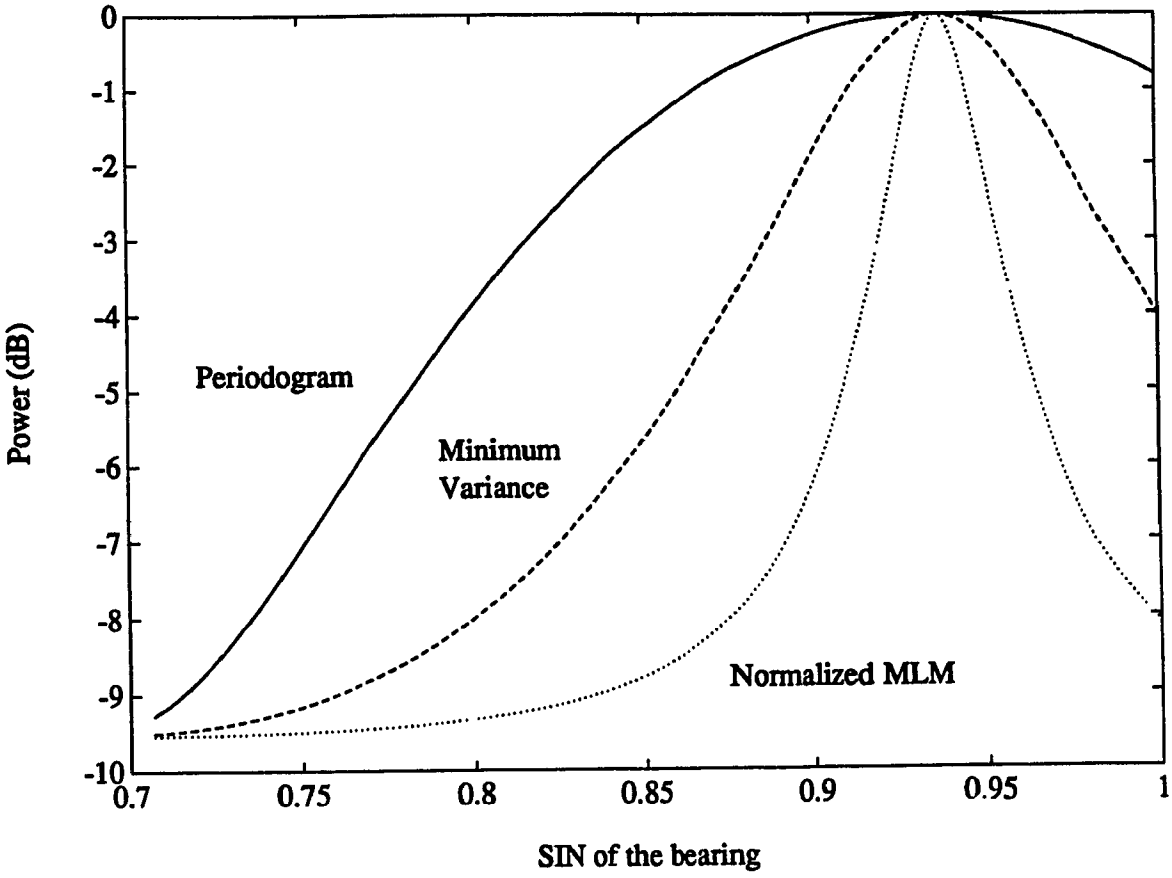

Figure 2.7: Comparison of the output spectrum of the NMLM, MV and BT

Blackman–Tukey method. The same scenario introduced in the previous section is used for this experiment. The NMLM estimator, when compared to the Minimum Variance results in *true* power spectral density estimates. It was the result of a modification introduced in the Capon Minimum Variance method. An increase in *resolution* measured by the width of the main peak is achieved. As will be shown later, this increase is obtained at a relatively high cost.

2.7 Rayleigh Estimates

Spectral estimates can be regarded as quadratic functions [37]. Capon suggested a spectral estimation method in which a non–quadratic function is used. The Minimum Variance, offered higher resolution as demonstrated by narrower peaks and had less smoothing effect on the true spectrum. However, the effect of a finite observation time was not inves-

tigated. Pisarenko introduced a new class of spectral estimators based on non–linear and non–quadratic functions that exploits the eigenvalues and eigenvectors structure and properties of the autocorrelation matrix. This class includes the conventional Blackman–Tukey and the high resolution Capon method.

The rationale behind using the eigenvalues of the autocorrelation matrix in spectral estimation lies in the fact that these eigenvalues $\lambda_1, \ldots, \lambda_M$ tend when $M \rightarrow \infty$ to the frequency values of the spectrum of $\mathcal{Z}(\omega)$ at $2\pi i/M$ such that [13]

$$\lambda_i \rightarrow \mathcal{Z}(2\pi i/M) \quad \text{as} \quad M \rightarrow \infty \tag{2.71}$$

The sample correlation matrix $\hat{\mathbf{R}}$ is expressed as $\hat{\mathbf{R}} = \{\hat{r}_{ik}\}$ where

$$\hat{r}_{ik} = \frac{1}{N} \sum_{m=1}^{N} x(t_i) x^*(t_k) \tag{2.72}$$

where $x(t_i)$ and $x^*(t_k)$ are ordinary stationary processes of time representing the sampled version of the received signal at the array. Using Pisarenko's notation, the conventional and high–resolution estimators are given by

$$\mathcal{Z}_C(\omega) = \frac{1}{M} \sum_{i=1}^{M} \sum_{k=1}^{M} \hat{r}_{ik} e^{j\omega(t_i - t_k)} \tag{2.73}$$

and

$$\mathcal{Z}_{HR}(\omega) = \frac{1}{M} \left[\sum_{i=1}^{M} \sum_{k=1}^{M} \hat{R}_{ik} e^{j\omega(t_i - t_k)} \right]^{-1} \tag{2.74}$$

where $\{\hat{R}_{ik}\}$ is the inverse of the matrix $\{\hat{r}_{ik}\}$. With the eigenvalues of the sample correlation matrix $\hat{\mathbf{R}}$, denoted by λ_i and the corresponding eigenvectors by $U_i = [u_{i1}, \ldots, u_{iM}]$, where $i = 1, \ldots, M$, the matrix can be represented as

$$\hat{\mathbf{R}} = \sum_{i=1}^{M} \lambda_i U_i U_i^* \tag{2.75}$$

Similarly for the inverse of $\mathbf{R}$ and using the properties of the eigenvalues

$$\hat{\mathbf{R}}^{-1} = \sum_{i=1}^{M} (\lambda_i)^{-1} U_i U_i^* \tag{2.76}$$

Introducing the new form of the correlation matrix in the expression of the conventional estimator (i.e. Eq. 2.73), results in

$$\mathcal{Z}_C(\omega) = \sum_{i=1}^{M} \lambda_i \left| \sum_{k=1}^{M} u_{ki} M^{-\frac{1}{2}} e^{j\omega t_k} \right|^2 \tag{2.77}$$

For the High resolution estimator, the eigenvalue–representation applied to 2.74 results in

$$\mathcal{Z}_{HR}(\omega) = \left[\sum_{i=1}^{M} \lambda_i^{-1} \left| \sum_{k=1}^{M} u_{ki} M^{-\frac{1}{2}} e^{j\omega t_k} \right|^2 \right]^{-1} \tag{2.78}$$

Let $F(x)$ be an arbitrary strictly monotone function defined over the interval $(0, \infty)$. The inverse function $f(F)$ is also strictly monotone and continuous, such that

$$f(F(x)) \equiv x \tag{2.79}$$

For a given class of functions $F(x)$, applied to the matrix $\hat{\mathbf{R}}$, the result can be expressed as a function of the eigenvalues of $\hat{\mathbf{R}}$ such that

$$F(\hat{\mathbf{R}}) = \{\hat{F}_{ik}\} = \sum_{l=1}^{M} F(\lambda_l) u_{il} u_{kl}^* \tag{2.80}$$

Since the function $F(x)$ is defined only for $x > 0$ and all the eigenvalues of $\hat{\mathbf{R}}$ are positive, a new spectral estimate in terms of $F(x)$, was introduced by Pisarenko as

$$\mathcal{Z}(\omega) = f\left[\sum_{i=1}^{M} F(\lambda_i) \left| \sum_{k=1}^{M} u_{ki} M^{\frac{1}{2}} e^{-j\omega t_k} \right|^2 \right] \tag{2.81}$$

From the above expression, if $F(x)$ is a unity or null function such that $F(x) = x$ then Eq. 2.81 is equivalent to that representing the conventional estimator. Also, with the function $F(x) = x^{-1}$ and its inverse $f(F(x)) = (x^{-1})^{-1}$, expression 2.81 will result in the high resolution estimator. The new family defines a class of non–quadratic non–linear spectral estimators. Each monotone invertible function $F(x)$ results in a new spectral estimator and the choice of the function will depend on the application and the problem at hand. Factors such as the necessary resolution, bias and form of the spectrum also contribute in the selection process of $F(x)$. One such function presented by Pisarenko is $F(x) = x^q$ with $f(F) = F^{1/q}$. Using this function, the resulting estimator is rewritten as

$$\mathcal{Z}_q(\omega) = \left[\sum_{i=1}^{M} \lambda_i^{q} \left| \sum_{k=1}^{M} u_{ki} M^{\frac{1}{2}} e^{j\omega t_k} \right|^2 \right]^{1/q} \tag{2.82}$$

This family of spectral estimators was labelled by Pisarenko as *Power Function Estimators* [37]. His work was further extended and classified by Lagunas into two families [23]:

- spectral estimates based on objectives derived from a power function of $\mathcal{Z}(\omega)$:

$$\min \int_{-\pi}^{\pi} (\mathcal{Z}(\omega))^{(1/q)}\, d\omega \quad \text{or} \quad \int_{-\pi}^{\pi} (\mathcal{Z}(\omega))^{q}\, d\omega \tag{2.83}$$

- Spectral estimates that use powers of the original data autocorrelation matrix **R**:

$$\mathbf{s}^*\mathbf{R}^q\mathbf{s} \text{ or } \mathbf{s}^*\mathbf{R}^{1/q}\mathbf{s} \tag{2.84}$$

Based on the second family and from the previous results by Pisarenko with $F(x) = x^q$ in Eq. 2.82, convergence to the true power density function is achieved when the estimator is defined as

$$\mathcal{Z}_q = (\mathbf{s}^*\mathbf{R}^q\mathbf{s})^{1/q} \tag{2.85}$$

where **s** is the hypothesized steering vector and **R** is the correlation matrix. In view of this, Lagunas extended it and proposed the Rayleigh family of power spectrum estimates expressed as:

$$\mathcal{Z}_q = \frac{\mathbf{s}^*\mathbf{R}^{-(q-1)}\mathbf{s}}{\mathbf{s}^*\mathbf{R}^{-q}\mathbf{s}} \tag{2.86}$$

with the parameter q denoting the order of the Rayleigh estimates. It can be seen from the above expression that this family of spectral estimates includes the Blackman–Tukey, the Minimum Variance and the Normalized Maximum Likelihood Method as outlined below:

$$q = 0 \quad \mathbf{s}^*\mathbf{R}\mathbf{s} \quad \text{Blackman–Tukey} \tag{2.87}$$

$$q = 1 \quad \frac{1}{\mathbf{s}^*\mathbf{R}^{-1}\mathbf{s}} \quad \text{Minimum Variance} \tag{2.88}$$

$$q = 2 \quad \frac{\mathbf{s}^*\mathbf{R}^{-1}\mathbf{s}}{\mathbf{s}^*\mathbf{R}^{-2}\mathbf{s}} \quad \text{Normalized Maximum Likelihood} \tag{2.89}$$

This family generalizes the Normalized Maximum Likelihood Method in the form of a quotient with two quadratic terms in consecutive order. The designation of Rayleigh estimate is the result of the close resemblance with the Rayleigh quotient used in the minimax principle for the eigenvalues, and having the following form [42]:

$$R(x) = \frac{x^T A x}{x^T M x} \tag{2.90}$$

In the next chapter, the Rayleigh family of power spectrum estimates will be analyzed. Closed form expressions for the output spectrum, bandwidth or beamwidth and sensitivity to mismatch for an order q estimate, will be derived. Several other properties of this family will be investigated and numerical results will be presented to support and compare the different expressions.

Chapter 3

Rayleigh Family

3.1 Introduction

In this chapter, the Rayleigh family of power spectrum estimates will be studied. A common notation and various conventions to be used throughout this work will first be presented. The output spectrum of the Rayleigh family will be analyzed. Expressions for the matched case response and the not matched case response will be derived, for arbitrary orders of estimates. Closed form expressions for the bandwidth, defined as the width of the main peak at the -3dB point, and the sensitivity to mismatch, for an arbitrary order estimate will also be derived. For the different characteristics (i.e. output spectrum, bandwidth and sensitivity to mismatch), numerical results will be presented to support the different expressions. Finally, various properties of the Rayleigh family will be considered. The effect of the size of the correlation matrix as it goes to infinity and the order q of the estimate on the output spectrum will be studied. A look at the statistical stability of the Rayleigh family through Monte–Carlo simulations will follow.

3.2 Preliminary Definitions

This section presents some concepts and definitions that will be applied throughout the analysis of the Rayleigh family. A geometric approach will be used in an attempt to simplify the different expressions thus leading to better understood results. This approach adds flexibility to the development of this work and permits the extension of the expressions with relative ease.

3.2.1 Generalized Angle

The generalized angle used by Cox [9] is a convenient expression to represent the angle between two vectors. Let $\mathbf{a}$ and $\mathbf{b}$ be two vectors of the same length and let $\mathbf{C}$ be a positive definite Hermitian matrix. The inner product of the two vectors is defined as $\mathbf{a^*Cb}$. In the resulting multidimensional space, the cosine squared of the generalized angle between the two vectors with respect to the space of C is:

$$\cos^2(\mathbf{a},\mathbf{b};\mathbf{C}) = \frac{|\mathbf{a^*Cb}|^2}{\{(\mathbf{a^*Ca})(\mathbf{b^*Cb})\}} \tag{3.1}$$

Due to the Schwartz inequality, the magnitude of this cosine is bounded between 0 and 1.

$$0 \leq \cos^2(\mathbf{a},\mathbf{b};\mathbf{C}) \leq 1 \tag{3.2}$$

The generalized angle can also be defined in terms of $\sin^2(\mathbf{a},\mathbf{b};\mathbf{C})$ as

$$\sin^2(\mathbf{a},\mathbf{b};\mathbf{C}) = 1 - \cos^2(\mathbf{a},\mathbf{b};\mathbf{C})$$

The matrix $\mathbf{C}$ in the array processing context denotes the space M-dimentional complex vectors with the inner product as defined. Two cases are of special interest in this work: $\mathbf{C} = \mathbf{Q}$, the arbitrary noise case assumed known for the analysis and $\mathbf{C} = \mathbf{I}$, the white noise case where I is the identity matrix. When the optimum processor is considered in an arbitrary noise environment (i.e. $\mathbf{C} = \mathbf{Q}$) some emphasis is given to the components with less noise (small eigenvalues) in the matrix $\mathbf{Q}$. This is best accomplished by using the metric $\mathbf{Q^{-1}}$, the inverse of the noise matrix Q, to stress those small components that play an important role, as will be shown later in this chapter [9]. Rewriting expression 3.1 in terms of $\mathbf{Q^{-1}}$ results in:

$$\sin^2(\mathbf{a},\mathbf{b};\mathbf{Q^{-1}}) = 1 - \frac{|\mathbf{a^*Q^{-1}b}|^2}{\{(\mathbf{a^*Q^{-1}a})(\mathbf{b^*Q^{-1}b})\}} \tag{3.3}$$

When the noise environment is assumed white, the noise matrix $\mathbf{Q}$ is replaced by $\mathbf{I}$, the identity matrix, and the resulting expression is written as $\sin^2(\mathbf{a},\mathbf{b};\mathbf{I})$. This expression will be used to study the effect on the various estimators of the angular difference between the true steering vector and the hypothesized one used. When vectors $\mathbf{a}$ and $\mathbf{b}$ are orthogonal, ($\mathbf{a} \perp \mathbf{b}$), then $\cos^2(\mathbf{a},\mathbf{b};\mathbf{I}) = 0$. Similarly, when $\mathbf{a}$ and $\mathbf{b}$ are perfectly aligned ($\mathbf{a} \parallel \mathbf{b}$), $\cos^2(\mathbf{a},\mathbf{b};\mathbf{I}) = 1$.

3.2.2 Expression for S/N and $\mathbf{R}^{-1}$

The power spectral estimate $\mathcal{Z}(\omega)$ at the output of a beamformer is given by

$$\mathcal{Z}(\omega) = \mathbf{w}(\omega)^* \mathbf{R}(\omega) \mathbf{w}(\omega) \tag{3.4}$$

where $\mathbf{w}(\omega)$ is the weight vector and $\mathrm{R}(\omega)$ is the signal plus noise correlation matrix defined in 2.44 and reproduced below for convenience

$$\mathrm{R}(\omega) = \sigma_s^2 \mathbf{d}(\omega)\mathbf{d}^*(\omega) + \sigma_n^2(\omega)\mathbf{Q}(\omega) \tag{3.5}$$

Since the process under investigation is assumed to be narrowband the dependency of the various terms on (ω) will not be shown explicitly. In many applications, the relative magnitude of the signal and noise power levels is an important criterion frequently used for comparison and classification purposes. From the previous expression where σ_n^2 is the input noise spectral level averaged across the sensors and σ_s^2 is the average input power spectrum of the wave, the input signal–to–noise ratio is defined as

$$S/N_i = \frac{\sigma_s^2}{\sigma_n^2} \tag{3.6}$$

Substituting 3.5 in 3.4 will result in

$$\mathcal{Z} = \sigma_n^2 \mathbf{w}^* \mathbf{Q} \mathbf{w} + \sigma_s^2 \mathbf{w}^* \mathbf{d} \mathbf{d}^* \mathbf{w} \tag{3.7}$$

This can also be written as:

$$\mathcal{Z} = \underbrace{\sigma_n^2 \mathbf{w}^* \mathbf{Q} \mathbf{w}}_{\text{noise}} + \underbrace{\sigma_s^2 |\mathbf{w}^* \mathbf{d}|^2}_{\text{signal}} \tag{3.8}$$

The ratio of both terms represents the output signal-to-noise ratio expressed as

$$S/N_o = \frac{\sigma_s^2 |\mathbf{w}^* \mathbf{d}|^2}{\sigma_n^2 \mathbf{w}^* \mathbf{Q} \mathbf{w}} \tag{3.9}$$

Given the following weight vector

$$\mathbf{w} = \frac{\mathbf{Q}^{-1}\mathbf{s}}{\mathbf{s}^* \mathbf{Q}^{-1} \mathbf{s}} \tag{3.10}$$

where $\mathbf{s}$ is the previously defined hypothesized direction vector. Introducing the weight vector in 3.4, expanding the correlation matrix and setting $\mathbf{s} = \mathbf{d}$, the ouput signal to noise ratio is equal to

$$S/N = \mathbf{d}^* \mathbf{Q}^{-1} \mathbf{d} \frac{\sigma_s^2}{\sigma_n^2} \tag{3.11}$$

Under the white noise assumption with $\mathbf{Q} = \mathbf{I}$ and using the fact that $\mathbf{d}^*\mathbf{d} = M$, the previous expression is further simplified and results in :

$$S/N = M\frac{\sigma_s^2}{\sigma_n^2} \tag{3.12}$$

This definition represents the signal-to-noise ratio expression used throughout this work. When substituting the different weight vectors w into 2.37, an expression for the inverse of the correlation matrix, represented by 3.5 will be required. Such an expression is obtained by applying the method of Modification [16]. Considering the general noise case, where the noise matrix is $\mathbf{Q}$, the inverse relation is given by:

$$\mathbf{R}^{-1} = \frac{1}{(\sigma_n^2)}\left\{\mathbf{Q}^{-1} - \frac{\mathbf{Q}^{-1}\mathbf{d}\mathbf{d}^*\mathbf{Q}^{-1}(\sigma_s^2/\sigma_n^2)}{1+\mathbf{d}^*\mathbf{Q}^{-1}\mathbf{d}(\sigma_s^2/\sigma_n^2)}\right\} \tag{3.13}$$

Similarly, for the white noise case, substituting $\mathbf{Q}$ by $\mathbf{I}$ and simplifying results in

$$\mathbf{R}^{-1} = \frac{1}{(\sigma_n^2)}\left\{\mathbf{I} - \frac{\mathbf{d}\mathbf{d}^*(\sigma_s^2/\sigma_n^2)}{1+M(\sigma_s^2/\sigma_n^2)}\right\} \tag{3.14}$$

3.2.3 Useful Identities

Other useful expressions that often occur when the output spectrum is evaluated for different weight vectors are presented below.

$$\mathbf{s}^*\mathbf{R}^{-1}\mathbf{s} \tag{3.15}$$

$$\left|\mathbf{s}^*\mathbf{R}^{-1}\mathbf{d}\right|^2 \tag{3.16}$$

$$\mathbf{s}^*\mathbf{R}^{-1}\mathbf{Q}\mathbf{R}^{-1}\mathbf{s} \tag{3.17}$$

These three terms, when combined with the expression of the inverse correlation matrix, the generalized angle, and the signal-to-noise ratio, are then expanded into the following relationships:

$$\mathbf{s}^*\mathbf{R}^{-1}\mathbf{s} = \frac{\mathbf{s}^*\mathbf{Q}^{-1}\mathbf{s}}{\sigma_n^2}\left\{\frac{1+(S/N)\sin^2(\mathbf{s},\mathbf{d};\mathbf{Q}^{-1})}{1+(S/N)}\right\} \tag{3.18}$$

$$\left|\mathbf{s}^*\mathbf{R}^{-1}\mathbf{d}\right|^2 = \frac{(\mathbf{s}^*\mathbf{Q}^{-1}\mathbf{s})(\mathbf{d}^*\mathbf{Q}^{-1}\mathbf{d})\cos^2(\mathbf{s},\mathbf{d};\mathbf{Q}^{-1})}{\sigma_n^4(1+S/N)^2} \tag{3.19}$$

$$\mathbf{s}^*\mathbf{R}^{-1}\mathbf{Q}\mathbf{R}^{-1}\mathbf{s} = \frac{\mathbf{s}^*\mathbf{Q}^{-1}\mathbf{s}}{\sigma_n^4}\left\{\frac{1+\{2(S/N)+(S/N)^2\}\sin^2(\mathbf{s},\mathbf{d};\mathbf{Q}^{-1})}{(1+S/N)^2}\right\} \tag{3.20}$$

For a complete derivation of 3.18, 3.19 and 3.20, the reader is referred to [9].

Using these expressions, it is possible to reformulate the output spectrum of the MV and NMLM as a function of the generalized angle difference between the hypothesized steering vector and the true direction vector. For the Minimum Variance estimator expressed as

$$\mathcal{Z} = \frac{1}{\mathbf{s}^*\mathbf{R}^{-1}\mathbf{s}} \tag{3.21}$$

introduced in an arbitrary noise environment, substituting 3.18 in 2.52 results in:

$$\mathcal{Z}_{MV} = \frac{\{\sigma_n^2/(\mathbf{s}^*\mathbf{Q}^{-1}\mathbf{s})\}\{1+(S/N)\}}{1+(S/N)\sin^2(\mathbf{s},\mathbf{d};\mathbf{Q}^{-1})} \tag{3.22}$$

and for the white noise case where $\mathbf{Q} = \mathbf{I}$ we have:

$$\mathcal{Z}_{MV} = \frac{\{\sigma_n^2/m\}\{1+(S/N)\}}{1+(S/N)\sin^2(\mathbf{s},\mathbf{d};\mathbf{I})} \tag{3.23}$$

Similarly, for the Normalized Maximum Likelihood method expressed as

$$\mathcal{Z} = \frac{\mathbf{s}^*\mathbf{R}^{-1}\mathbf{s}}{\mathbf{s}^*\mathbf{R}^{-2}\mathbf{s}} \tag{3.24}$$

by introducing 3.18 in the numerator, 3.20 in the denominator, and considering the white noise case, we obtain:

$$\mathcal{Z}_{NMLM} = \sigma_n^2 + \frac{\sigma_s^2\cos^2(\mathbf{s},\mathbf{d};\mathbf{I})}{1+\{2(S/N)+(S/N)^2\}\sin^2(\mathbf{s},\mathbf{d};\mathbf{I})} \tag{3.25}$$

3.3 Output Spectrum

In this section, the power spectrum at the output of the Rayleigh estimate will be studied and a closed form expression for the output of the arbitrary order q estimator will be derived. This expression will be used to observe the *peaky* characteristic and convergence rate of the estimate, as a function of the order, and the generalized angle difference between the hypothesized steering vector and the true direction vector. From equation 2.86 representing the Rayleigh estimate, one can see that an expression for the correlation matrix $\mathbf{R}$ when raised to a power q is needed. Such an expression will be derived in the next section and holds for the single source case.

3.3.1 $\mathbf{R}^{-q}$ and $\mathbf{R}^{-(q-1)}$

The correlation matrix, $\mathbf{R}$ was previously defined as:

$$\mathbf{R} = \sigma_n^2\mathbf{Q} + \sigma_s^2\mathbf{d}\mathbf{d}^*$$

Applying the spectral theorem in linear algebra, since $\mathbf{R}$ is Hermitian, it can be decomposed in term of its eigenvalues and eigenvectors in the following way

$$\mathbf{R} = \mathbf{U}\Lambda\mathbf{U}^*$$

where $\mathbf{U}$ represents the orthogonal eigenvectors $[\mathbf{u}_1, \ldots, \mathbf{u}_M]$ and Λ the corresponding eigenvalues $[\lambda_1, \ldots, \lambda_M]$. When $\mathbf{R}$ is raised to the power q, the eigenvalues of $\mathbf{R}^q$ are $\lambda_1^q, \ldots, \lambda_M^q$, the q^{th} power of the eigenvalues of $\mathbf{R}$, and each eigenvector of $\mathbf{R}$ is still an eigenvector of $\mathbf{R}^q$ [42] such that:

$$\mathbf{R}^q = \mathbf{U}\Lambda^q\mathbf{U}^*$$

The eigenvalues matrix Λ^q further expanded can be expressed as

$$\Lambda^q = \begin{bmatrix} \frac{1}{M}(\sigma_n^2 + M\sigma_s^2)^q & & & 0 \\ & (\sigma_n^2)^q & & \\ & & \ddots & \\ 0 & & & (\sigma_n^2)^q \end{bmatrix}$$

Using the mathematical identity

$$(x+y)^q = \sum_{i=0}^{q} \binom{q}{i} x^i y^{q-i}$$

it is possible to rewrite the first element of Λ^q as

$$(\sigma_n^2 + M\sigma_s^2)^q = \sum_{i=0}^{q} \binom{q}{i} (M\sigma_s^2)^i (\sigma_n^2)^{q-i}$$

By factoring $(\sigma_n^2)^q$ out of the above expression, the result is given by

$$(\sigma_n^2 + M\sigma_s^2)^q = (\sigma_n^2)^q + \sum_{i=1}^{q} \binom{q}{i} (M\sigma_s^2)^i (\sigma_n^2)^{q-i} \tag{3.26}$$

The matrix $\mathbf{R}^q$ is now reformulated as

$$\mathbf{R}^q = (\sigma_n^2)^q\mathbf{Q} + \frac{1}{M}\sum_{i=1}^{q} \binom{q}{i} (M\sigma_s^2)^i (\sigma_n^2)^{q-i}\mathbf{d}\mathbf{d}^* \tag{3.27}$$

The inverse of the previous equation is derived by using the power property of the Hermitian matrix. Expressing $\mathbf{R}^{-q}$ as $(\mathbf{R}^q)^{-1}$ and applying the matrix inversion identity results in:

$$\mathbf{R}^{-q} = (\mathbf{R}^q)^{-1} \tag{3.28}$$

$$= \left\{(\sigma_n^2)^q\mathbf{Q} + \frac{1}{M}\sum_{i=1}^{q} \binom{q}{i} (M\sigma_s^2)^i (\sigma_n^2)^{q-i}\mathbf{d}\mathbf{d}^*\right\}^{-1} \tag{3.29}$$

$$= \frac{1}{(\sigma_n^2)^q}\left\{\mathbf{Q}^{-1} - \frac{\mathbf{Q}^{-1}\mathbf{d}\mathbf{d}^*\mathbf{Q}^{-1}\beta_q}{1 + \mathbf{d}^*\mathbf{Q}^{-1}\mathbf{d}\beta_q}\right\} \tag{3.30}$$

where β_q is given by

$$\beta_q = \frac{\sum_{i=1}^{q} \binom{q}{i} (M\sigma_s^2)^i (\sigma_n^2)^{q-i}}{M(\sigma_n^2)^q} \tag{3.31}$$

For the Rayleigh spectral estimate expressed as

$$\mathcal{Z} = \frac{\mathbf{s}^*\mathbf{R}^{-(q-1)}\mathbf{s}}{\mathbf{s}^*\mathbf{R}^{-q}\mathbf{s}} \tag{3.32}$$

replacing q by $(q-1)$ in Eq. 3.30 will result in the expression for the $\mathbf{R}^{-(q-1)}$ present in the numerator. To complete the analysis of the Rayleigh estimate structure, a complete expression for the numerator and a similar one for the denominator are needed. The expanded representation of $\mathbf{R}^{-q}$ is introduced in the denominator and considering the general noise matrix $\mathbf{Q}$, the result is:

$$\mathbf{s}^*\mathbf{R}^{-q}\mathbf{s} = \frac{1}{(\sigma_n^2)^q}\left\{\mathbf{s}^*\mathbf{Q}^{-1}\mathbf{s} - \frac{\mathbf{s}^*\mathbf{Q}^{-1}\mathbf{d}\mathbf{d}^*\mathbf{Q}^{-1}\mathbf{s}\beta_q}{1+\mathbf{d}^*\mathbf{Q}^{-1}\mathbf{d}\beta_q}\right\} \tag{3.33}$$

$$= \frac{\mathbf{s}^*\mathbf{Q}^{-1}\mathbf{s}}{(\sigma_n^2)^q}\left\{I - \frac{|\mathbf{s}^*\mathbf{Q}^{-1}\mathbf{d}|^2\beta_q}{(\mathbf{s}^*\mathbf{Q}^{-1}\mathbf{s})(1+\mathbf{d}^*\mathbf{Q}^{-1}\mathbf{d}\beta_q)}\right\} \tag{3.34}$$

When the noise environment is assumed white, (i.e. $\mathbf{Q} = \mathbf{I}$), the above expression is simplified as

$$\mathbf{s}^*\mathbf{R}^{-q}\mathbf{s} = \frac{M}{(\sigma_n^2)^q}\left\{I - \frac{|\mathbf{s}^*\mathbf{d}|^2\beta_q}{M(1+M\beta_q)}\right\} \tag{3.35}$$

It is useful to introduce in the previous expression the signal-to-noise ratio and the generalized angle in order to better understand their effect on the output spectrum of the Rayleigh family. The signal-to-noise ratio given in 3.11 can be rewritten as

$$\frac{\sigma_s^2}{\sigma_n^2} = \frac{S/N}{\mathbf{d}^*\mathbf{Q}^{-1}\mathbf{d}} \tag{3.36}$$

Similarly, β_q can be further factored and written as:

$$\beta_q = \frac{\sigma_s^2}{\sigma_n^2}\underbrace{\frac{\sum_{i=1}^{q}\binom{q}{i}M^i(\sigma_s^2)^{i-1}(\sigma_n^2)^{q-i}}{M(\sigma_n^2)^{q-1}}}_{\alpha_q} \tag{3.37}$$

$$= \frac{S/N}{\mathbf{d}^*\mathbf{Q}^{-1}\mathbf{d}}\underbrace{\frac{\sum_{i=1}^{q}\binom{q}{i}M^i(\sigma_s^2)^{i-1}(\sigma_n^2)^{q-i}}{M(\sigma_n^2)^{q-1}}}_{\alpha_q} \tag{3.38}$$

The second term on the right hand side will be designated by α_q for its dependency on the order q of the estimate. Introducing the above relation into expression 3.34

$$\mathbf{s}^*\mathbf{R}^{-q}\mathbf{s} = \frac{\mathbf{s}^*\mathbf{Q}^{-1}\mathbf{s}}{(\sigma_n^2)^q}\left\{I - \frac{|\mathbf{s}^*\mathbf{Q}^{-1}\mathbf{d}|^2}{\mathbf{s}^*\mathbf{Q}^{-1}\mathbf{s}}\frac{S/N}{\mathbf{d}^*\mathbf{Q}^{-1}\mathbf{d}}\frac{\alpha_q}{1+(S/N)\alpha_q}\right\} \tag{3.39}$$

q	α_q
1	1
2	$2+(S/N)$
3	$3+3(S/N)+(S/N)^2$
4	$4+6(S/N)+4(S/N)^2+(S/N)^3$

Table 3.1: Values of α_q for $q = 1$ to 4

With the generalized angle, equation 3.39 is rewritten as

$$\mathbf{s}^*\mathbf{R}^{-q}\mathbf{s} = \frac{\mathbf{s}^*\mathbf{Q}^{-1}\mathbf{s}}{(\sigma_n^2)^q}\left\{I - \frac{\cos^2(\mathbf{s},\mathbf{d};\mathbf{Q}^{-1})(S/N)\alpha_q}{1+(S/N)\alpha_q}\right\} \tag{3.40}$$

Following a simplification operation, the denominator of the Rayleigh estimate of order q is

$$\mathbf{s}^*\mathbf{R}^{-q}\mathbf{s} = \frac{\mathbf{s}^*\mathbf{Q}^{-1}\mathbf{s}}{(\sigma_n^2)^q}\left\{\frac{1+\sin^2(\mathbf{s},\mathbf{d};\mathbf{Q}^{-1})(S/N)\alpha_q}{1+(S/N)\alpha_q}\right\} \tag{3.41}$$

For the white noise case, we have

$$\mathbf{s}^*\mathbf{R}^{-q}\mathbf{s} = \frac{M}{(\sigma_n^2)^q}\left\{\frac{1+\sin^2(\mathbf{s},\mathbf{d};\mathbf{I})(S/N)\alpha_q}{1+(S/N)\alpha_q}\right\} \tag{3.42}$$

It will be useful to expand the term α_q for several values of q, to further simplify the different expressions of Rayleigh estimate. The results for $q = 1 \ldots 4$ are summarized in table 3.1. When q is set to 1 in 3.34, the result is equivalent to Eq. 21 presented by Cox [9]. When $q = 2$, it is equivalent to Eq. 23 in the same work. The numerator of the Rayleigh estimate is described by the same expression, with $(-q)$ replaced by $(-(q-1))$. The complete Rayleigh estimate expression is obtained by forming the ratio and is given as:

$$\frac{\mathbf{s}^*\mathbf{R}^{-(q-1)}\mathbf{s}}{\mathbf{s}^*\mathbf{R}^{-q}\mathbf{s}} = \sigma_n^2 \frac{\left\{\frac{1+\sin^2(\mathbf{s},\mathbf{d};\mathbf{I})(S/N)\alpha_{q-1}}{1+(S/N)\alpha_{q-1}}\right\}}{\left\{\frac{1+\sin^2(\mathbf{s},\mathbf{d};\mathbf{I})(S/N)\alpha_q}{1+(S/N)\alpha_q}\right\}} \tag{3.43}$$

In a typical beamforming application, the response of the system will depend on the steering vector $\mathbf{s}$ representing directions of hypothesized signal. Throughout the scanning process, the different directio: of interest will be used to steer the array and *look* in some specific directions. As the array is steered, one of the directions of interest will ideally coincide with a true location of a source. For that case, the array is said to be *matched* since the hypothesized steering vector is equal to the true direction vector. Steering off the main point, mismatch in the array response will result and the array is said to be *not-matched* to the true direction vector. This behavior can be summarized as follow:

- *matched case*: $\mathbf{s} = \mathbf{d}$, this implies that $\sin^2(\mathbf{s}, \mathbf{d}; \mathbf{I}) = 0$ or $\cos^2(\mathbf{s}, \mathbf{d}; \mathbf{I}) = 1$
- *not matched case*: $\mathbf{s} \neq \mathbf{d}$, the effect of $\sin^2(\mathbf{s}, \mathbf{d}; \mathbf{I})$ must be considered

3.3.2 Matched Case Response

In this section, the output spectrum level of the array, when the hypothesized steering vector is perfectly aligned with the true direction vector will be analyzed. A closed form expression for the BT, MV, NMLM and the Rayleigh estimate of order q will also be derived.

Blackman–Tukey

For the Blackman–Tukey estimator, the output characteristic under perfect conditions will first be investigated. When the array is said to be matched (i.e. the hypothesized and the actual direction vector are aligned), the two vectors $\mathbf{s}$ and $\mathbf{d}$ are equal and their product $\mathbf{s}^*\mathbf{d}$ and $\mathbf{d}^*\mathbf{s}$ is equal to M. Using these properties and introducing the expanded form of the correlation matrix from Eq. 3.5 in the Blackman–Tukey estimator results in the following match case response:

$$\mathcal{Z}_{BT} = \frac{1}{M}\mathbf{s}^*\mathbf{R}\mathbf{s} = \sigma_n^2 + M\sigma_s^2 \tag{3.44}$$

Minimum Variance

The generalized angle will be used in the Minimum Variance estimator matched case response analysis. Under ideal conditions, the angle between the hypothesized and true direction vector is equal to 0 resulting in $\sin^2(\mathbf{s}, \mathbf{d}; \mathbf{I}) = 0$. The output spectrum of the estimator is written as

$$\mathcal{Z}_{MV} = \frac{M}{\mathbf{s}^*\mathbf{R}^{-1}\mathbf{s}} = \frac{M}{\frac{M}{\sigma_n^2}\left\{\frac{1}{1+(S/N)\alpha_q}\right\}} \tag{3.45}$$

Substituting α_q, when $q = 1$, by its equivalent expression from table 3.1 and further simplifying results in the following for the matched case response

$$\mathcal{Z}_{MV} = \sigma_n^2 + M\sigma_s^2 \tag{3.46}$$

Normalized Maximum Likelihood

Applying the same procedure used in the Minimum Variance estimate, to the Normalized Maximum Likelihood method, we have

$$\text{NMLM} = \frac{\mathbf{s}^*\mathbf{R}^{-1}\mathbf{s}}{\mathbf{s}^*\mathbf{R}^{-2}\mathbf{s}} = \frac{M/(\sigma_n^2 + M\sigma_s^2)}{M/(\sigma_n^2 + M\sigma_s^2)^2} \tag{3.47}$$

After further simplifications, the output spectrum in the matched case is expressed as

$$\mathcal{Z}_{NMLM} = \sigma_n^2 + M\sigma_s^2 \tag{3.48}$$

It can be seen from expression 3.44, 3.46 and 3.48, that the output level, when **s** is perfectly aligned with **d**, is maintained at a constant value as a function of $q = 0$, 1 and 2. This value is also a function of the power of the input signal and noise components and of the number of elements in the array.

Rayleigh Estimate of Order q

For the Rayleigh estimate of order q, where $q > 2$, we can derive an expression for the numerator, an expression for the denominator, then form the ratio. In the matched case, with $\sin^2(\mathbf{s}, \mathbf{d}; \mathbf{I}) = 0$, the denominator is expressed as

$$\mathbf{s}^*\mathbf{R}^{-q}\mathbf{s} = \frac{M}{(\sigma_n^2)^q}\left\{\frac{1}{1 + (S/N)\alpha_q}\right\} \tag{3.49}$$

Replacing α_q by 3.31, (S/N) by $M\frac{\sigma_s^2}{\sigma_n^2}$ and following a first simplification step results in

$$\frac{M}{(\sigma_n^2)^q + \sigma_s^2 \sum_{i=1}^{q} \binom{q}{i} M^i (\sigma_s^2)^{i-1} (\sigma_n^2)^{q-i}} \tag{3.50}$$

After some algebraic manipulations and grouping of the various elements, the denominator of the Rayleigh estimate under matched case response is

$$\frac{M}{(\sigma_n^2 + M\sigma_s^2)^q} \tag{3.51}$$

Substituting q with $q-1$ results in the expression of the numerator of the Rayleigh estimate.

$$\frac{M}{(\sigma_n^2 + M\sigma_s^2)^{q-1}} \tag{3.52}$$

Forming the ratio of 3.51 and 3.52 and simplifying, the resulting expression represents the output spectrum for the Rayleigh estimate of order q written as follows:

$$\mathcal{Z}_q = \sigma_n^2 + M\sigma_s^2 \tag{3.53}$$

An equivalent form, using the definition of the signal to noise ratio, is

$$\mathcal{Z}_q = \sigma_n^2\{1 + (S/N)\} \tag{3.54}$$

We can conclude that in the matched case, when the look direction coincides with a true source location, for the BT, MV, NMLM and Rayleigh estimate of order q, the output is always maintained at a constant value. Any higher order estimate will not result in an improved maximum signal-to-noise level or a higher output level. For the matched case considered, the maximum signal-to-noise ratio is achieved using any member of the Rayleigh family and when the noise field is gaussian, the various estimators are equivalent. The Capon method can therefore be considered as the optimum estimator.

3.3.3 Not–Matched Case Response

When the array system is steered *off target*, the $\sin^2(\mathbf{s}, \mathbf{d}; \mathbf{I})$ element is no longer equal to zero and must be taken into account. The behavior of the output for different values of angles is also of interest. The response to a mismatch will be studied for the MV, NMLM and Rayleigh estimate of order q. By taking the reciprocal of expression 3.18, the following represents the output spectrum of the Minimum Variance estimator, in the white noise case:

$$\frac{1}{\mathbf{s}^*\mathbf{R}^{-1}\mathbf{s}} = \frac{(\sigma_n^2/M)\{1 + (S/N)\}}{1 + (S/N)\sin^2(\mathbf{s}, \mathbf{d}; \mathbf{I})} \tag{3.55}$$

A similar expression for the Normalized Maximum Likelihood Method or Rayleigh estimate of order 2 can be derived by substituting 3.18 in the numerator and 3.20 in the denominator. After further simplifications and considering the white noise case results in:

$$\frac{\mathbf{s}^*\mathbf{R}^{-1}\mathbf{s}}{\mathbf{s}^*\mathbf{R}^{-2}\mathbf{s}} = \sigma_n^2 \frac{\left\{\frac{1+\sin^2(\mathbf{s},\mathbf{d};\mathbf{I})(S/N)}{1+(S/N)}\right\}}{\left\{\frac{1+\sin^2(\mathbf{s},\mathbf{d};\mathbf{I})(S/N)\{2+(S/N)\}}{1+2(S/N)+(S/N)^2}\right\}} \tag{3.56}$$

For the Rayleigh estimate of order q, the general expression of the output spectrum given by 3.43 and reproduced below for convenience will be used.

$$\frac{\mathbf{s}^*\mathbf{R}^{-(q-1)}\mathbf{s}}{\mathbf{s}^*\mathbf{R}^{-q}\mathbf{s}} = \frac{1}{\sigma_n^2} \frac{\left\{\frac{1+\sin^2(\mathbf{s},\mathbf{d};\mathbf{I})(S/N)\alpha_{q-1}}{1+(S/N)\alpha_{q-1}}\right\}}{\left\{\frac{1+\sin^2(\mathbf{s},\mathbf{d};\mathbf{I})(S/N)\alpha_q}{1+(S/N)\alpha_q}\right\}}$$

It is important to note at this point that using the above expression and setting $q = 1$ will result in the Minimum Variance output spectrum expression; equivalent to Eq. 32 by

Cox [9]. The response of the array will reach a maximum value equal to $\sigma_n^2 + M\sigma_s^2$ when the array is perfectly matched and decrease to σ_n^2 when the hypothesized steering vector is orthogonal to the true one. This behavior can be summarized as follows

$$\sigma_n^2 \leq Z_q \leq \sigma_n^2\{1 + (S/N)\} \tag{3.57}$$

3.3.4 Results

To visualize the behavior of Rayleigh estimates graphically, a simulation scenario was set up. The field consisted of a single source introduced at 110.4884° with background white noise and a signal-to-noise ratio of 0dB (i.e. $\sigma_s^2/\sigma_n^2 = 1$). A horizontal array of 8 sensors was combined with Rayleigh estimates of order 1 to 5. Initially, the correlation matrix for the given target, operating frequency and number of sensors in the array for the infinite observation interval case was formed. Under normal conditions, the true correlation matrix is not available and an estimated version must be computed instead, from the available input data. In the following two experiments, the observation interval is assumed to be of infinite length. The true correlation matrix, once formed, will be inserted in the Rayleigh estimate expression. Later in this work, the effect of using a shorter observation interval on the performance of the Rayleigh estimate will be considered. The array was steered from 90° to 135° and the results are presented in Fig. 3.1. This plot represents the output power spectrum versus the sin of the bearing angle for Rayleigh estimates of order 1 to 5. The following observations can be made from Fig. 3.1:

- As predicted in the previous section, any estimate is always a bound for the next higher order one.
- The peak indicating the presence of a source is located at the exact source bearing of 110.4884°
- The maximum output level when the hypothesized steering vector is matched to the true one is equal to its predicted level of

$$(1 + M\frac{\sigma_s^2}{\sigma_n^2}) = (1 + 8 \times 1) = 9$$

The effect of an increase in the number of sensors in the array from 8 to 16 will be considered next. The experiment was repeated with 16 sensors and the results are presented in Fig. 3.2.

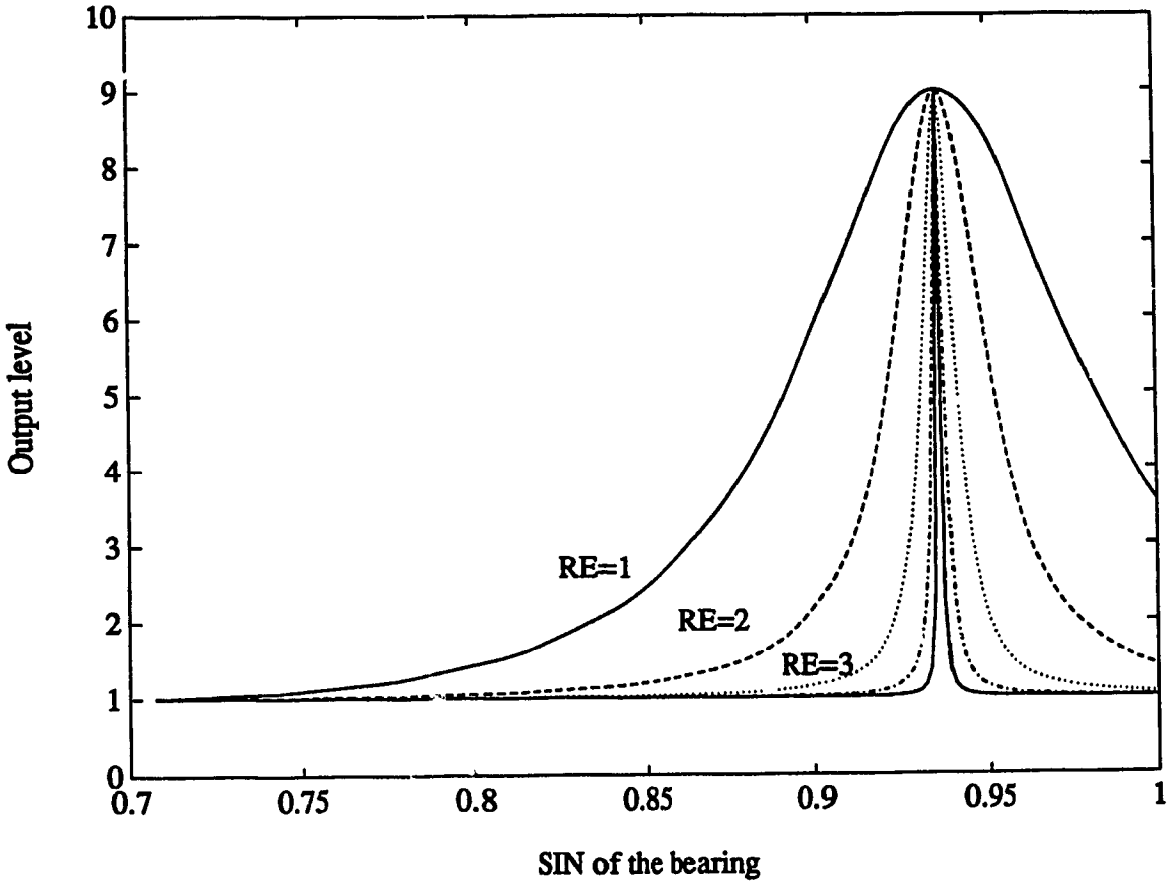

Figure 3.1: Rayleigh estimate $q = 1$ to 5, infinite observ. int. M=8

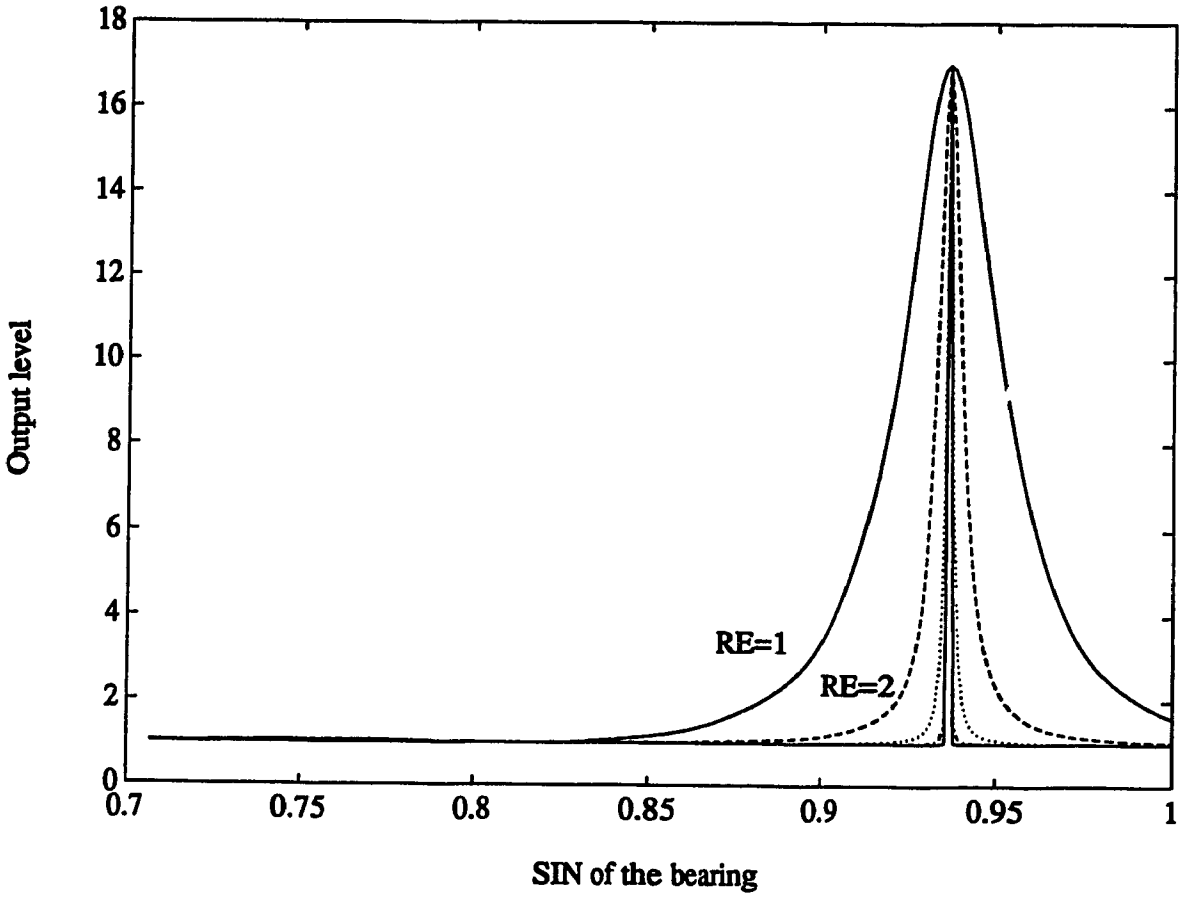

Figure 3.2: Rayleigh estimate $q = 1$ to 5, infinite observ. int. M=16

The previously mentioned observations hold for these results, with the maximum output level now equal to $(1 + 16 \times 1) = 17$. Increasing the number of sensors to 16 resulted in sharper peaks, as seen in Fig. 3.2 by the narrower peaks. This result was predicted in the introduction of Chap. 2 where an increase in the resolution of the estimator, measured by the narrower peaks, can be achieved by increasing the number of elements in the array. It is possible to conclude that the number of sensors plays an important role in the *resolution* of the estimator. This will also be demonstrated in a subsequent section. The background level of 1, evident in both figures is due to the gaussian noise field. When the hypothesized steering vector is orthogonal to the true steering vector, the generalized angle between them being 90° will result in

$$\sin^2(\mathbf{s}, \mathbf{d}; \mathbf{I}) = 1$$

Introducing this condition in Eq. 3.43 and simplifying, the resulting expression is equal to σ_n^2. The minimum output level of a Rayleigh estimate of order q is therefore equal to the noise power σ_n^2.

3.4 Bandwidth Analysis

To study and compare the performance of different spectral estimation methods, a common criterion must be selected. The resolution, statistical stability and robustness are examples of such criteria. There exists no uniquely agreed upon measure for the resolution of a given spectral estimator. Different definitions were proposed by several authors, each with their own arguments to support them. For example, the resolution can be the ability of a spectral estimator to reveal the presence of two equal energy sources which have nearly equal bearing [18]. In this case, the sources are said to be resolved and two peaks, each representing a source will appear on the spectral plot. Better resolved bearings correspond to narrower spectral peaks. As the peak sharpness increases, it is an indication that the bearings are better resolved. In the present work, the case of a single source is considered. The measure of resolution proposed by Lacoss is used [22]. It is defined as the width of the main peak at the -3dB point. This point corresponds to the level where the output power is at half its maximum value. In this section, the resolution as defined by the peak-width or beam-width for the estimator of order q will be analyzed and a closed form expression will be derived.

Let ϕ_v denote the point where the output spectrum is at its maximum level (i.e. when the hypothesized steering vector is matched to the true direction vector) and ϕ_3 will correspond to the -3dB point, we can then write

$$\mathcal{Z}_{\phi_3} = \frac{1}{2}\mathcal{Z}_{\phi_v} \tag{3.58}$$

Before proceeding with the derivation of the closed form expression representing the width of the main peak of the Rayleigh estimate of order q, some preliminary definitions are necessary. Using the fact that the product of $\mathbf{s}^*\mathbf{s}$ and $\mathbf{d}^*\mathbf{d}$ are both normalized to be equal to M, the number of sensors in the array, it is convenient to introduce the following definition by Lacoss, used throughout the bandwidth analysis[22]

$$B_M(\phi) = \frac{1}{M}\sum_{k=0}^{M-1} e^{\jmath\phi k} \tag{3.59}$$

Consequently,

$$|\mathbf{s}^*\mathbf{d}|^2 = M^2|B_M(\phi_v - \phi)|^2 \tag{3.60}$$

Using the previously derived expression of $\mathbf{s}^*\mathbf{R}^{-q}\mathbf{s}$, given by 3.34 and reproduced below

$$\mathbf{s}^*\mathbf{R}^{-q}\mathbf{s} = \frac{1}{(\sigma_n^2)^q}\left\{M - \frac{|\mathbf{s}^*\mathbf{d}|^2\alpha_q}{1+M\alpha_q}\right\} \tag{3.61}$$

$|\mathbf{s}^*\mathbf{d}|^2$, in the above equation, can be replaced by 3.60, resulting in:

$$\mathbf{s}^*\mathbf{R}^{-q}\mathbf{s} = \frac{1}{(\sigma_n^2)^q}\left\{M - \frac{M^2|B_M(\phi_v - \phi)|^2\alpha_q}{1+M\alpha_q}\right\} \tag{3.62}$$

$$= \frac{M}{(\sigma_n^2)^q}\left\{1 - \frac{M|B_M(\phi_v - \phi)|^2\alpha_q}{1+M\alpha_q}\right\} \tag{3.63}$$

By examining the denominator of the previous equation and comparing it with 3.31, the expression of α_q, the common M term is simplified and a new entity α'_q is defined as;

$$\alpha'_q = \frac{\sum_{i=1}^{q}\binom{q}{i}(M\sigma_s^2)^i(\sigma_n^2)^{q-i}}{(\sigma_n^2)^q} \tag{3.64}$$

A similar mathematical identity is used to rewrite α'_q as a function of the signal-to-noise ratio in the following way,

$$\alpha'_q = \sum_{i=1}^{q}\binom{q}{i}(S/N)^i \tag{3.65}$$

Furthermore, $(1+\alpha'_q)$ can be written as:

$$1+\alpha'_q = 1+\sum_{i=1}^{q}\binom{q}{i}(S/N)^i \tag{3.66}$$

$$= (1+S/N)^q \tag{3.67}$$

Introducing 3.65 and 3.67, the two previously defined identities, in 3.63, and repeating the same procedure for the numerator of the Rayleigh estimate yields the following complete expression

$$\mathcal{Z}_\phi = \sigma_n^2 \frac{\left\{1-\frac{\alpha'_{q-1}|B_M(\phi_v-\phi)|^2}{(1+S/N)^{q-1}}\right\}}{\left\{1-\frac{\alpha'_q|B_M(\phi_v-\phi)|^2}{(1+S/N)^q}\right\}} \tag{3.68}$$

When $\phi=\phi_v$, the point where the output level reaches it maximum value, the expression of $|B_M(\phi_v-\phi)|^2$ is then equal to 1. Similarly, when the array system is perfectly matched (i.e. $\mathbf{s}=\mathbf{d}$) and 3.54 is used to represent the maximum output level, Eq. 3.68 can then be equated to half this maximum value, resulting in:

$$\sigma_n^2 \frac{\left\{1-\frac{\alpha'_{q-1}|B_M(\phi_3)|^2}{(1+S/N)^{q-1}}\right\}}{\left\{1-\frac{\alpha'_q|B_M(\phi_3)|^2}{(1+S/N)^q}\right\}} = \frac{1}{2}\left\{\sigma_n^2(1+S/N)\right\} \tag{3.69}$$

With some algebraic manipulations, the above expression is rewritten as follow

$$\frac{(1+S/N)^{q-1}-\alpha'_{q-1}|B_M(\phi_3)|^2}{(1+S/N)^q-\alpha'_q|B_M(\phi_3)|^2} = \frac{1}{2} \tag{3.70}$$

$$(1+S/N)^{q-1}-\alpha'_{q-1}|B_M(\phi_3)|^2 = \frac{1}{2}(1+S/N)^q - \frac{1}{2}\alpha'_q|B_M(\phi_3)|^2 \tag{3.71}$$

$$(1+S/N)^{q-1}-\frac{1}{2}(1+S/N)^q = \alpha'_{q-1}|B_M(\phi_3)|^2 - \frac{1}{2}\alpha'_q|B_M(\phi_3)|^2 \tag{3.72}$$

The term $|B_M(\phi_3)|^2$ being a function of the element of interest, is isolated as follows

$$|B_M(\phi_3)|^2 = \frac{2(1+S/N)^{q-1}-(1+S/N)^q}{2\alpha'_{q-1}-\alpha'_q} \tag{3.73}$$

From the definition of α'_q given in 3.64, we can rewrite

$$(1+S/N)^q = 1+\alpha'_q \tag{3.74}$$

and similarly

$$(1+S/N)^{q-1} = 1+\alpha'_{q-1} \tag{3.75}$$

Substituting the above two new identities in 3.73, results in

$$|B_M(\phi_3)|^2 = \frac{2(1+\alpha'_{q-1}) - (1+\alpha'_q)}{2\alpha'_{q-1} - \alpha'_q} \tag{3.76}$$

An approximate solution for the -3dB point is obtained using a first order Taylor series expansion of $|B_M(\phi_3)|^2$. The truncated expression is

$$\begin{aligned} |B_M(\phi_3)|^2 &= B_M(\phi_3)B^*_M(\phi_3) && (3.77) \\ &= \simeq 1 - \frac{\phi_3^2(M^2-1)}{12} && (3.78) \end{aligned}$$

Combining this result with 3.76 and isolating ϕ_3, we have

$$\phi_3 = \sqrt{\frac{-12}{(M^2-1)(2\alpha'_{q-1} - \alpha'_q)}} \tag{3.79}$$

Assuming that $M^2 - 1 \gg 1$ will permit us to factor the M term from the denominator and simplify the expression, the result is

$$\phi_3 = \frac{2}{M}\sqrt{\frac{3}{\alpha'_q - 2\alpha'_{q-1}}} \tag{3.80}$$

where α'_q and α'_{q-1} can be replaced by 3.74 and 3.75 respectively. The final expression representing the bandwidth of the Rayleigh estimate of order q is

$$\phi_3 = \frac{2}{M}\sqrt{\frac{3}{(1+S/N)^q - 2(1+S/N)^{q-1} + 1}} \tag{3.81}$$

It is evident that the *resolution* of the Rayleigh family of spectral estimates is dependent on the number of elements in the array and the signal-to-noise ratio. As the number of sensors increases, ϕ_3 decreases and the width of the main peak decreases, signifying a resolution increase. Similarly, as the order of the estimate increases, the width of the main peak will also decrease. A sharper peak is considered in the present context as an indication of a increase in resolution. The relationship between the order of the estimate and the signal-to-noise ratio is illustrated in Fig. 3.3.

To verify the validity of the approximate solution, an experiment was set up. The environment comprised of a single source introduced at 110.4884°, the array was steered from 90° to 135° and the MV, NMLM and Rayleigh estimate of order 3 and 4 were used. Initially, the output spectrum response of the 4 estimators for the infinite time case, illustrated in Fig. 3.4, was calculated. The exact values of the main peak width were obtained.

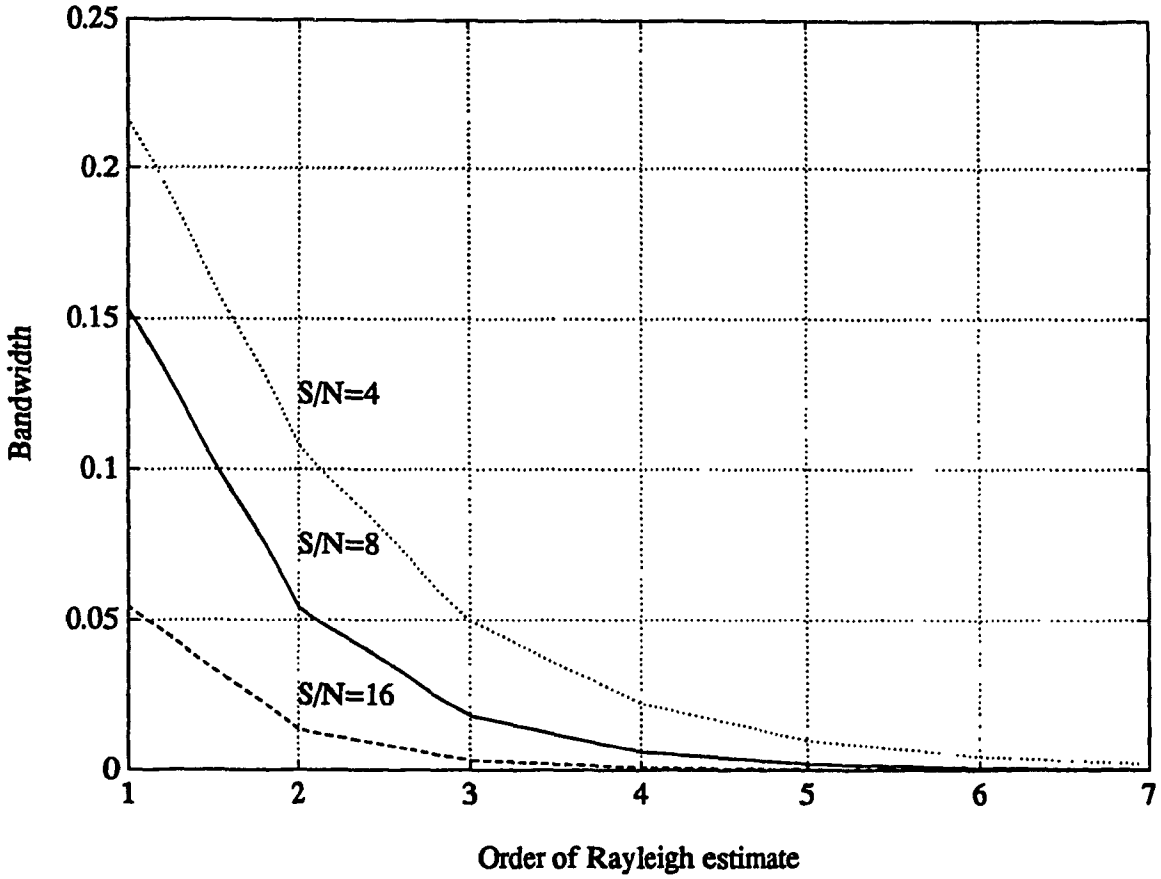

Figure 3.3: Bandwidth of Rayleigh estimates $q = 1$ to 4

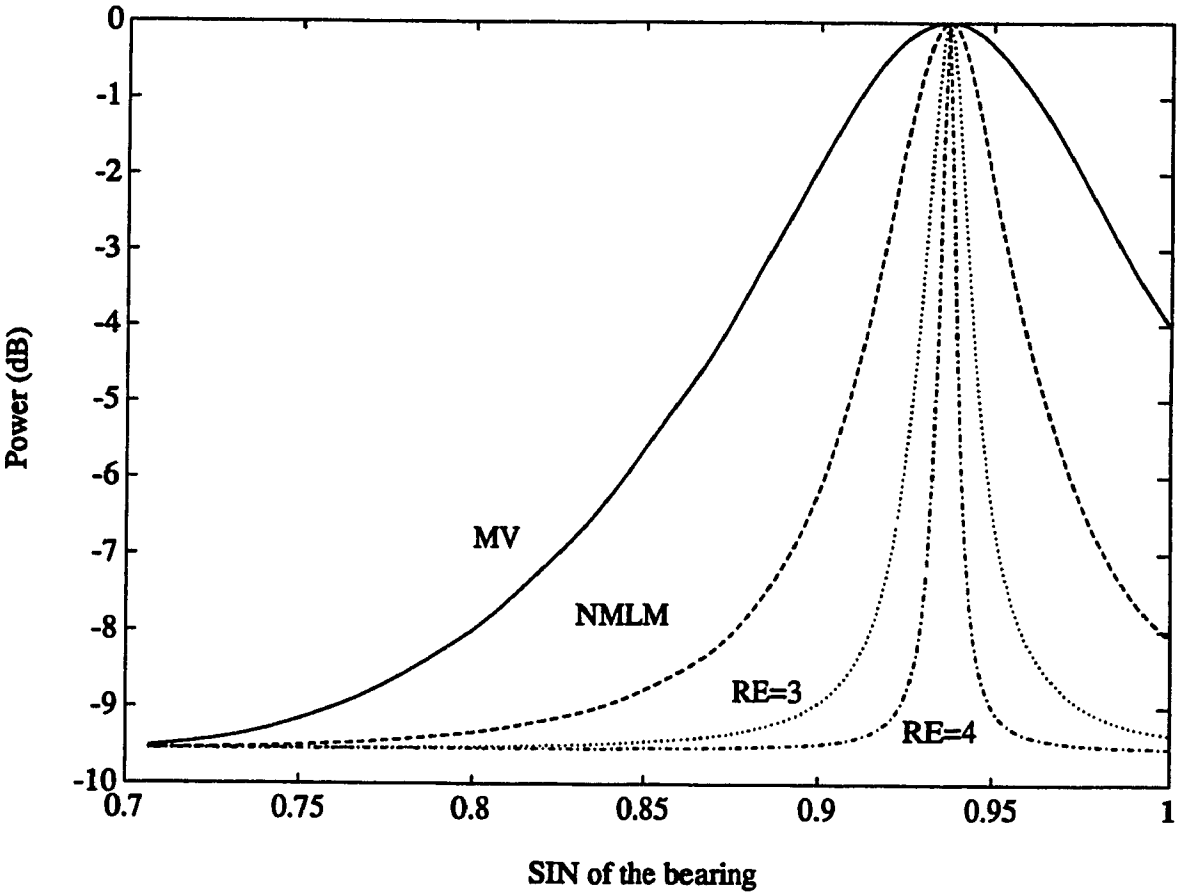

Figure 3.4: Beam plot of Rayleigh estimates $q = 1$ to 4

Estimator	S/N=8		S/N=4	
	Exact	Approx.	Exact	Approx.
Minimum Variance	0.1031	0.0975	0.1492	0.1378
Normalized MLM	0.0362	0.0344	0.0708	0.0689
Rayleigh $q = 3$	0.0115	0.0116	0.0323	0.0316
Rayleigh $q = 4$	0.0038	0.0039	0.0146	0.0142

Table 3.2: Exact versus approximate values for RE of order 1 to 4

These values were then compared to those obtained by directly applying equation 3.81 to the same scenario. It is important to point out that a conversion between spatial frequency and $\sin(\phi)$ was required, the resulting values from the approximate expression must be multiplied by a factor of $2/\pi$.

The experiment was repeated a second time with a different signal-to-noise ratio and the results are given in the table 3.2. It is clear that the exact values and those obtained from the approximate solution are very close. Any discrepancy can be attributed to the first order Taylor series expansion. When $q = 1$, the Minimum Variance estimator, 3.81 yields the same results as those derived by Lacoss in [22], thus confirming the validity of the approximate solution expression. As will be shown later, the increase in resolution observed in the various results is achieved at the expense of the statistical stability of the Rayleigh estimate. Th reduction in size of the observation interval will affect the response of a given estimator and in turn affect it's reponse and width of the main peak.

3.5 Sensitivity Analysis

In a typical array signal processing operation, the measured array output is fitted to a predicted model. Any error in the predicted model will result in a degradation in the output. These errors can originate from incomplete knowledge about the ocean model, sensor position error or other factors. The effect of the mismatch resulting from the use of a hypothesized version of the true steering vector on the estimator response represents the main element of interest in the present analysis. This mismatch will affect the output power level. By investigating the effect of various angular separations between the hypothesized steering vector and the true one, through the use of the generalized angle expression, the sensitivity of the estimator can be calculated.

As seen in the previous section, the correlation matrix $\mathbf{R}$ plays an important role in the Rayleigh Estimate. In most applications, an estimated version of the matrix $\mathbf{R}$ is formed from a finite–length sample of time and then used in the source detection and localization process. Since the true correlation matrix is not available, the goodness of the estimated version of $\mathbf{R}$ will affect the detection performance of the system. To concentrate only on the sensitivity criterion of the Rayleigh estimate, the true correlation matrix, rather than the estimated version, will be used in the following analysis.

The power ratio introduced by Gingras [12] has been used to qualify the sensitivity to mismatch of the Rayleigh family of spectrum estimate. It is expressed as the ratio of the output spectrum resulting from imprecise information to that obtained using the exact model and is given by

$$\rho = \frac{\mathcal{Z}_{\mathbf{s}\neq\mathbf{d}}}{\mathcal{Z}_{\mathbf{s}=\mathbf{d}}} = \frac{\mathcal{Z}(\text{not matched})}{\mathcal{Z}(\text{matched})} \tag{3.82}$$

When there is no mismatch, $\mathbf{s} = \mathbf{d}$ and consequently $\rho = 1$. Given the output spectrum expression of a Rayleigh estimate of order q, the effect of mismatch on the output will be examined under white (uncorrelated) noise. Setting the matrix $\mathbf{Q} = \mathbf{I}$, will allow us to work with simpler expressions. Under these conditions, the correlation matrix is given by

$$\mathbf{R} = \sigma_n^2\mathbf{I} + \sigma_s^2\mathbf{d}\mathbf{d}^*$$

The power ratio for the Blackman–Tukey, Minimum Variance and Normalized Maximum Likelihood estimators will first be derived. These results will then be used to extend the power ratio to the Rayleigh family. A closed form expression describing the sensitivity of an estimator of arbitrary order q for various values of mismatch will be derived. This expression will be used to graphically visualize and compare the power ratio of different estimators. This will be followed by a discussion on the significance of the power ratio. For comparison purposes, a common reference will be maintained with Gingras's work. In this section the product of $\mathbf{s}^*\mathbf{s}$ and $\mathbf{d}^*\mathbf{d}$ are normalized to 1 rather than M as used so far throughout this work.

3.5.1 Sensitivity of the BT

For the Blackman–Tukey expressed as

$$\mathcal{Z}_{BT} = \mathbf{s}^*\mathbf{R}\mathbf{s} \tag{3.83}$$

and from [9], we can derive the matched and not-matched case response to form the power ratio. Expanding the Blackman–Tukey to account for the different terms in the correlation matrix results in:

$$\mathcal{Z}_{BT} = \sigma_n^2 M + \sigma_s^2 |\mathbf{s}^* \mathbf{d}|^2 \qquad \text{for } \mathbf{s} \neq \mathbf{d} \tag{3.84}$$

This expression also corresponds to the not-matched case response of the estimator. For the matched case, $|\mathbf{s}^* \mathbf{d}|^2$ can be replaced by its equivalent $\cos^2(\mathbf{s}, \mathbf{d}; \mathbf{I})$ term and in turn, this term is set to 1 when $\mathbf{s} = \mathbf{d}$, yielding the following:

$$\mathcal{Z}_{BT} = \sigma_n^2 M + \sigma_s^2 \qquad \text{for } \mathbf{s} = \mathbf{d} \tag{3.85}$$

Forming the ratio ρ with 3.84 and 3.85, we obtain

$$\rho = \frac{\sigma_n^2 M + \sigma_s^2 |\mathbf{s}^* \mathbf{d}|^2}{\sigma_n^2 M + \sigma_s^2} \tag{3.86}$$

Comparison of the results derived in this work with those by Gingras [12], for the Blackman–Tukey case, is inorder. The S/N expression given by 3.12 is used to group the terms such that

$$\rho = 1 - \frac{S/N}{1 + S/N} \left\{ 1 - |\mathbf{s}^* \mathbf{d}|^2 \right\} \tag{3.87}$$

The above result corresponds to Eq. 20 presented by Gingras [12].

3.5.2 Sensitivity of the MV

From the analysis of the properties of the Minimum Variance estimator, and using expression 3.46 and 3.55, reproduced below, to represent the matched and not matched case response respectively

$$\mathcal{Z}_{MV} = \sigma_n^2 + M\sigma_s^2 \qquad \text{for } \mathbf{s} = \mathbf{d}$$

$$\mathcal{Z}_{MV} = \frac{(\sigma_n^2/M)\{1 + (S/N)\}}{1 + (S/N)\sin^2(\mathbf{s}, \mathbf{d}; \mathbf{I})} \qquad \text{for } \mathbf{s} \neq \mathbf{d}$$

we can form the power ratio ρ. The result after simplification is:

$$\rho_{MV} = \frac{1/M}{1 + (S/N)\sin^2(\mathbf{s}, \mathbf{d}; \mathbf{I})} \tag{3.88}$$

Substituting $\sin^2(\mathbf{s}, \mathbf{d}; \mathbf{I})$ by $1 - |\mathbf{s}^* \mathbf{d}|^2$ results in

$$\rho_{MV} = \left\{ 1 + \frac{\sigma_s^2}{\sigma_n^2} \left[1 - |\mathbf{s}^* \mathbf{d}|^2 \right] \right\}^{-1} \tag{3.89}$$

This corresponds to Eq. 21 presented by Gingras in the same work.

3.5.3 Sensitivity of the NMLM

The same method is repeated for the Normalized Maximum Likelihood estimator. It was shown in an earlier section that the output spectrum in the matched case is always constant and is therefore equal to

$$\mathcal{Z}_{NMLM} = \sigma_n^2 + M\sigma_s^2 \qquad \text{for } \mathbf{s} = \mathbf{d}$$

for the not-matched case, we have from 3.56

$$\mathcal{Z}_{NMLM} = \sigma_n^2 \frac{\left\{\frac{1+\sin^2(\mathbf{s},\mathbf{d};\mathbf{I})(S/N)}{1+(S/N)}\right\}}{\left\{\frac{1+\sin^2(\mathbf{s},\mathbf{d};\mathbf{I})(S/N)(2+(S/N))}{1+2(S/N)+(S/N)^2}\right\}} \qquad \text{for } \mathbf{s} \neq \mathbf{d}$$

Similarly, forming the power ratio and further simplifying results in:

$$\rho = \frac{1+(S/N)(1-|\mathbf{s}^*\mathbf{d}|^2)}{1+\left\{2(S/N)+(S/N)^2\right\}(1-|\mathbf{s}^*\mathbf{d}|^2)} \tag{3.90}$$

3.5.4 Sensitivity of the Rayleigh Family

We have now obtained expressions for the sensitivity to mismatch of the BT, MV and NMLM spectral estimators, in the white noise case. Generalizing the power ratio ρ on the Rayleigh family of spectral estimates will help predict the sensitivity of any estimator of order q. The power ratio expression for the Rayleigh estimate of order 3, will first be derived to visualize any emerging pattern. With $q = 3$, we have

$$\rho = \frac{1+(S/N)\left\{1-|\mathbf{s}^*\mathbf{d}|^2\right\}\{2+S/N\}}{1+(S/N)\left\{1-|\mathbf{s}^*\mathbf{d}|^2\right\}(3+3(S/N)+(S/N)^2)} \tag{3.91}$$

From this expression, and by examining table 3.1, we can notice the occurrence of the expanded version of α_{q-1} and α_q on the right hand side of both the numerator and denominator. This element is included in the final expression of the power ratio. The sensitivity of the Rayleigh estimate of order q is

$$\rho = \frac{1+(S/N)\left\{1-|\mathbf{s}^*\mathbf{d}|^2\right\}\alpha_{q-1}}{1+(S/N)\left\{1-|\mathbf{s}^*\mathbf{d}|^2\right\}\alpha_q} \tag{3.92}$$

3.5.5 Sensitivity Results

The above derived expression is used to graphically visualize the effect of a mismatch on the output spectrum level. The generalized angle expression is simplified as

$$\cos^2(\mathbf{s},\mathbf{d};\mathbf{I}) = \frac{|\mathbf{s}^*\mathbf{I}\mathbf{d}|^2}{\{(\mathbf{s}^*\mathbf{I}\mathbf{s})(\mathbf{d}^*\mathbf{I}\mathbf{d})\}} \tag{3.93}$$

$$= |\mathbf{s}^*\mathbf{d}|^2 \tag{3.94}$$

The effect of a mismatch expressed by an angular difference between the hypothesized steering vector and the true one, on the spectrum response of different order of Rayleigh estimates will be presented. The sensitivity of the estimator is indicated by the change in the peak level at the true location when a mismatch is introduced. Since $|\mathbf{s}^*\mathbf{d}|^2$ is equivalent to the angular mismatch expressed by $\cos^2(\mathbf{s},\mathbf{d};\mathbf{I})$, it is bounded between 0 and 1 such as

$$0 \leq |\mathbf{s}^*\mathbf{d}|^2 \leq 1$$

When the hypothesized steering vector is orthogonal to the true direction vector, their product is equal to 0 ($\cos 90° = 0$), the power ratio expression given in 3.92 is simplified as:

$$\rho = \frac{1+(S/N)\alpha_{q-1}}{1+(S/N)\alpha_q} \tag{3.95}$$

Since

$$1+(S/N)\alpha_{q-1} = (1+S/N)^{q-1} \tag{3.96}$$

$$1+(S/N)\alpha_q = (1+S/N)^q \tag{3.97}$$

Introducing these two properties in the power ratio expression and simplifying results in a lower bound on the sensitivity to mismatch equal to

$$\frac{1}{1+S/N} \tag{3.98}$$

Under no mismatch, both vectors are perfectly aligned and the power ratio is equal to 1. It then follows for the white noise case that the power ratio is bounded such that

$$\frac{1}{1+S/N} \leq \rho \leq 1 \tag{3.99}$$

As mismatch is introduced, the order of the Rayleigh estimate plays an important role in its sensitivity. Fig. 3.5 illustrates the power ratio measure of sensitivity of Rayleigh estimates

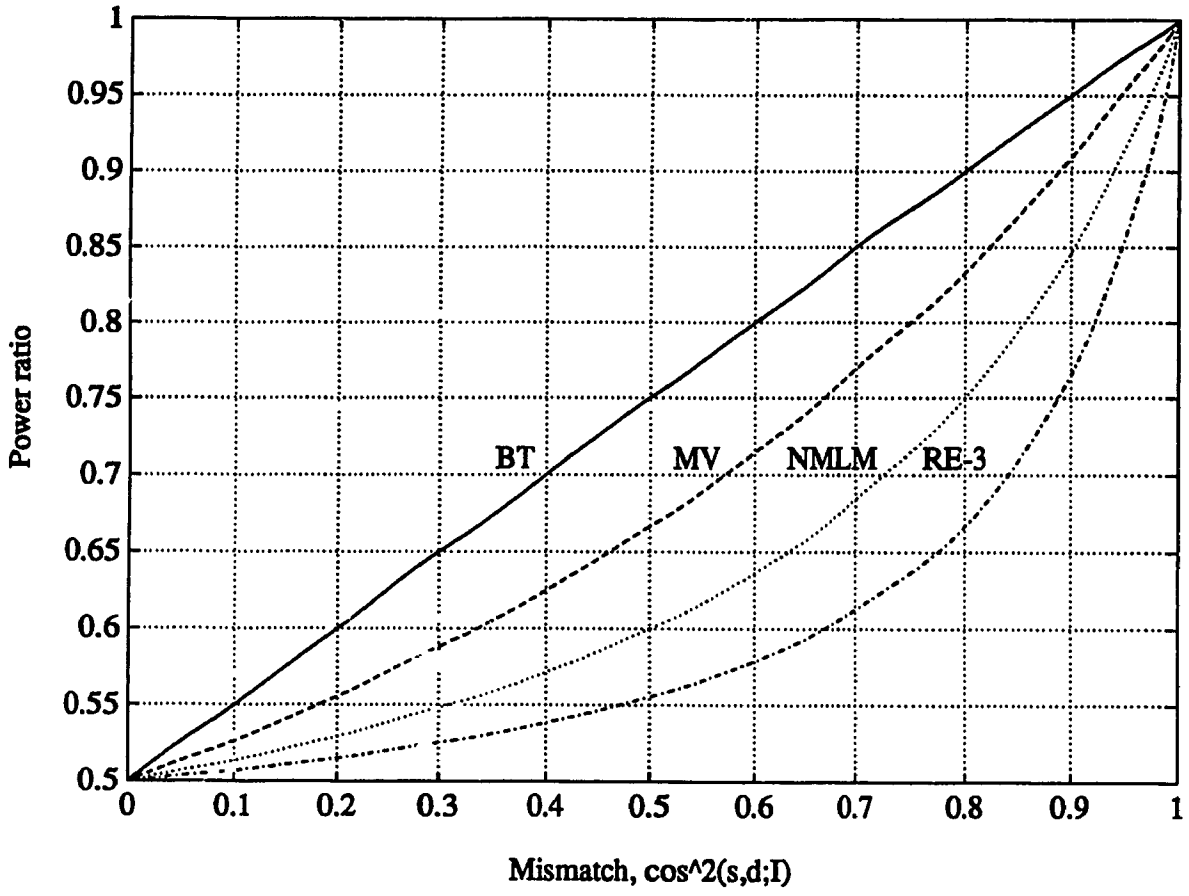

Figure 3.5: Sensitivity of the Rayleigh estimates $q = 1$ to 4, S/N=1

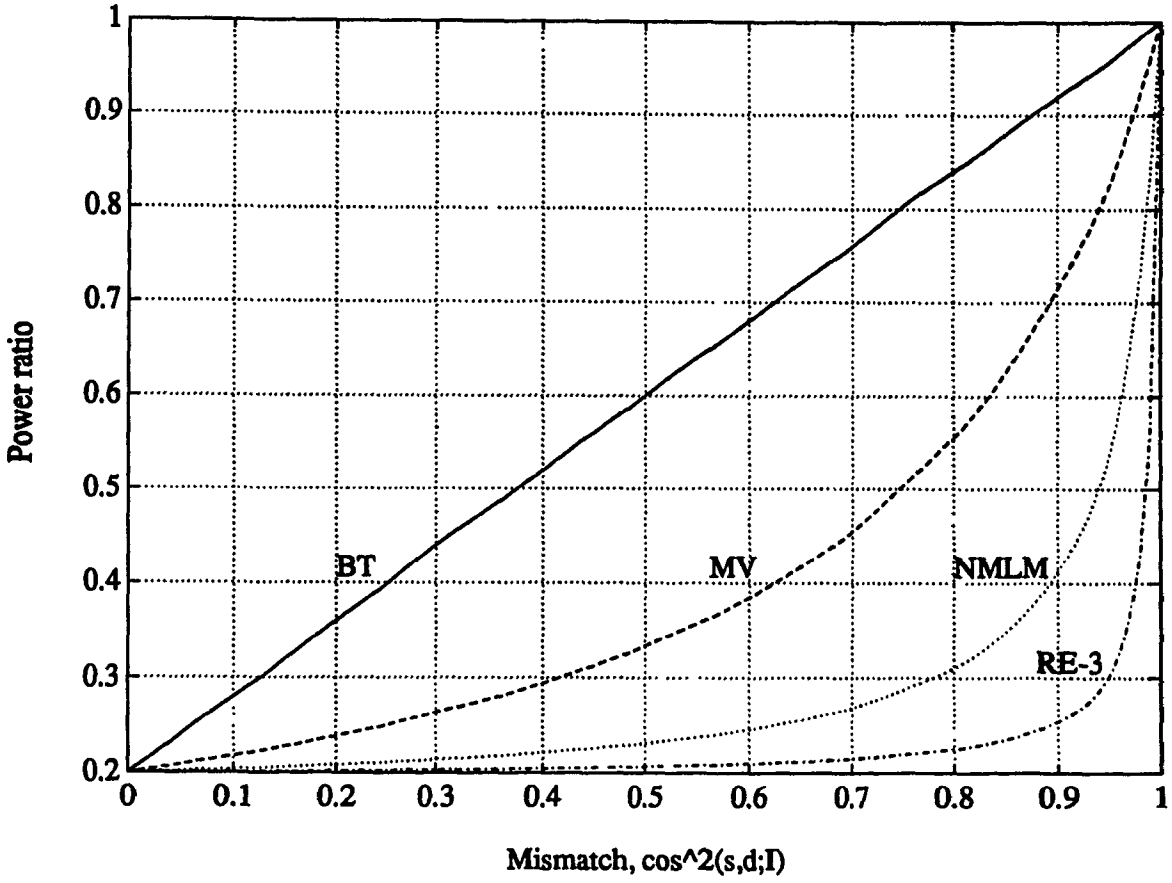

Figure 3.6: Sensitivity of the Rayleigh estimates $q = 1$ to 4, S/N=4

of order 1 to 4. The plot represents the normalized output spectrum level versus the mismatch expressed as the $\cos^2$ of the angular difference between the true and hypothesized steering vectors. When both vectors are aligned, the different order estimators have their normalized output level equal to 1. With increased mismatch, the value of the peak level will drop rapidly. The experiment was repeated a second time with a new signal-to-noise ratio equal to 4 and expressed as

$$(S/N)_i = \frac{\sigma_s^2}{\sigma_n^2} = 4 \tag{3.100}$$

In this case, the predicted lower and upper bounds for the power ratio are

$$0.2 \leq \rho \leq 1$$

The results are presented in Fig. 3.6. It is possibleto observe the following:

- The impact of mismatch is greater at higher signal-to-noise ratios; this was also observed by Gingras [12]. The lower bound given by 3.98 illustrates the inverse relationship between the mismatch and the signal-to-noise ratio.

- The impact of mismatch is more severe as the order of the Rayleigh estimate increases.

$$\rho_{BT} \geq \rho_{MV} \geq \rho_{NMLM} \geq RE_3 \geq \cdots \tag{3.101}$$

From the sensitivity analysis of the Rayleigh family, it is evident that the increase in resolution, observed in the previous section in the narrower peaks is achieved at the expense of the sensitivity of the estimator. A minimum mismatch of 5° will seriously affect the output of the order 3 estimator.

3.6 Other Properties of Rayleigh Estimates

In the previous section of this chapter, expressions for the output spectrum, bandwidth and sensitivity to mismatch of the Rayleigh family were derived. These expressions are used to visualize the trade-off between the order of the estimate and its various properties. In this section, additional characteristics of the Rayleigh family are presented. The effect of the order or size M of the correlation matrix on the convergence of the estimate. Similarly, the effect of increasing the order q and asymptotic statistical stability of the Rayleigh estimate will be presented.

3.6.1 Asymptotic Convergence of the Estimate

An important property of any spectral estimate is its convergence to the true power spectral density of the process. In this section this behavior will be investigated [23]. The effect of an increase in the size of the correlation matrix on the resulting estimate is considered. This is equivalent to an increase in the physical size of the array.

Let $\lambda_i, i = 1, \ldots, M$ denote the eigenvalues of $\mathbf{R}$ and $\mathbf{u}_i$ the corresponding eigenvectors, the correlation matrix can be written as:

$$\mathbf{R} = \sum_{i=1}^{M} \lambda_i \mathbf{u}_i \mathbf{u}_i^* \tag{3.102}$$

As the size of the correlation matrix increases and goes to infinity, ($M \rightarrow \infty$), we can use the asymptotic property of the eigenvalues stated as [39,13]

$$\lim_{M \rightarrow \infty} \lambda_i = \mathcal{Z}(\omega_o)$$

Thus, the eigenvalue for a particular frequency ω_o is the value of the power of the process at that particular frequency [46]. They are approximated by samples of the power spectrum. For example, if $\mathcal{Z}(\omega)$ is white, than all the eigenvalues are equal to σ_n^2. Similarly, if the $\mathcal{Z}(\omega)$ has k lines in its spectrum, then the correlation matrix is of rank k and has only k non-zeros eigenvalues [39]. Furthermore, the corresponding eigenvector will tend to equally spaced steering vector in the spatial domain. As $M \rightarrow \infty$, it is possible to write

$$\mathbf{R} = \sum_{i=1}^{M} \lambda_i \mathbf{u}_i \mathbf{u}_i^* \tag{3.103}$$

$$= \sum_{i=1}^{M} \mathcal{Z}(\omega_i) \mathbf{s}_i \mathbf{s}_i^* \tag{3.104}$$

where $\mathbf{s}_i$ is the steering vector corresponding to the spatial frequency ω_i. With M very large, the hypothesized steering vector $\mathbf{s}$ with spatial frequency of interest ω_o will ultimately coincide with one of the eigenvectors $\mathbf{s}_i = \mathbf{u}_i$ such that

$$\mathbf{s} = \mathbf{s}_i$$

Using the above property and considering the case where $\omega = \omega_o$, then

$$\mathbf{s}^* \mathbf{R} \mathbf{s} = \mathcal{Z}(\omega_o) \mathbf{s}^* \mathbf{s}_i \mathbf{s}_i^* \mathbf{s} \tag{3.105}$$

Extending the above result to the Rayleigh estimate case and using the property of the eigenvalues to raise them to the power q results in

$$\mathbf{s}^* \mathbf{R}^{-q} \mathbf{s} = \mathcal{Z}^{-q}(\omega_o) \mathbf{s}^* \mathbf{s}_i \mathbf{s}_i^* \mathbf{s} \tag{3.106}$$

Since the inner product of the hypothesized steering vector and the steering vector $\mathbf{s}_i = \mathbf{u}_i$ is equal to M, the above expression is further simplified as

$$\mathbf{s}^* \mathbf{R}^{-q} \mathbf{s} = M^2 \mathcal{Z}^{-q}(\omega_o) \tag{3.107}$$

For the numerator of the Rayleigh estimate, the equivalent expression is given by

$$\mathbf{s}^* \mathbf{R}^{-(q-1)} \mathbf{s} = M^2 \mathcal{Z}^{-(q-1)}(\omega_o) \tag{3.108}$$

Forming the ratio of the numerator and denominator and simplifying

$$\frac{M^2 \mathcal{Z}^{-(q-1)}(\omega_o)}{M^2 \mathcal{Z}^{-q}(\omega_o)} = \mathcal{Z}(\omega_o) \tag{3.109}$$

From the previous results, it is possible to conclude that for any order q of the Rayleigh estimate, convergence to the true power density as the size of the correlation matrix goes to infinity is achieved. It is important to note that the correlation matrix used in an estimated version of the true correlation matrix and the convergence to the true spectrum also depends on the approach used to estimate $\hat{\mathbf{R}}$. This can be summarized as

$$\lim_{M \to \infty} \hat{\mathcal{Z}}_q(\omega_o) = \mathcal{Z}(\omega_o) \tag{3.110}$$

3.6.2 Effect of the Order q

In section 3.3.2, it was shown that the value of the output spectrum level in the matched case is independent of the order of the estimate and is always equal to

$$\mathcal{Z}_q = \sigma_n^2(1 + S/N) \qquad \text{when } \mathbf{s} = \mathbf{d}$$

Below, the effect of varying the order q on the off-main-peak values is investigated [24]. For a given $\mathbf{R}$, we can write

$$\mathbf{s}^* \mathbf{R} \mathbf{s} = \sum_{i=1}^{M} \lambda_i |\mathbf{s}^* \mathbf{u}_i|^2 \tag{3.111}$$

Extending to the general case of order q, and using the eigenvalues properties of the correlation matrix, the denominator of the Rayleigh estimate can be written as

$$\mathbf{s}^* \mathbf{R}^{-q} \mathbf{s} = \sum_{i=1}^{M} \lambda_i^{-q} |\mathbf{s}^* \mathbf{u}_i|^2 \tag{3.112}$$

As the order $q \rightarrow \infty$, the smallest eigenvalues, λ_{min}, becomes more significant when raised to a large negative power. The Rayleigh ratio can now be expressed in terms of the smallest of the eigenvalues as

$$\lim_{q \to \infty} \frac{\lambda_{min}^{-(q-1)}}{\lambda_{min}^{-q}} = \lambda_{min} \tag{3.113}$$

In the white noise case, and by examining the structure of the matrix $\mathbf{R}$, this smallest eigenvalue is equal to the noise power σ_n^2 and constitutes a minimum threshold for the resulting estimator. It was found that the sensitivity of the estimator is related to the condition of data correlation matrix, given by the ratio of the largest eigenvalue to its

smallest [28]. Thus as the order increases and goes to infinity, the smallest eigenvalue will gain importance and the effect of the noise on the output spectrum becomes more apparent and must be taken into consideration.

3.6.3 Threshold Effect

The objective of spectral estimation is to achieve a high degree of resolution with a relatively short number of data segments. There exist an inherent trade-off between the resolution of the estimator and its statistical stability with a finite amount of data. The correlation matrix plays an important role in the evaluation of the Rayleigh estimate. Best results are achieved when it is formed with the maximum available input data. In practice, the spatial correlation matrix never takes the form of 3.5 and is estimated from the available time series at the sensors output. This estimate is the result of using time averages as an approximation to the corresponding ensemble average. With the time series denoted by $\mathbf{x}(t)$, it is sectioned in segments of length T and the Fourier transform of each section is evaluated. The resulting frequency domain version of the i-th segment is denoted by $\mathbf{X}_i(f)$. The spatial correlation matrix is *estimated* by averaging the outer product of this vector with itself as follows [18]

$$\hat{\mathbf{R}} = \frac{1}{N}\sum_{i=1}^{N} X_i X_i^* \tag{3.114}$$

In this section, the relation between the number of data segments (N), the accuracy of the estimate and its statistical variability will be considered. The mean and the normalized variance expressed as $\sigma/\overline{x}$, are used to measure the effect the number of data segments has on the performance of the estimators. It is expected that as the number of segments increases, the resulting estimator will be more *robust* and consequently, its variance will decrease.

Capon and Goodman presented an expression for the mean and the variance of the Minimum Variance or Rayleigh estimate of order 1, as a function of, among other parameters, the number of sensors and the number of data segments [7]. This analysis was based on the study of the properties of a random matrix, its probability distribution function being a Wishart distribution. Expressions for the statistics of the Rayleigh estimate of arbitrary order q represent an extensive undertaking due to the nature and complexity of the Rayleigh estimate expression. The probability distribution of a ratio of two random matrices raised to an arbitrary power must be examined. This is an issue considered beyond

Order	No. of snapshots				
	60	100	200	500	1000
2	100	100	100	100	100
3	50	76	98	100	100
4	8.5	17	31	66.5	92.5
5	0	(3)	4.5	21	27

Table 3.3: Detection performance of various Rayleigh estimates

the scope of this work.

An alternative approach based on *Monte–Carlo methods* was used instead. Repeated trials of the same experiment were executed. The mean and the normalized variance were calculated for different orders of Rayleigh estimates. The following scenario was devised: a target was introduced at a bearing of 109.9768° with a signal-to-noise ratio of 0dB. For a Rayleigh estimate of a given order and with fixed observation intervals, the experiment was repeated 200 times. The number of trials in the experiment should be large enough to generate good estimates of the mean and the variance of the process. The objective is to study the effect of the length of the observation interval on the detection capability of the estimate. Following each trial, 2 values were retained:

- The bearing of the peak values
- The output level at the peak.

For each order of Rayleigh estimates, the *spatial bandwidth* was calculated using Eq. 3.81 from section 3.4. The location of the peak in the current trial was then compared to the true one. If the peak occurred within the predicted spatial frequency band, the source was labelled as detected and resolved and the trial was tagged appropriately. The estimated correlation matrix was generated using one of the following number of *snapshots* [60 100 200 500 1000]. It is evident that as the number of data segments increases, the estimated correlation matrix will converge to the true one. The results expressed in detection percentage are given in table 3.3.

From table. 3.3, it is possible to observe that the detection/non-detection threshold increases rapidly as the order of the Rayleigh estimate increases. To achieve an adequate detection percentage of 90%, an order 2 with 60 snapshots is sufficient. However for higher resolution results, approximately 200 snapshots are required for the order 3, 1000 for the

order 4 and over 5000 for the order 5 Rayleigh estimate. Table 3.4 and 3.5 represent the mean value and the standard deviation of the peak value of the Rayleigh estimate of order 2 to 5 for various number of data segments used to form the correlation matrix. It is possible to observe in Table 3.4 that as the number of data segments increases, the peak value of the estimate converges to the predicted value of 9 and at the same time the variance decreases. As for the mean and variance of the bearing or location of the peak, the results are presented in Table 3.6 and Table 3.7. It is also possible to observe that similarly, with an increase in the number of data segments, the mean value of the peak decreases and exhibit less variability demonstrated by a decreasing variance. It is possible to conclude that as the observation interval increases, the peak value will converge to the predicted value and the location of this peak will correspond to the true bearing.

Since the localization of the source at the position is the parameter of interest, convergence to the true bearing along with the minimum variability is the desired objective. Figure 3.7 illustrates the normalized variance of the different orders of Rayleigh estimates for various values of snapshots. The variance values are those presented in Table 3.7. From the figure, it is possible to observe that for a given number of snapshots, as the order of the Rayleigh estimates increases, the resulting variance also increases. However as the number of snapshots increases, the variance of the different estimates decreases. Combining the results presented in Table 3.3 and the figure under consideration, it is possible to confirm the trade–off existing between the resolution and the variance of the estimates. Under ideal conditions (i.e. infinite time case or maximum number of data segments), increasing the order of the Rayleigh estimates results in an increase in resolution as seen in the previous section by the narrower peaks. However, using a fixed size number of segments (i.e. 200) results in poorer detection performance as the Rayleigh order increases and similarly an increase in the variance of the estimate. A large increase in the number of snapshots is needed to offset the detection performance deterioration of the estimate and consequently decrease the variance. A closed–form expression describing the relationship between the order of the Rayleigh estimate and the variance should be useful in predicting the performance of the estimate and could represent the basis for future work due to the nature of the issues involved.

nsnap	Order of estimate			
	2	3	4	5
60	4.0945	1.2701	0.8342	
100	5.4387	1.8053	0.9578	0.8657
200	7.0666	2.9878	1.2041	0.9494
500	8.2955	5.1415	1.8223	1.0625
1000	8.7490	6.9611	2.9428	1.2501
Exact value = 9				

Table 3.4: Mean value of peak level for RE = 2 to 5

nsnap	Order of estimate			
	2	3	4	5
60	0.2421	0.2571	0.1345	
100	0.1873	0.2628	0.1333	0.1055
200	0.1244	0.2512	0.1754	0.0766
500	0.0554	0.1318	0.1610	0.0661
1000	0.0309	0.0751	0.1586	0.0849

Table 3.5: Normalized variance of peak level for RE = 2 to 5

nsnap	Order of estimate			
	2	3	4	5
60	110.1590	110.5605	111.0201	
100	110.1461	110.4320	110.4007	111.6780
200	110.1362	110.1533	109.7631	109.6379
500	110.1329	110.1452	110.1635	109.4223
1000	110.1212	110.1277	110.1341	110.1574
Exact value = 109.9768				

Table 3.6: Mean value of peak bearing for RE = 2 to 5

nsnap	Order of estimate			
	2	3	4	5
60	0.0083	0.0395	0.0988	
100	0.0063	0.0238	0.0704	0.1010
200	0.0038	0.0041	0.0415	0.0845
500	0.0022	0.0023	0.0025	0.0365
1000	0.0011	0.0011	0.0012	0.0013

Table 3.7: Normalized variance of peak bearing for RE = 2 to 5

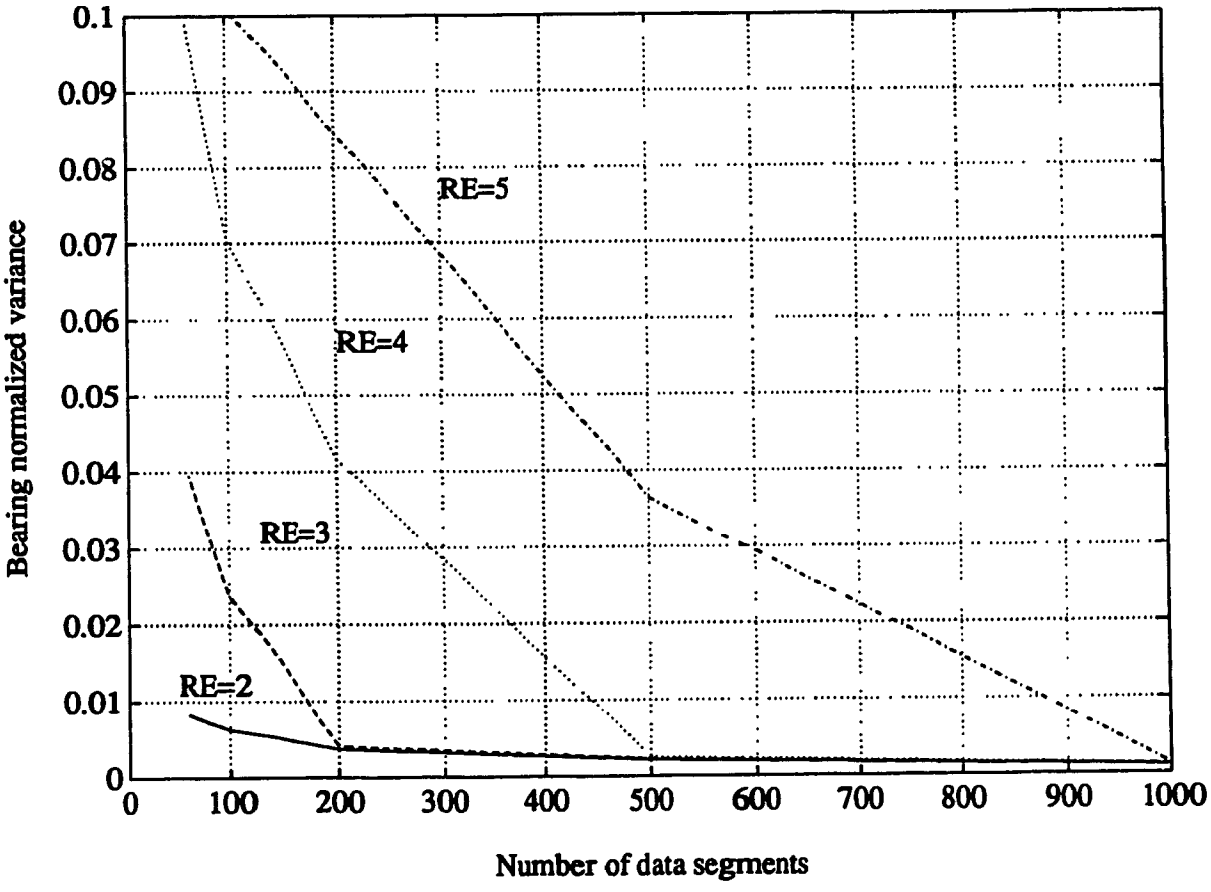

Figure 3.7: Bearing variance for RE = 2 to 5

Chapter 4

Acoustical models

4.1 Introduction

In recent years there has been an increasing interest in merging signals processing with propagation models. In conventional beamforming, signals radiated by a source are modelled as plane waves. However, in complex multipath propagation conditions, a more realistic propagation model is required and accurate treatment of the physics of acoustic wave propagation is essential. Matched–Field Processing (MFP) is one such approach to this problem. The plane wave beamformer steers the array by matching the measured field with plane waves for all look directions. The measured sensor array output is fitted with versions of the predicted fields for the different source location, through a propagation model. This model accounts for the refractive, multipath and sound speed profile [1].

There are many underwater acoustic propagation models each of which has its own advantages and disadvantages. This chapter is concerned with the study of three such models. They offer different modelling techniques for the sound propagation in the ocean ranging from the simplest method to the very sophisticated. The most complete propagation model will then be combined with the beamformers presented so far to form the basis for matched–field processing, discussed in the next chapter.

4.2 The Ocean Environment

The ocean can be regarded as a complex multilayer acoustic medium with properties that change daily and seasonally. For example, temperature and salinity have been

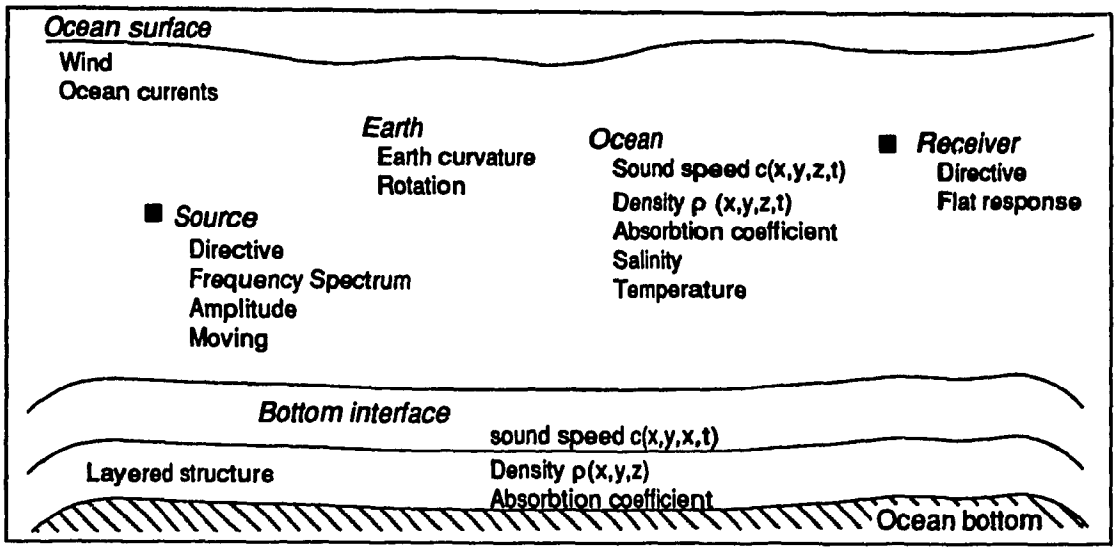

Figure 4.1: Representation of the ocean model

found to often change sharply over a few meters. Below the uppermost layer, there exists a thermocline, a layer in which the temperature rapidly decreases with increasing depth. The bottom of the thermocline corresponds to a minimum in the sound speed profile. This level represents the axis of the deep sound channel where the energy is confined by refraction [8]. Below this layer is a region of constant temperature. The different layers do not necessarily run parallel to the surface and may often follow the sea-bed contour. Their differing temperature and density may be sufficient to change the direction of sound waves. The knowledge of the characteristics of these layers is very important in the study of underwater acoustic transmission.

The sea is a better medium than air for long range sound transmission. Sound can propagate within the ocean for much greater distances than other forms of energy, and the detectability range can span several thousand kilometers. Moreover the sea has an acoustic impedance layer greater than that of air. It is the high speed of sound in the water combined with its low attenuation that facilitates the measurements of the echo in sonar systems. This leads to an increased interest in the study of sound propagation and consequently the development of the sonar field.

The study of sound propagation in the sea is a complex field due to the different

factors that affect it. Fig 4.1 is an attempt to summarize these elements and an explanation of the different roles they play will follow. In the figure, the 3 coordinates x, y, z are used to indicate a location, t represents the time, c is the sound speed, ρ is the medium density and α is the acoustic absorption coefficient. Other factors such as the earth curvature, ocean currents, wind flow and ship noise must also be taken into account. If all the parameters are allowed to vary simultaneously, a model of the ocean will be very difficult to formulate, instead some approximations must be made. These approximations will impose a constraint either on the model used to study the sound propagation or the signal processor used at the receiver end of the system.

4.3 Acoustic Principles

The propagation of sound in an *elastic* medium can be described mathematically by the solution of the wave equation using the appropriate boundary and medium conditions for a particular problem. The wave equation relates the acoustic pressure p at coordinates x, y, z with the time t. It is expressed as:

$$\frac{\partial^2 p}{\partial t^2} = c^2 \left(\frac{\partial^2 p}{\partial x^2} + \frac{\partial^2 p}{\partial y^2} + \frac{\partial^2 p}{\partial z^2} \right) \tag{4.1}$$

where c is the sound velocity. For various applications, it is often more convenient to describe and solve the wave equation in terms of cylindrical coordinates (r, z) where r is the range and z is the depth. Rewriting the wave equation in the new coordinates system results in [2]

$$\frac{\partial^2 p}{\partial r^2} + \frac{1}{r}\frac{\partial p}{\partial r} + \frac{\partial^2 p}{\partial z^2} - \frac{1}{\rho(z)}\frac{d\rho}{dz}\frac{\partial p}{\partial 2} + k^2(z)p = -\frac{1}{2\pi r}\delta(r)\delta(z - z_s) \tag{4.2}$$

In general, there is a variety of different types of solutions for any given partial differential equation. For a particular problem, one or more of these solutions can be applied to meet specific boundaries or initial conditions and results in a unique solution. Two theoretical approaches can be used to solve the wave equation. The development through specific boundary conditions into a solution in terms of normal modes. This approach is known as *normal-mode theory*. Normal modes define the preferred frequency of vibration of the system. They are combined additively through a summation of the contribution from the various frequencies to satisfy the boundary and source conditions of interest. The propagation is described in terms of characteristic functions called normal modes, each of

which is a solution of the equation. The result is a complicated function that gives little insight into the distribution of the energy in space and time [44].

The other solution is in terms of wave surfaces or rays also known as *Ray theory*. Ray methods are derived from the wave equation with the following condition: In Ray theory, the wave surfaces are the locations of points undergoing a transformation in time and space. The rays are normal to the wave surfaces and describe where in space the sound emanating from a source is being sent and its propagation direction through the medium. Ray acoustics similar to its analog in optics, presents a picture of the propagation in the form of a ray diagram. The underlying assumption for the validity of the ray treatment is that the acoustic wavelength is much smaller than the distance over which $c(z)$ changes, stated as

$$\psi \ll c(z)$$

where $c(z)$ is the sound velocity expressed as a function of depth. Ray theory offers the following advantages

- Rays are easily drawn using Snell's law or by using numerical algorithms.
- Sound distribution is easily visualized.
- Ray tracing is independent of the source.
- Boundary conditions are easily inserted.

However, several disadvantages exist [41]:

1. For relatively simple cases with few parameters, the ray tracing method doesn't require a large computational load. However for complex cases where multiple sound speed profiles and various boundary conditions exist, the ray tracing being an iterative process, will necessitate large computational resources.
2. Since there exists no closed form expression describing the ray behavior at the boundaries, the interface with bottom models and the large number of unknown parameters, the incident ray must be *told* the reflected angle.
3. Since ray tracing is essentially a numerical procedure whereby each ray is traced from the source, a variation in the parameter (e.g., new source depth or new range) will affect the ray trajectory and the procedure must be restarted.

4. Sound like light, is a phenomenon, not a ray process. Under specific conditions, the ray tracing approach is an approximate solution of the wave equation. The relation between the acoustic frequency, ray calculation and all the ocean parameters are not clearly defined.

4.4 Ray–Tracing

The assumption that sound speed varies with depth z is an indication that acoustic rays will be refracted and consequently a refractive index is defined. This index is a function of the depth

$$n(z) = c_1/c(z)$$

where c_1 is a fixed value of the sound speed. Using Snell's law, the angle θ formed by a ray with a horizontal boundary layer, where the sound speed is c is expressed by the following relation:

$$n = \frac{c_1}{c} = \frac{\cos\theta_1}{\cos\theta} \tag{4.3}$$

With the refractive index known, it is useful to trace the predicted sound field. The ray method will allow us to determine the ray path from a given source location, the change of intensity along the ray path and the travel time between the source and a receiver. A number of rays originate from the source at known angles with respect to the horizontal. Using Snell's law, the rays are traced forward. When a ray strikes the upper or lower boundary of the ocean, assumptions about its reflection and absorption must be applied. With $c(z)$ known at different depths, the travel time of an acoustic pulse along a calculated ray trajectory can be computed. The ability to calculate the total travel time of a ray helps in determining whether sound emitting from a source reaches a receiver. Also, the relative delay between arrivals of a ray aid in verifying if the sound originating from the source followed multiple paths.

Since there is no specific or definitive ray method due to the complex issues involved in the modeling of the ocean, several methods exist, each with its own set of approximations, omissions and so on. Even though each method will generate a ray plot, it is not guaranteed that two methods will yield equivalent results for the same problem. Different methods could be appropriate for different applications and a good understanding of a given ray tracing method along with its approximations and assumptions is important prior to its application.

When given a source and a receiver in an ocean model of known characteristics, it is of importance to the signal processor to be able to estimate or evaluate the angles of arrival of the rays originating from the source and the total travel time of a ray between the source and the receiver. This information is needed when forming the hypothesized pressure field used in matched-field processing and is presented in the next chapter. Prior to considering a specific ray tracing algorithm, several criterion must be taken into account:

- The ability to compute the angle of arrival and the total travel time of individual rays.
- The realism of the channel modeling.
- The computational complexity required.
- The flexibility of the algorithm.

In the following sections, three ray tracing methods will be presented, they are:

- Ray tracing in an isovelocity linear sound speed profile: the sound speed is assumed constant in both the horizontal and vertical layer. Complex boundary conditions are not considered and perfect refraction is assumed at both boundaries [44,5].
- Linear and Quadratic square slowness profile: two profiles are presented where the sound propagation is modelled as a linear or a quadratic function of the depth. Boundary conditions are not treated since the rays are confined to the SOFAR channel [30].
- Multiple–Profile Ray–Tracing Program: a rather complex and computational intensive numerical model where a wide range of parameters such as multiple profiles, the earth curvature correction and boundary conditions are taken into account [31].

Whenever appropriate, numerical examples and a sample ray diagram will be included. The three different methods will be compared and their respective advantages and disadvantages will be outlined.

4.5 Isovelocity Model

In the ocean, sound transmission is affected by such factors as temperature, pressure, chemical composition and details of the surface and bottom boundaries. For he isovelocity homogeneous medium presented in this section, it is assumed that the medium

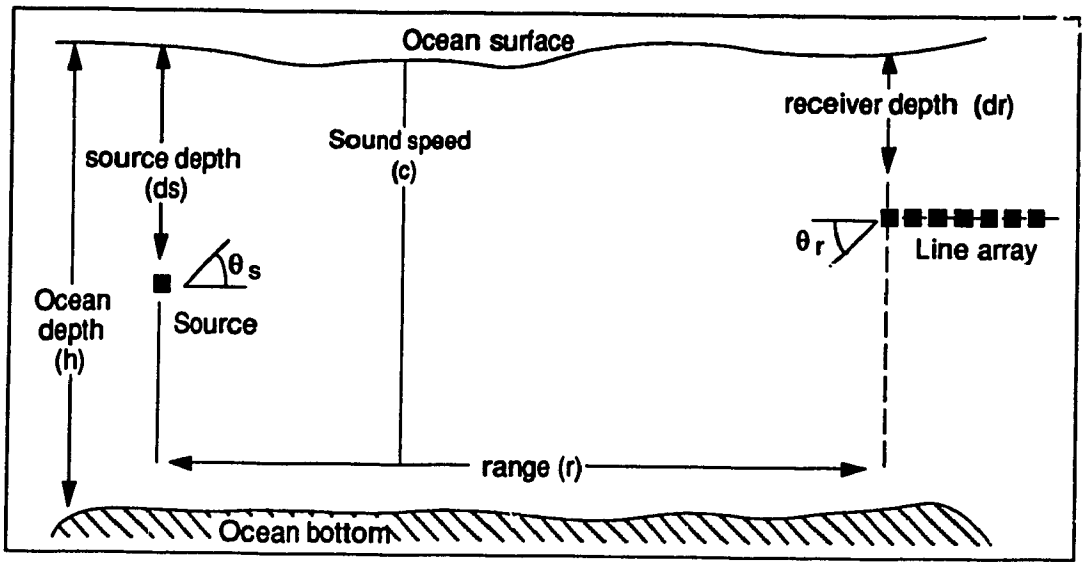

Figure 4.2: Isovelocity sound speed profile

properties are constant. All mechanical losses are zero. Reflection of the water-air interface and the bottom sediment layer is ideal resulting in the reflection angle being equal to the incident angle. This ocean model is illustrated in Fig. 4.2. The arrival angle with respect to the first sensor of an array, for any combination of source-receiver depth-range represents the element of interest. In this model, no restrictions are imposed on the relative location of the source and the receiver. The array used is a horizontal array of M sensors, and the sound propagation is constant in both the horizontal and vertical layer and between the different elements in the array. The ocean model will be presented first and a general expression for the arrival angle of a ray at the receiver will be derived. An expression for the total travel time along a ray path will follow.

In this model, rays travel along straight lines and Snell's law is used at the boundary to compute the reflection angle. The analysis mainly relies on trigonometric identities used to derive the specific angle θ_r of interest, the angle formed at the receiver between the ray and the horizontal plane. The solution of the wave equation for a given set of coordinates and source-receiver combination yields a fourth order equation. The roots of this equation along with the principles of mode interference result in 4 distinct initial angles [29,30]. These 4 angles form a group n and they *connect* the source to the receiver in the

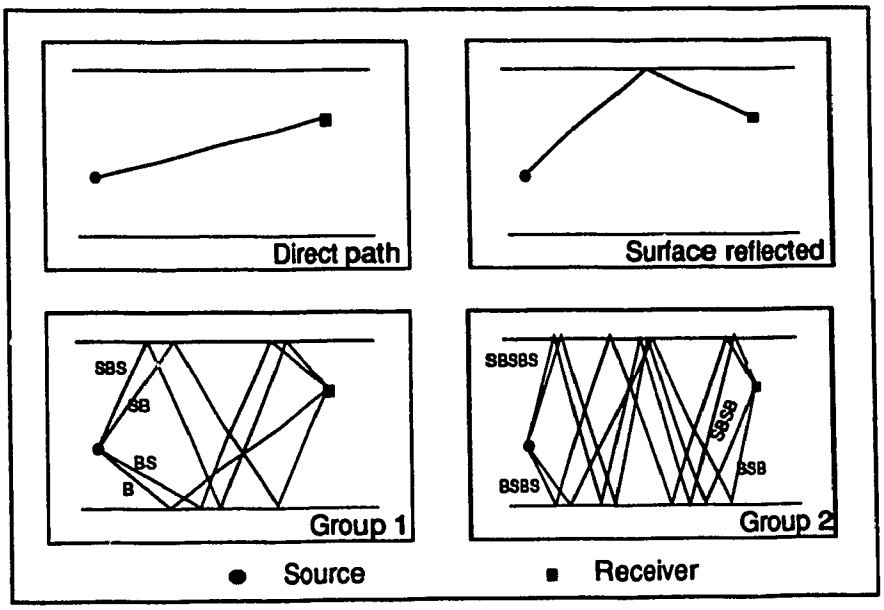

Figure 4.3: Path of rays members of group 1 and 2

following fashion:

- two rays with an equal number of surface and bottom reflections and opposing initial angle sign.
- a ray with an additional surface reflection and a positive initial angle
- a ray with an additional bottom reflection and a negative initial angle

In the analysis to follow, a surface and a bottom reflection will be denoted by S and B respectively. The ray from the source with a path that includes a bottom reflection, followed by a surface, then a bottom reflection is expressed as BSB. The rays'members of the first and second group ($n = 1, 2$) are illustrated in Fig. 4.3. Derivation of the expression for the arrival angle and the total travel time for the ray group of order 1 will follow. Ray absorption at both boundaries is neglected and incident rays are fully reflected such that the reflection and incidence angle are equal. The subscript i and r are used to denote incident and reflected rays and the prime will indicate the subsequent incident and reflected rays. For the SB ray in group $n = 1$ presented in Fig. 4.3, the total distance r traveled by the ray is expressed as

$$r = p_i \cos\theta + p_r \cos\theta + p_i' \cos\theta \tag{4.4}$$

where

$$p_i = d_s/\sin\theta \tag{4.5}$$

$$p_r = h/\sin\theta \tag{4.6}$$

$$p_i' = (h - d_r)/\sin\theta \tag{4.7}$$

Introducing p_i, p_r and p_i' into 4.4 and isolating θ, results in the following expression:

$$\theta = \tan^{-1}\frac{2h + d_s - d_r}{r} \tag{4.8}$$

It is possible to calculate the initial and arrival angle for a ray connecting the source with the receiver, separated by a distance r, given their respective depth and the height of the water column. The delay between the different ray arrivals plays an important role in the processing of the signals. It is appropriate to calculate the total travel time of each ray and calculating the difference between the various arrivals will result in the delay values. This time is designated by T and expressed by

$$T = \frac{\text{ray path length}}{\text{sound speed}} \tag{4.9}$$

where the ray path length is the sum of the length of the individual incident and reflected rays. In the case of the SB ray, this length is expressed as the sum of the source-surface, surface-bottom and bottom-receiver segments length, and given by:

$$p_i + p_r + p_i' \tag{4.10}$$

using 4.5, 4.6 and 4.7, the path length denoted by p_l is

$$p_l = \frac{2h + d_s - d_r}{\sin\theta} \tag{4.11}$$

Since the sound speed in this model is assumed constant in both the horizontal and vertical layers in the ocean, the expression of the total travel time is

$$T = \frac{2h + d_s - d_r}{c\sin\theta} \tag{4.12}$$

Using the same trigonometric approach, similar expressions are derived for the remaining rays of the same group. Two cases are still to be considered, the direct ray from the source to the receiver and the surface reflected ray, both presented in Fig. 4.3. For the direct path case, the range between the source and the receiver is given by

$$r = p_i\cos\theta \tag{4.13}$$

Ray	Angle θ	Tavel time T	Sign
D	$\tan^{-1}(d_s - d_r)/r$	$r/c\cos\theta$	$-$
S	$\tan^{-1}(d_s + d_r)/r$	$(d_s + d_r)/c\sin\theta$	$+$
B	$\tan^{-1}(2h - d_s - d_r)/r$	$(2h - d_s - d_r)/c\sin\theta$	$-$
BS	$\tan^{-1}(2h - d_s + d_r)/r$	$(2h - d_s + d_r)/c\sin\theta$	$+$
SB	$\tan^{-1}(2h + d_s - d_r)/r$	$(2h + d_s - d_r)/c\sin\theta$	$-$
SBS	$\tan^{-1}(2h + d_s + d_r)/r$	$(2h + d_s + d_r)/c\sin\theta$	$+$
BSB	$\tan^{-1}(4h - d_s - d_r)/r$	$(4h - d_s - d_r)/c\sin\theta$	$-$
BSBS	$\tan^{-1}(4h - d_s + d_r)/r$	$(4h - d_s + d_r)/c\sin\theta$	$+$
SBSB	$\tan^{-1}(4h + d_s - d_r)/r$	$(4h + d_s - d_r)/c\sin\theta$	$-$
SBSBS	$\tan^{-1}(4h + d_s + d_r)/r$	$(4h + d_s + d_r)/c\sin\theta$	$+$

Table 4.1: Arrival angle and travel time for ray groups 1 & 2

where

$$p_i = \frac{d_s - d_r}{\sin\theta} \tag{4.14}$$

Isolating θ to derive an expression for the arrival angle results in

$$\theta = \tan^{-1}\frac{d_s - d_r}{r} \tag{4.15}$$

Since the only ray connecting the source to the receiver in this case is the incident ray, the ray path length is equal to p_i and expressed as

$$p_l = p_i = \frac{r}{\cos\theta} \tag{4.16}$$

and the total travel time is

$$T = \frac{r}{c\cos\theta} \tag{4.17}$$

Similarly, for the special case of the surface reflected ray S, the arrival angle θ and the total travel time are

$$\theta = \tan^{-1}\frac{d_s + d_r}{r} \tag{4.18}$$

$$T = \frac{d_s + d_r}{c\sin\theta} \tag{4.19}$$

The results for the rays of the first and second group are summarized in Table 4.1. Typically, the receiver is positioned closer to the surface than the source (i.e. $d_s < d_r$). The previously derived expressions are representative of this case. If the source is a surface ship such that $d_s \geq d_r$, similar expressions can be derived using the same approach.

The isovelocity model presented in this section was used to derive closed form expressions for the initial angle and the total travel time of the rays. This model imposes no restrictions on the relative location of the source and the receiver. However, this simplicity is achieved at the expense of the realistic aspect of the ocean model. The assumption of constant sound speed and ideal reflection at the boundaries render the model unsuitable for serious applications. The following ray-tracing method proposes two different representations to achieve a more realistic modelling of the sound speed profile and an alternative approach to the handling of the boundaries.

4.6 Munk and Wunsh Model

The sound speed in the ocean is a function of the depth and therefore should be modelled appropriately. This relationship is usually described by a closed form expression or by a series of coordinates (depth, sound speed) at various points. In the work by Munk and Wunsh presented in this section, the sound speed in the ocean is expressed as a function of depth. Two different sound speed profiles are discussed: the Linear and the Quadratic model [30]. They are given by the following expressions:

$$S^2 = S_o^2(1 \pm z/a_{\pm}) \qquad (l) \tag{4.20}$$

$$S^2 = S_o^2(1 - z^2/a_{\pm}^2) \qquad (q) \tag{4.21}$$

where S is the sound slowness, the reciprocal of the sound speed c; S_o is the initial sound slowness; z_o represents the sound axis located at the minimum sound speed depth; z denotes the depth and is positive for values above z_o and negative for values below z_o and a is a constant that depends on the geographical area being considered.

In the linear model, the sound speed profile results from a layer with a negative gradient from the surface to a depth of z_o, above a region with a positive gradient from z_o to the bottom. The quadratic model uses a second order quadratic expression to describe the sound speed versus depth characteristics thereby allowing for a better and more realistic modelling of the sound channel. The Munk and Wunsh model is a range-independent propagation model where the sound speed is only a function of the depth and is constant across the horizontal layer. A constraint is imposed by the algorithm on the relative depth of the source and the receiver; both must be located on the sound axis at depth z_o. For the Northwest Atlantic region, this axis is situated at a depth of 1300 m [30]. This constraint

renders the proposed model inappropriate for sonar applications. The Sonar or Sonobouys are usually positioned at a depth less than 400 m and it is highly unlikely to have the sensor array and the target of interest at the same depth.

Since the sound channel consists of two regions with different gradients, the ray travel distance in the upper region denoted by X_+, and the distance travelled in the lower region, X_-, will not be equal. The + and − signs are used to denote the quantities and units associated with either the upper or lower section of the sound channel. The total travel distance of any ray, between the source and the receiver, can be expressed as the sum of the portion travelled in the upper region and that travelled in the lower region. Each ray has a total of p *turning points*. The sum of the number of positive and negative turning points is given by p and equal to

$$p = p_+ + p_-$$

The total travel distance for the single loop with one positive turning point and one negative is given by

$$x = X_+ + X_-$$

For the rays having multiple turning points, the total travel distance is now expressed as the sum of all the portions travelled in the positive and negative region, such as

$$x = \sum_{p_+} X_+ + \sum_{p_-} X_- \tag{4.22}$$

From the ray mode duality, a ray group n arriving at the receiver has four members. The 4 constituents of a given ray group are expressed as $\{+2n, -2n, +(2n-1), -(2n+1)\}$ and are shown in Fig. 4.4. Assuming that the distance between the source and the receiver denoted by x is known, we are interested in deriving an expression to calculate the arrival angles of all the rays that reach the receiver.

4.6.1 Linear Profile

For the linear model and from [30], the distance travelled by a ray in the upper and lower layers is given by

$$X_\pm = 4a_\pm \sin|\theta_o| \cos\theta_o \tag{4.23}$$

The objective is to rewrite the above equation in terms of the initial angle θ_o for each member of the ray group n. For the first two rays $(+2n, -2n)$, with $p_+ = p_- = n$, rearranging the

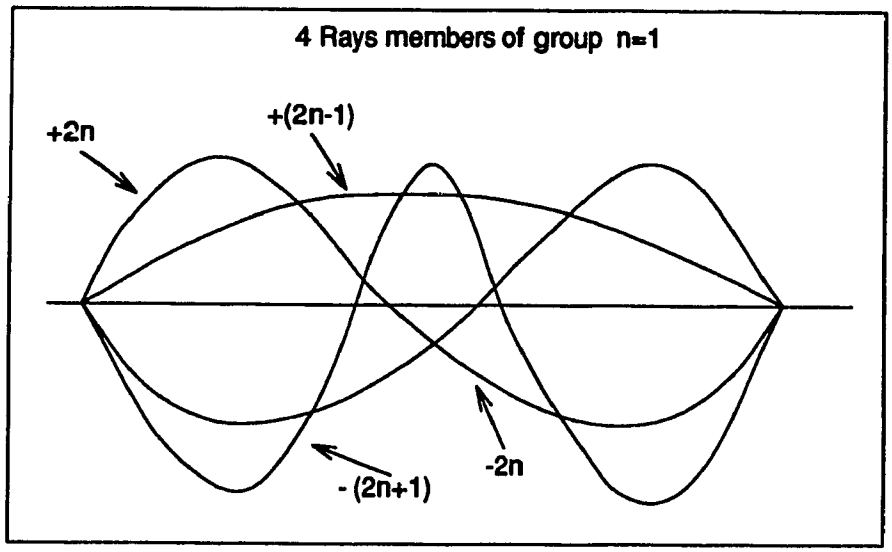

Figure 4.4: 4 constituents of ray group n

n	$+2n$	$-2n$	$+(2n-1)$	$-(2n+1)$
p_+	n	n	n	n
p_-	n	n	$n-1$	$n+1$
θ_o	$+$	$-$	$+$	$-$
t	nT	nT	$nT-T_-$	$nT+T_-$
x	nX	nX	$nX-X_-$	$nX+X_+$

Table 4.2: composition of the different rays

elements in the above expression results in

$$\frac{x}{4n(a_+ + a_-)} = \sin|\theta_o|\cos\theta_o \tag{4.24}$$

using the trigonometric identity $\sin 2\theta = 2\sin\theta\cos\theta$, we can write

$$\sin 2\theta_o = \frac{2x}{4n(a_+ + a_-)} \tag{4.25}$$

and consequently

$$\theta_{o1} = \theta_{o2} = \frac{1}{2}\sin^{-1}\frac{x}{2n(a_+ + a_-)} \tag{4.26}$$

Similarly, for the third and fourth constituent, $+(2n-1)$ and $-(2n+1)$ their respective initial angle is expressed as follows:

$$\theta_{o3} = \frac{1}{2}\sin^{-1}\frac{x}{2(na_+ + (n-1)a_-)} \tag{4.27}$$

and

$$\theta_{o4} = \frac{1}{2}\sin^{-1}\frac{x}{2(na_+ + (n+1)a_-)} \tag{4.28}$$

Given the range between the source and the receiver, and the gradient of the upper and lower layer in the ocean, the initial angle of an arbitrary ray group n can be computed from the previously derived expressions. The validity of these expressions can be verified against Fig. 2 in the work by Munk and Wunsh [30].

Travel Time Calculation

Since the sound speed in the ocean is not constant and various rays exist between any two points of interest, a delay will result from the different ray arrivals at the receiver. This delay is a function of the sound speed profile used in the modelling of the ocean. The total travel time can be expressed as the sum of the travel time in the upper and lower layers. For the single loop case with one turning point in each region (i.e. $p_+ = p_- = 1$), this is equal to

$$t = T_+ + T_-$$

For a ray group n, the total travel time is a function of the number of upper and lower turning points in the ray path, and is given by

$$t = p_+T_+ + p_-T_-$$

The travel time for the distance travelled in the upper and lower layers in the linear model case is expressed as [30]

$$T_\pm = \frac{4}{3}a_\pm S_o \sin|\theta_o|(1 + 2\cos^2\theta_o) \tag{4.29}$$

for the general case of ray group n, the total travel time is rewritten as

$$t = \frac{4}{3}(a_+p_+ + a_-p_-)S_o \sin|\theta_o|(1 + 2\cos^2\theta_o) \tag{4.30}$$

Using the results presented in Table 4.2, combined with a priori knowledge of the two values of a_+ and a_- for a specific geographic region, it is possible to calculate the initial angle and the total travel time for different ray groups. It is important to observe that for a given range x, only certain rays can reach the receiver. This is the result of the limit imposed by the domain of the function $\sin^{-1}$.

4.6.2 Quadratic Profile

For the quadratic profile, a similar approach can be used to obtain the different expressions of interest. The results are summarized below. From the work by Munk and Wunsh, the upper and lower loop ranges are

$$X_{\pm} = \pi a_{\pm} \cos\theta_o \tag{4.31}$$

Isolating θ_o and considering the 3 distinct initial angles will yield the following expressions

$$\theta_{o1} = \theta_{o2} = \cos^{-1} \frac{x}{\pi n(a_+ + a_-)} \tag{4.32}$$

$$\theta_{o3} = \cos^{-1} \frac{x}{\pi(na_+ + (n-1)a_-)} \tag{4.33}$$

$$\theta_{o4} = \cos^{-1} \frac{x}{\pi(na_+ + (n+1)a_-)} \tag{4.34}$$

A similar procedure is used and the total travel time is given by

$$t = \frac{\pi}{2}(a_+ p_+ + a_- p_-) S_o (1 + \cos^2\theta_o) \tag{4.35}$$

4.6.3 Numerical Example

A source-receiver scenario will be used to demonstrate the various expressions derived and sample calculations for both the linear and quadratic model will be presented. Due to the availability of the data, the Northwest Atlantic region was choosen. From Munk and Wunsh and for the linear model, $a_+ = 25.354$ and $a_- = 50.708$; for the quadratic model, $a_+ = 5.305$ and $a_- = 10.61$. The minimum sound speed axis is taken at a depth of 1.3 km. For a distance $x = 60$ km separating the source from the receiver, the initial angle of the first constituent and the total travel time, for different ray groups n when both models were used are summarized in table 4.3. From these results, we can observe that the axial arrivals are last for the linear model and first for the quadratic. As the order increases, the near–axial arrivals become more clustered for the quadratic than for the linear model and the time difference between successive arrivals will decrease. Likewise, the frequency of the arrivals at the receiver will increase with time.

The Munk and Wunsh acoustic modelling system was presented. It offers closed form expressions for deriving the initial angle and total travel time of a given ray group. With the range separating the source from the receiver known along with the medium gradient information (a_+, a_-), it is possible to calculate the necessary information of interest.

	Linear		Quadratic	
n	θ	t	θ	t
1	11.6147	39.7327		
2	5.6869	39.9347		
3	3.7773	39.9711		
10	1.1302	39.9974	83.1077	169.0616
11	1.0274	39.9979	83.7369	185.5095
12	0.9418	39.9982	84.2607	201.9939
20	0.5650	39.9994	86.5601	334.5230
21	0.5381	39.9994	86.7241	351.1320
22	0.5136	39.9995	86.8731	367.7462

Table 4.3: Linear and Quadratic model results

However, for practical applications this method has some drawbacks. The Munk and Wunsh approach is concerned with range-independent sound channel propagation and concentrates on geometry where both the source and the receiver are located on the sound axis, more specifically, at the depth of the minimum sound speed. For sonar applications, this geometry does not reflect a realistic scenario since both the sources and the receiver are rarely located at the same depth in the neighborhood of 1300 m $\sim$ 1500 m. Off-axis geometry, boundary conditions and absorption or losses are not considered by this model.

4.7 Multiple–Profile Ray–Tracing Program

From the introduction of this chapter, rays propagating in the ocean are affected by such factors as depth, sound speed, boundary conditions and temperature. These factors are also interrelated. The isovelocity and the Munk and Wunsh ray tracing approaches do not take into account all of the different parameters, and the resulting models do not represent the real behavior of sound propagating in the ocean. These methods are relatively simple due to the closed form nature of the different expressions. However, the major drawback lies in the assumptions and the simplistic model used. Several techniques are available, and have been applied in propagation studies. Most widely used at the current time is computer modelling where a mathematical model of the ocean is set up and solved by a computer program. Due to the complex structure of the ocean, there exists an inherent difficulty in realistically modelling it. Consequently, the result of these computer techniques

will be closely tied to the completeness of the parameters considered by the program. In this section, the ocean model used by the Multiple–Profile Ray–Tracing Program (MPP) will be described [31,45]. A sample input scenario along with the output results will be presented.

The Multiple–Profile Ray–Tracing Program represents a more complete and realistic ray tracing and modelling technique. This software package attempts to make use of the maximum number of available parameters to render a realistic and complete view of ray propagation in the ocean. This is accomplished at the expense of a high computational load. The MPP package uses the following parameters in its modelling of the ocean:

- The position of the source and the receiver as a function of range-depth coordinates.
- The sound speed profile as a series of depth versus sound speed points.
- Multiple sound speed profiles.
- Bathymetric points.
- Absorption coefficient.
- Surface and bottom reflection losses.
- Surface duct propagation losses.
- Earth curvature correction.

It is evident that this model offers improvements over the two previous ray tracing approaches, with respect to the following:

- No restrictions are imposed on the location of the source and the receiver.
- Better modelling of the sound speed profile with the option of being range-dependent.
- Accounts for the temperature effect and the boundary conditions.

Using such a technique, it is possible to trace, with an iterative method, all the rays between two points at arbitrary locations. The initial angle, arrival angle, total travel time and propagation loss are among the parameters calculated by the program. A description of the main parameters of the MPP program is given in the next section. This is followed by an outline of the steps performed by the program on the input data file to yield the desired values.

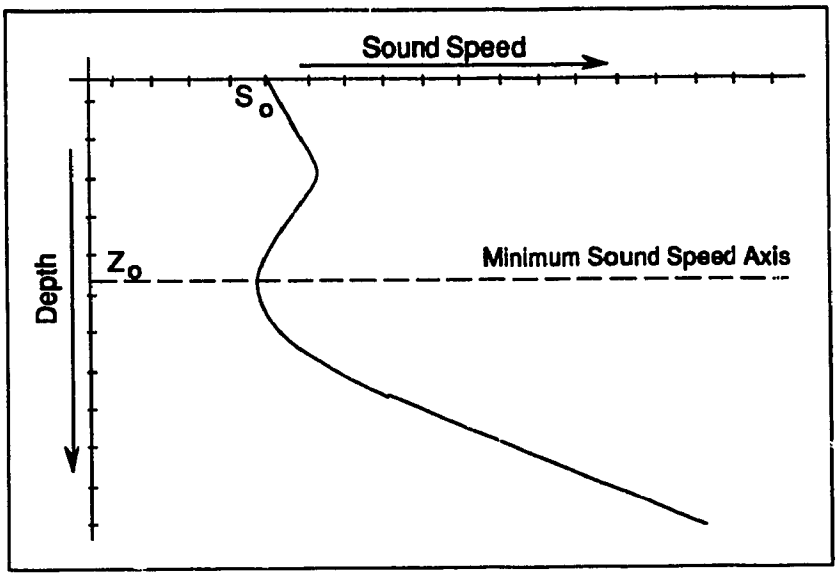

Figure 4.5: Complex sound speed profile

4.7.1 Model Description

Position of Source and Receiver (target)

Contrary to the Munk and Wunsh model where both source and receiver were positioned at the minimum sound speed depth, in the MPP program, the depth of the source and receiver are two independent parameters expressed in meters from the ocean surface. Two additional parameters representing the range of the source and receiver with respect to a fixed reference point, such as the position of an observer, are required; these values are given in kilometers.

Sound Speed Profile

The second input parameter to the program is the sound speed profile. In the isovelocity ray tracing model, the sound speed was assumed constant in both the vertical and horizontal layer. In the work by Munk and Wunsh, a linear and a quadratic mo' ' -re used to represent the sound propagation in the ocean. The quadratic model is adequate but cannot be used to model complex profiles such as the one illustrated in Fig. 4.5 since a closed form expression describing the profile is not available. In the MPP program, the sound

speed profile consists of a series of depth versus speed coordinates. Using this approach, arbitrary and complex profiles can be modeled, including the constant (isovelocity), bilinear and quadratic. Complex profiles can be described by introducing a large set of coordinates. Range dependent profiles represent a feature of the MPP program. Over a considerable distance, several sound speed profiles can be specified each with its respective range. An option is also available to generate a number of interpolated profiles between two consecutive ones.

Bathymetry and Bottom Loss

A number of bathymetric points can be included in the input model and are expressed in terms of range and depth, thus taking into account the temperature's effect on the sound speed. Bottom loss information can be specified for various types of sediments and range domains. Over a given distance, the ocean floor can be divided into regions. These regions are called domains and for each domain the loss is specified for the different angles that a ray can form with the bottom. The angles considered by the MPP program are the critical, grazing and normal angle.

Other Parameters

The previously mentioned parameters are mainly used to build the ocean model. This model will be used in the ray-tracing process where all the rays between the source and receiver are computed. In some instances, this number of rays can be quite large, and will require a very high computational load. Additional input parameters are required to bracket the range of rays. Two angular values $\theta_{\min}$ and $\theta_{\max}$ with respect to the horizontal plane are needed to form a range of angles of interest where the eigenray search will take place. Being an iterative process, a number a rays are *shot out* from the source. These rays are then traced to the receiver. The larger this number, the smaller the search grid, and the longer the program will need to run to completion. Two parameters must be specified to control the execution of the program. The first is the number of rays included between $\theta_{\min}$ and $\theta_{\max}$, used in the search procedure. The maximum number of iterations must be also be specified. Since exact results are very difficult to achieve in an iterative process, minimum and maximum tolerances can also be fixed for various parameters to introduce a form of flexibility. Having assembled all this information in an input file, the MPP program

is invoked. The execution of the MPP program can be described as a five step procedure:

Pass 1 The input file containing the ocean profile, the source and receiver information and the different MPP parameters is read. The information is grouped and several files are created to be used by the remaining modules of the program.

Pass 2 The ocean model is built from the input data file by first reading the sound speed profiles. All the data is read in and checked for errors. The bottoms are extended to a depth of 10000 m. Bottom loss information is assembled and introduced in the profile and the data is written to disk. Profiles are then read in pairs. If two consecutive profiles are the same and connections between the different layers are properly specified, then rectangularization of the region can proceed and the ocean can be regarded as a series of layers. If two profiles are not the same, then the range depth plane is divided into triangular regions and the gradient for each region is then calculated. If specified, spherical earth correction is considered and finally the regions are written to disk.

Pass 3 This pass is concerned with the identification of all the ray pairs that travel the specified range and reach the receiver. The data is read and the initialization procedure is started. With the range-depth plane divided into sectors, the location of the source and the receiver in terms of sectors must first be determined. As the ray is being traced through the different sectors, the intersection with sector boundaries is computed. A test is made as to whether the ray reached the bottom. The nature of the reflection, the grazing angle and the bottom-reflection loss (in dB) of a ray striking the bottom at angle θ and range r is computed. An arrival test is also performed to verify the position of the ray with respect to the desired arrival range. The velocity of the sector is then calculated and the travel time between the current and the previous point on the ray trajectory is computed. This is followed by an update of ray transmission loss value. A test is performed to verify if the ray should be cut. This step is initiated if the maximum transmission loss specified by the user (150 dB) was exceeded, the ray angle was too steep or the ray turned back. The processing of the arrival information for each ray then follows and data is written to disk.

Pass 4 In the previous pass, each ray pair was marked with one of eight identifiers (e.g. ray crossed receiver depth, badly bracketed receiver, good diffraction field, etc. ...)

Parameter	value
Source depth	1200 m
Receiver depth	1200 m
Source–receiver separation	150 km
Minimum angle in eigenray search	2°
Maximum angle in eigenray search	30°
Number of rays shot out from source	50
Number of passes allowed	10
Number of sound speed profiles	2
Number of layers in sound profile	20

Table 4.4: Sample MPP parameters

This information is used to sort the rays and discard those with bad results. Only two types of rays are saved: those with a good diffraction field indicating that the ray travelled the exact range but did not necessarily reach the receiver depth, and those that reached the receiver or fell within the acceptable receiver tolerance.

Pass 5 Finally, the remaining information is sorted on different criteria (order of decreasing initial angle, order of increasing travel time and order of increasing transmission loss) and appropriate output files are created.

4.7.2 Sample Ray–Trace

A sample run of the Multiple–Profile Ray–Tracing Program is presented in this section. The different rays travelling from the source to the receiver are traced and the results are presented graphically as a ray diagram. The field consists of a source and a receiver, both situated at a depth of 1200 m and separated by a range of 150 km. 50 rays are *shot out* from the source. Under ideal conditions all the rays radiating from the source, in a circular range of 360°, should be traced. However, since the procedure is computationally intensive, a subset of this angular range was used. With the horizontal plane serving as a reference, the rays having an initial angle between 2° and 30° were considered. The result is a subset of the full ray field, sufficient for the purposes of this example. Being an iterative process, the maximum number of iterations is specified as 10 and two equal sound speed profiles are used. One loss domain and two bathymetric points are also considered. The different parameters are illustrated in Fig. 4.6 and summarized in table. 4.4.

A commented version of the sample input is presented in Fig. 4.7 to show the format of the input data required by the MPP program. In this file, the depth of the source and the receiver are specified in meters. The range information follows along with the range of angular values of interest. Several parameters are also included in order to control the exhaustive nature of the process. The number of sound speed profiles are then listed as a series of depth versus speed coordinates. Any number of profiles can be included to add more realism to the overall scenario. Finally the bathymetry information and the different reflection coefficients are specified. Various other parameters controlling the tolerance used by the MPP program can also be modified. They include the vertical and horizontal minimum miss distance, the maximum error allowed in the time computation, the minimum angle separation and the maximum transmission loss. These values however are specified in the different source code modules and changing them necessitates a recompilation of the FORTRAN code.

Following the completion of the program, the resulting ray information (total travel time, initial angle, arrival angle and transmission loss) is presented in Table 4.5. From the information presented in the table it is possible to observe that 25 rays were traced between the source and the receiver. These rays fall within the specified angular limits of 2° and 30°. The transmission loss in column 4 gives an indication of the attenuation suffered by the propagating signal in the channel under consideration. The corresponding ray diagram of ray trace between the source and the receiver is presented in Fig. 4.8. Only a subset of the 25 rays resulting from the MPP program are present in this figure. They are the rays numbered 11 to 17 in the result table. The remaining rays are excluded from the figure for reasons of clarity. From the figure, it is evident that some of the rays have undergone a surface reflection. The arrival structure of the rays along with the travel time will be most useful in the matched field processing presented in the next chapter. This information will be used to evaluate, in a real ocean environment, the performance of the coherent and incoherent approaches.

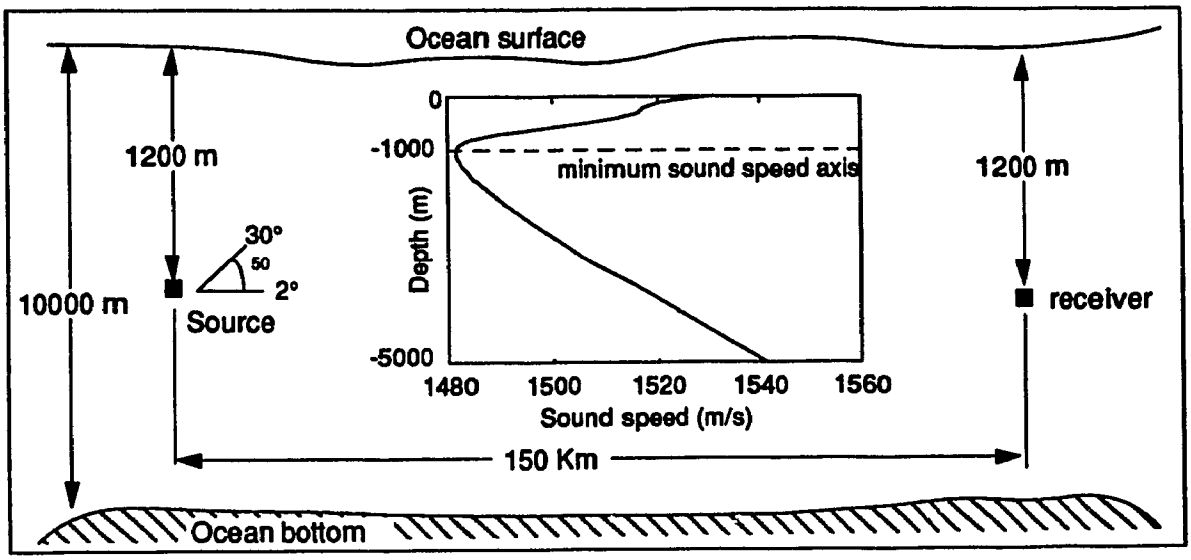

Figure 4.6: Profile of the sample MPP run

	Travel time (sec)	Init. angle (deg)	Arriv. angle (deg)	Loss (dB)
1	112.8119	29.8441826	29.8489415	106.1
2	110.5390	27.7130218	-27.7172588	106.0
⋮				
11	101.3511	16.4476696	16.4448006	109.7
12	100.4757	12.3630368	-12.3598561	117.6
13	100.4756	12.3167661	-12.3136147	112.1
14	100.9267	10.8160421	10.8147401	102.6
15	101.0691	9.5530824	-9.5529797	101.8
16	101.2038	4.9009048	4.9354433	99.9
17	101.2104	3.2015784	3.2992357	103.0
⋮				
24	101.1087	2.9340165	0.0911641	96.0
25	101.1442	2.8521036	-0.1114116	70.3

Table 4.5: Sample results sorted in order of decreasing initial angle

```
 This is a Sample run for MPP2 - MPPTEST.DAT
1200. 1200.                    Source Depth, Receiver (Target) Depth (m)
0.    150.                     Source Range, Receiver Range (km)
2.0  10.0                      Min. Ray Angle, Max. Ray Angle (deg)
-50 10 150 50                  # of Rays, Max. Passes, Max. Reflections, bottom
 1    1                        No curvature correction, Yes print connections
 2                             # of Range Profiles to follow
 0.0  20    2                  Range #1 (km), # of layers, # interp'd profiles
   0.0  1529.57                Depth (m), Soundspeed
 100.0  1520.32                  :          :
 200.0  1517.26                  :          :
 300.0  1516.11
   :      :
2000.0  1490.49
3000.0  1505.99
4000.0  1523.12
5000.0  1541.04
  3                            Number of connections
  1 1                            Connection - layer 1 to 1
  6 6                                  :           6 to 6
  9 9                                  :           9 to 9
 1010.0  20    0                Range #1 (km), # of layers, # interp'd profiles
   0.0  1532.57                Depth (m), Soundspeed
 100.0  1522.32                  :          :
 200.0  1519.26                  :          :
 300.0  1518.11
   :      :
2000.0  1492.49
3000.0  1507.99
4000.0  1525.12
5000.0  1543.04
2  1  2                        # Bathymetric pts, # loss domains,type
0     5000.0                   Range (km), Depth (m)
1010  5000.0                     :          :
0.0                            Starting range (km) of Bottom Loss Domain
0.0  0.0  90.0  0.0            Crt. ang., loss@graz,loss@crit,loss@norm
```

Figure 4.7: MPP sample input file

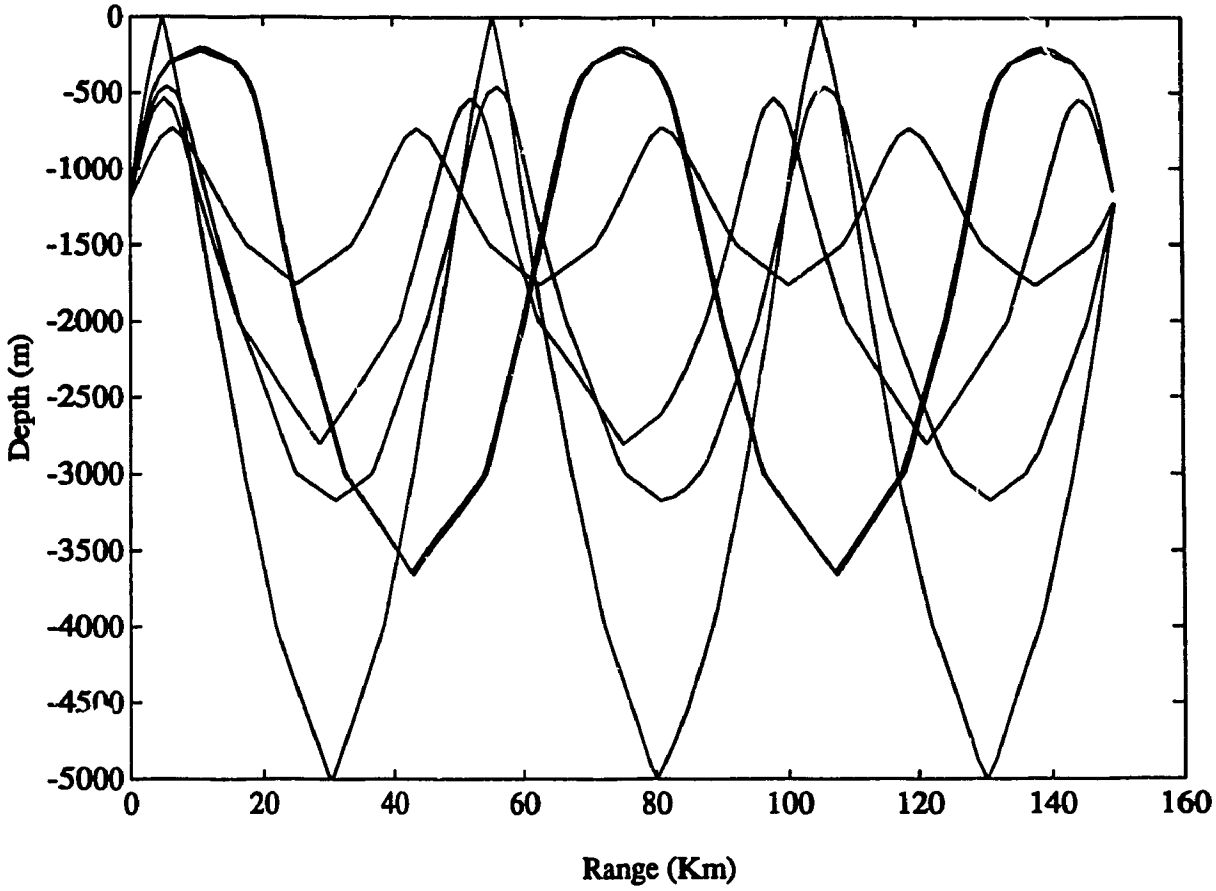

Figure 4.8: Ray diagram generated by the MPP program

Chapter 5

Matched–Field Processing

5.1 Introduction

Conventional beamforming is an effective approach to the localization of an underwater source when the received signal consists of a few plane waves. However, a more general approach is required to handle the complex field case that arises in the ocean at moderate ranges [3]. Matched–field processing is a parameter estimation technique for localizing an underwater source from its signal field, pro. . .ing in a acoustic wave guide [1]. The matched–field processor takes the same form as traditional estimators (e.g. the Blackman–Tukey, the Minimum Variance or the Normalized Maximum Likelihood method), except that the plane wave replica vector is replaced by a replica vector derived from a propagation model [38]. The one dimensional (1D) hypothesized bearing beamformer is now replaced by a three dimentional look position (range, bearing and depth), by exploring the complete propagation characteristics of the ocean channel.

Traditional Matched–Field Processing methods such as the Coherent MV method use complete pressure field model with its two main components: the arrival structure of the rays at the receiver and the relative travel time delay. These two quantities are the direct result of the solution of the wave equation. Best results are achieved in matched–field processing when the *a priori* information concerning the acoustic medium is complete and as close as possible to the real conditions. This information is not readily available and fluctuates on a constant basis. It was found by Krolik *et al* [21] that the coherent approach to MFP is very sensitive to any errors in the relative time delay structure.

Two approaches to increasing the stability and robustness of the matched–field

processor are possible. The first such approach is to concentrate on the physical nature of the acoustic medium in order to collect the maximum amount of information necessary for the coherent MFP method. This alternative is not very practical due to the complex nature of the medium. The second approach, proposed by Krolik *et al*, suggest the use of a higher resolution estimator combined with only the arrival structure information of the pressure field model. The result is a high resolution MFP that is more robust to changes in the medium profile. Rather than using the coherent matched–field processor with the full pressure field model resulting in a highly sensitive to mismatch method, the combination of the incoherent method with less acoustic information results in a more robust processor. A trade–off between the completeness of the model and the robustness of the processor exists.

In this chapter, the coherent matched–field processor is presented. It represents a general estimator utilizing the complete pressure field model. A new approach, the incoherent approach formulated by Krolik *et al* is then presented for the case of the Minimum Variance or Rayleigh estimate of order 1. The two methods are then compared in a real ocean environment using the MPP ray tracing program in an attempt to verify and confirm their respective robustness.

5.2 Pressure Field Model

In this section the model used in the development of the coherent and incoheren matched–field processors will be presented. The pressure field model describes the acoustic pressure field at the receiver, as a function of the arrival structure of the rays and the relative delay. The difference between the two processors lies in the amount of model information each processor uses.

An M–sensor horizontal array is used for the detection process. In the cylindrical coordinates system the vector $\Phi = (r, z, \phi)$ will be used to describe the position of the element of interest as a function of range, depth and bearing. Sound can travel in the ocean through a number of different paths, a phenomenon known as multipath which represents a fundamental aspect of the present development. With L denoting the maximum number of paths. From Chap. 2, the received signal at the array, at time t and sensor m, is described as

$$x_m(t) = s(t - \tau_m) + n_m(t) \tag{5.1}$$

where $s(t)$ represents the signal component, $n_m(t)$, the added noise and τ_m, the propagation

delay to sensor m of the ray. This expression can now be extended to the general case of L multipath arrivals $l = 1, \ldots, L$. From the frequency domain approach, the signal received at sensor m is now given by

$$Y_m(\omega) = \sum_{l=1}^{L} S_l(\omega) a_l(\Phi) e^{-j\omega\tau_{lm}} + N_m(\omega) \tag{5.2}$$

The parameter τ_{lm} represents the total propagation delay of the l–th path to the m–th sensor. From Eq. 2.7, adding the multipath component to the expression and using the first sensor ($m = 0$) as the reference, results in

$$\tau_{lm} = \tau_{l0} - m\varphi_l(\Phi) \tag{5.3}$$

$$= \tau_{l0} - \frac{m\ell \sin\phi \cos\theta}{c} \tag{5.4}$$

In the above equation, θ is the elevation angle formed between the ray and the horizontal plane and $\varphi_l(\Phi)$ is the delay of the l–th path through the array. For the narrowband case considered here, the dependency of the various terms on the frequency component will not be shown explicitly. Since the signal and noise are uncorrelated, it was shown in section 2.2 and [26] that the correlation matrix can be expressed as the sum of the individual correlation matrices, more specifically that of the signal and the noise. Considering the case where all the multipath arrivals are correlated, the correlation matrix $\mathbf{R}$ is written as

$$\mathbf{R} = \mathbf{R}_N + \sigma_s^2 \mathbf{p}(\Phi)\mathbf{p}^*(\Phi) \tag{5.5}$$

With the above information at hand, the objective is to find $\hat{\Phi}$ for which the new hypothesized steering vector $\mathbf{p}(\omega, \hat{\Phi})$ matches the true $\mathbf{p}(\omega, \Phi)$. The vector $\mathbf{p}(\omega, \Phi)$ represents the $M \times 1$ vector of pressures at each sensor in the array such as

$$\mathbf{p}(\omega; \Phi) = [p_0(\omega; \Phi), p_1(\omega; \Phi), \ldots, p_{M-1}(\omega; \Phi)]^T$$

In the case of the minimum variance spectral estimator, the processor is described by

$$\mathcal{Z}_{MV}(\omega; \hat{\Phi}) = \frac{1}{\mathbf{p}^*(\omega, \hat{\Phi})\mathbf{R}^{-1}(\omega)\mathbf{p}(\omega, \hat{\Phi})} \tag{5.6}$$

When the received signals at the array are equal such that $S_l(\omega) = S_1(\omega)$ for $l = 2, \ldots, L$, Eq. 5.2 is rewritten as

$$\mathbf{V}(\Phi)\mathbf{a}(\Phi) \tag{5.7}$$

where $\mathbf{V}(\Phi)$ is the $M \times L$ matrix of steering vectors defined as

$$\mathbf{V}(\Phi) = [\mathbf{v}(\omega, \varphi_l(\Phi)), \mathbf{v}(\omega, \varphi_l(\Phi)), \ldots, \mathbf{v}(\omega, \varphi_l(\Phi)),] \tag{5.8}$$

and having as individual columns the steering vector of the l–th arrival expressed as

$$\mathbf{v}(\omega, \varphi_l(\Phi)) = [1, e^{\jmath\omega 1\varphi_1(\Phi)}, \ldots, e^{\jmath\omega(M-1)\varphi_1(\Phi)}]^T \tag{5.9}$$

The vector $\mathbf{a}(\Phi)$ is the $L \times 1$ vector of complex coherence between paths written as

$$\mathbf{a}(\Phi) = [a_1(\Phi)e^{-\jmath\omega\tau_1(\Phi)}, a_2(\Phi)e^{-\jmath\omega\tau_2(\Phi)}, \ldots, a_L(\Phi)e^{-\jmath\omega\tau_L(\Phi)}]^T \tag{5.10}$$

The hypothesized direction vector can now be defined as

$$\mathbf{p}(\Phi) = \mathbf{V}(\Phi)\mathbf{a}(\Phi) \tag{5.11}$$

In the various analysis throughout this work, the different projection vectors were normalized to have unit length. Using the same concept, the unit length replica vector $\mathbf{p}(\Phi)$ for a source at location Φ, is given by:

$$\mathbf{p}(\Phi) = \frac{\mathbf{V}(\Phi)\mathbf{a}(\Phi)}{|\mathbf{V}(\Phi)\mathbf{a}(\Phi)|} \tag{5.12}$$

The vector function $\mathbf{p}(\Phi)$ represents the true source location parameters space. The matrix $\mathbf{V}(\omega)$ determines the coefficient of the set of linear equations relating the predicted power field $\mathbf{p}(\Phi)$ to the function $\mathbf{a}(\Phi)$.

5.3 Coherent Matched–Field Processing

From the previous development, a new steering vector $\mathbf{p}(\Phi)$ was presented. Using this direction vector, the matched–field processor can now be defined. From the results presented in chap. 2 of this work, it was shown that given the array correlation matrix $\mathbf{R}$ and $\mathbf{w}$, the weight vector for a general processor, the matched–field processor array power response function is given by

$$\mathcal{Z}(\hat{\Phi}) = \mathbf{w}^*\mathbf{R}(\Phi)\mathbf{w} \tag{5.13}$$

Several processors can result by introducing a different definition for the weight vector $\mathbf{w}$. For the Blackman–Tukey method, this vector is equal to the direction or hypothesized vector such that

$$\mathbf{w} = \mathbf{p}(\hat{\Phi})$$

The resulting spacial spectral estimate is

$$\mathcal{Z}_{BT}(\hat{\Phi}) = \mathbf{p}^*(\hat{\Phi})\mathbf{R}(\Phi)\mathbf{p}(\hat{\Phi}) \tag{5.14}$$

Similarly, for the Capon Minimum Variance processor, the beamformer weight vector is expressed as

$$\mathbf{w} = \frac{\mathbf{R}^{-1}(\Phi)\mathbf{p}(\hat{\Phi})}{\mathbf{p}^*(\hat{\Phi})\mathbf{R}^{-1}(\Phi)\mathbf{p}(\hat{\Phi})}$$

and the resulting estimate is

$$\mathcal{Z}_{MV}(\hat{\Phi}) = \frac{1}{\mathbf{p}^*(\hat{\Phi})\mathbf{R}^{-1}(\Phi)\mathbf{p}(\hat{\Phi})} \tag{5.15}$$

Expanding these results to the Rayleigh family of spectral estimates in terms of the pressure field model, the following expression is obtained

$$\mathcal{Z}_{RE}(\hat{\Phi}) = \frac{\mathbf{p}^*(\hat{\Phi})\mathbf{R}^{-(q-1)}(\Phi)\mathbf{p}(\hat{\Phi})}{\mathbf{p}^*(\hat{\Phi})\mathbf{R}^{-q}(\Phi)\mathbf{p}(\hat{\Phi})} \tag{5.16}$$

where q is know as the order of the Rayleigh estimate. The various methods presented are based on coherent matched–field processing. An estimate of the actual source location vector Φ is obtained by introducing the hypothesized location vector $\hat{\Phi}$. Coherent matched–field processing consists of finding $\hat{\Phi}$ for which the hypothesized direction vector $\mathbf{p}(\hat{\Phi})$ best matches the true direction vector $\mathbf{p}(\Phi)$.

In the coherent model, a priori knowledge of $\mathbf{V}(\hat{\Phi})$ and $\mathbf{a}(\hat{\Phi})$ is required to generate the hypothesized direction vector $\mathbf{p}(\hat{\Phi})$. The difficulty in coherent matched–field processing occurs when the propagation model used to generate the hypothesized direction vector differs from the true ocean model. The sensitivity of the various coherent matched–field processor was demonstrated in Chap. 3 by studying the effect of a mismatch between the hypothesized and the true direction vector on the resulting estimate. It was shown in Chap. 2 that the received signal has mainly two components: an elevation angle with respect to the horizontal plane and a travel time or relative delay. Expressions were derived to compute the relative delay between different multipath arrivals. This delay is:

$$\tau_m = \tau_0 - \frac{m\ell \sin\phi \cos\theta}{c} \tag{5.17}$$

Due to the structure of both $\mathbf{V}(\hat{\Phi})$ and $\mathbf{a}(\hat{\Phi})$ terms, small errors in the elevation angle will not seriously affect the model and will result in minor model mismatch. However, small

errors in the delay will result in phase errors that affect the vector $\mathbf{a}(\hat{\Phi})$ and lead to a serious degradation at the output.

To avoid the model mismatch, a new matched–field processor relying only on the arrival structure was proposed by Krolik *et al* [21]. The angle of arrival information is used in the matched–field processor regardless of the correlation between the different arrivals. The new approach is known as the incoherent method and will be presented next.

5.4 Incoherent Matched–Field Processing

The incoherent approach to matched–field processing was originally reported by Krolik *et al* [21]. It corresponds to multiple linear constraints in the multipath arrival direction. When applied to the minimum variance or Rayleigh estimate of order 1, it can be expressed as the following minimization problem

$$\textbf{minimize} \quad \mathbf{w}^*\mathbf{R}(\Phi)\mathbf{w} \tag{5.18}$$

$$\textbf{subject to} \quad \mathbf{V}^*(\hat{\Phi})\mathbf{w} = 1_L \tag{5.19}$$

Only the $\mathbf{V}(\hat{\Phi})$ $M \times L$ matrix is used in the constraint. The optimum weight vector that satisfies the above condition is given by

$$\mathbf{w}_{opt} = \frac{\mathbf{R}^{-1}(\Phi)\mathbf{V}(\hat{\Phi})}{\mathbf{V}^*(\hat{\Phi})\mathbf{R}^{-1}(\Phi)\mathbf{V}(\hat{\Phi})}\, 1_L \tag{5.20}$$

Substituting the above expression into the minimization problem will yield the desired spectral estimate. Two issues were considered in the derivation of the incoherent matched–field processor. Often the columns of $\mathbf{V}(\hat{\Phi})$ are nearly colinear resulting in a nearly singular term in the denominator of the optimum vector. This is resolved by using a pseudo inverse of smaller rank equivalent to only using the most significant eigenvectors. The second issue arises in a white noise environment. Although not very practical in a real ocean model, when the noise field is white, the beamformer power output will vary with the field Φ. The problem is avoided by normalizing the output by the norm of $\mathbf{w}_{opt}$. Taking these two issues into account, the resulting incoherent processor is expressed as

$$\mathcal{Z}_{MV}(\hat{\Phi}) = \frac{\mathbf{w}_{opt}^*\mathbf{R}(\Phi)\mathbf{w}_{opt}}{\mathbf{w}_{opt}^*\mathbf{w}_{opt}} \tag{5.21}$$

5.5 Comparative Results

Having presented the coherent and incoherent approaches to matched–field processing, the main objective of this section is to verify the robustness of each method. Rather than using a hypothetical ocean model, the MPP program presented in the previous chapter will be used to generate the necessary information. Therefore, the combination of a real ocean model with both matched–field processing approaches can be used as a serious measure of performance. The procedure used in this comparative study will first be described. The various results will follow and any observations and conclusions will then be presented. A one dimensional approach in range only was chosen over the two dimensional ambiguity surface of range and depth due to the large computational load involved in the ray tracing operation.

The scenario used by the MPP program is described in Table 5.1 and also illustrated in Figure 5.1. An imaginary source was introduced at a range of 60 km and the area of interest covered the range from 20 km to 80 km. Starting at one end, the MPP program was used to generate the ray traces for the specified range. This necessitated modifying the MPP program to allow it to run continuously and sweep over a specified range of interest. For each range of interest, the location of the receiver was then incremented by a value varying between 100 m and 1 km, thus sweeping was performed at irregular intervals. The result was 185 files covering the entire range of interest. Using these files, a specified range vector and the original profile, the match field processing program was able to extract the arrival structure and compute the relative time delay. In this experiment, the same information was used to build the original field and in the detection process. The two processors (coherent and incoherent) were applied to the resulting data and the final results are presented in Fig. 5.3. From the figure, it is possible to observe that both methods exhibit a peak at 60 km, an indication of the presence of the source. Also, the power level at the location of the peak is higher for the coherent MFP.

In the second part of the experiment, the objective is to observe the behavior of both processors when a perturbation is applied in the data. An *error* was introduced in the sound speed profile and a new set of ray traces was generated with the MPP program. The pressure field with the source at 60 km was generated using the information from experiment 1 and the detection would take place using a field generated from the new set of files. This approach is equivalent to the presence of an error in the assumed value of any

Parameter	value
Source depth	400 m
Receiver depth	75 m
Source–receiver separation	60 km
Minimum angle in eigenray search	−60°
Maximum angle in eigenray search	+60°
Number of rays shot out from source	120
Number of passes allowed	10
Number of sound speed profiles	2
Number of layers in sound profile	20

Table 5.1: MPP parameters used to form the ocean model

parameter. For each range specified in the range vector of interest, and similar to the first experiment, the corresponding file was read and the arrival structure and delay information were extracted. The results of the two methods are presented in Fig. 5.4. It is evident from the figure that the coherent MFP behaved poorly, whereas the incoherent processor successfully detected the presence of the source.

A comparison of the coherent versus the incoherent for both experiments is presented in Fig. 5.5. The small change in the sound speed profile affected the relative time delay between ray arrivals, and consequently the performance of the coherent matched–field processor. Since the incoherent matched–field processor relies only on the arrival structure (i.e. the matrix $\mathbf{V}$), its performance is not affected by the change introduced in the sound speed profile. With the ocean or medium characteristics unknown a priori, the use of the two fields techniques constitute a close approximation to a real life case, where the assumed model does not match the real underlying one. It is possible to conclude that the incoherent MV is a matched–field processor more robust to model mismatch under realistic conditions than the coherent MV.

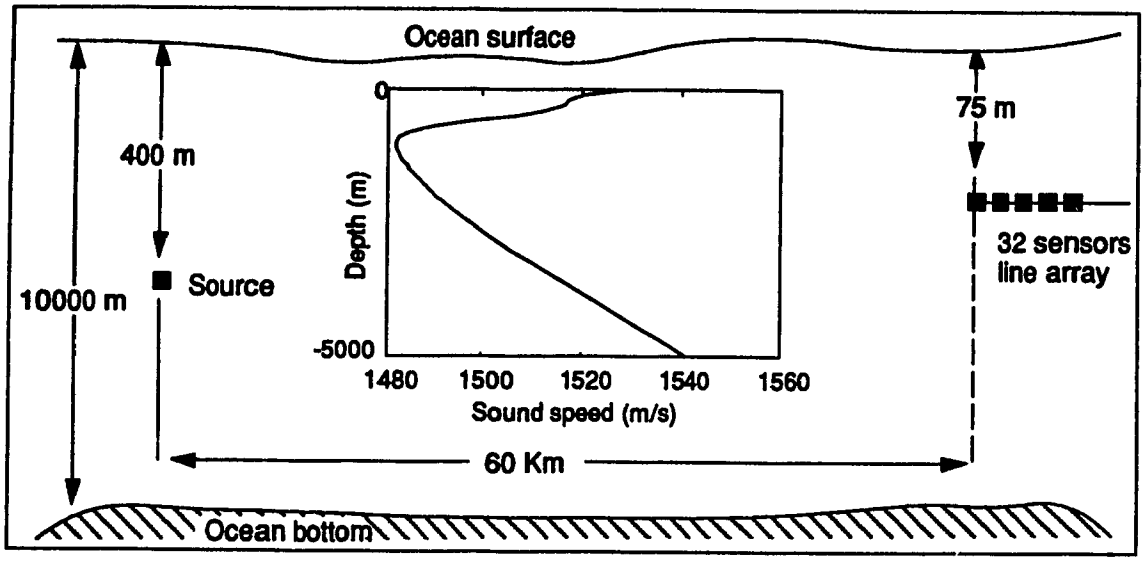

Figure 5.1: Scenario used by the MPP program

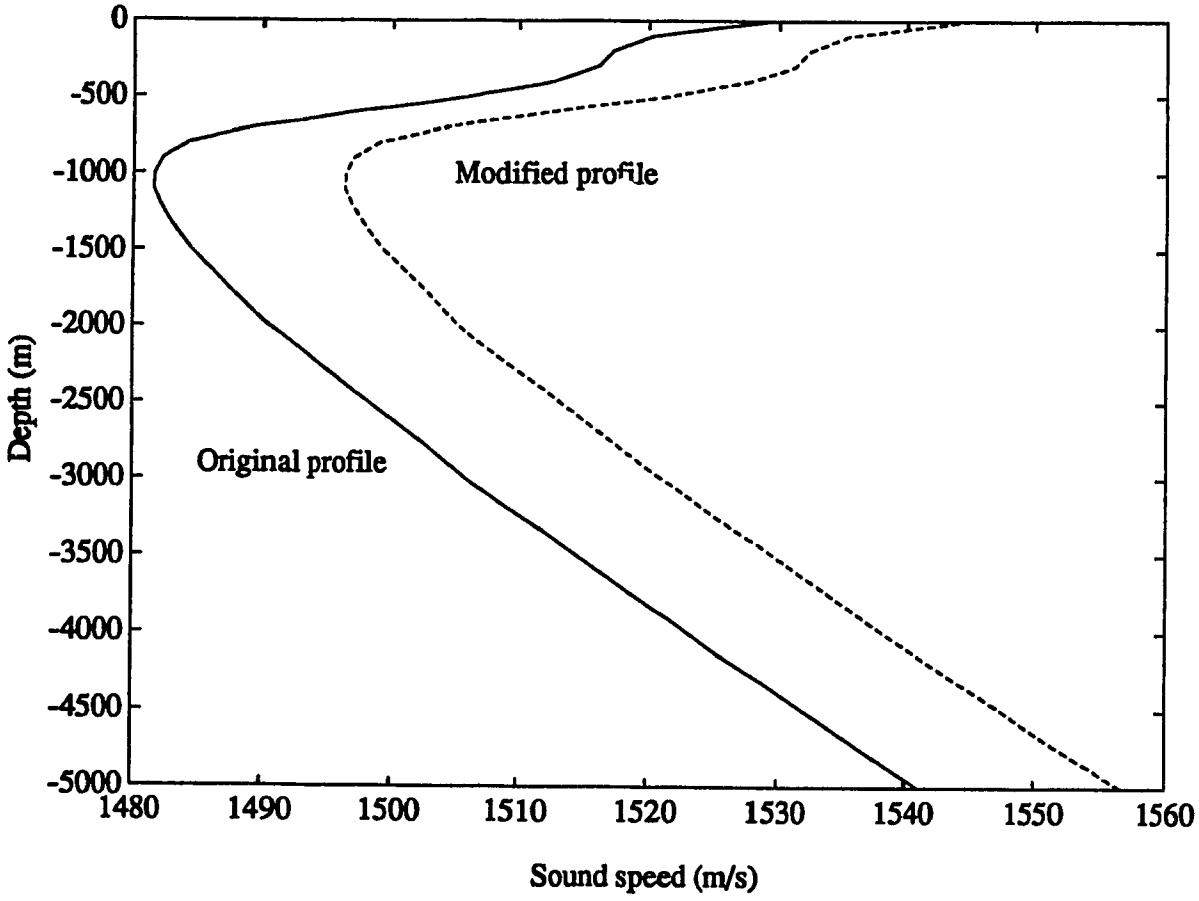

Figure 5.2: Original and modified sound speed profiles

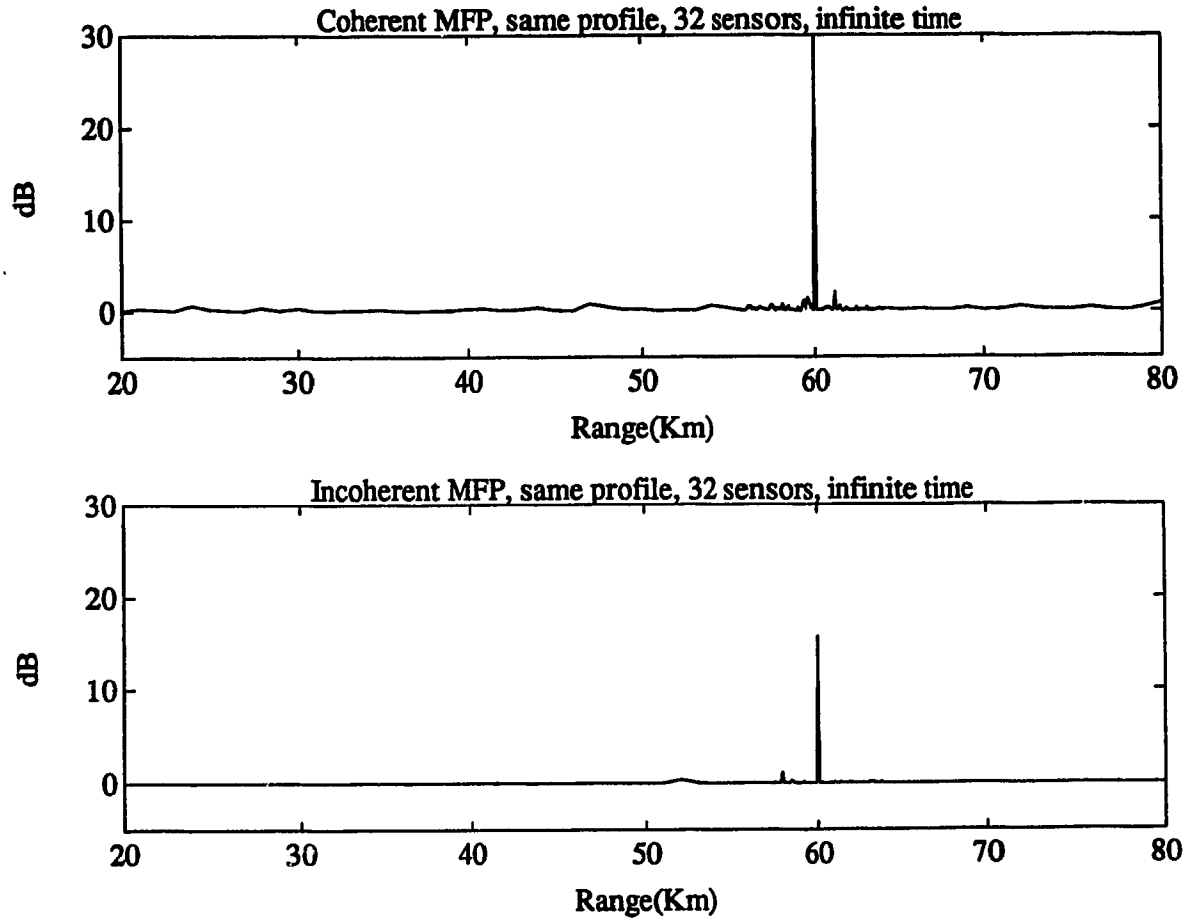

Figure 5.3: Coherent vs. Incoherent MFP, same field

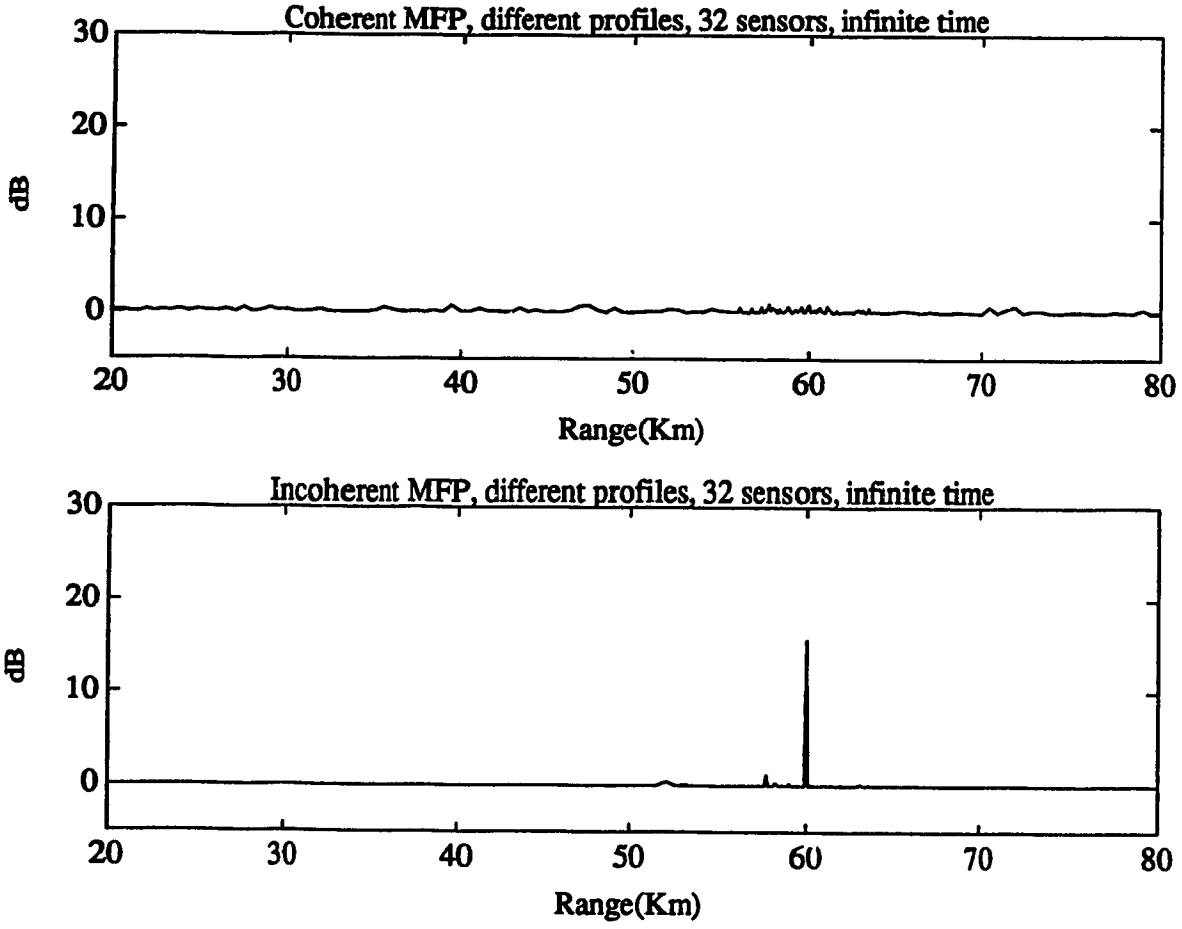

Figure 5.4: Coherent vs. Incoherent MFP, different fields

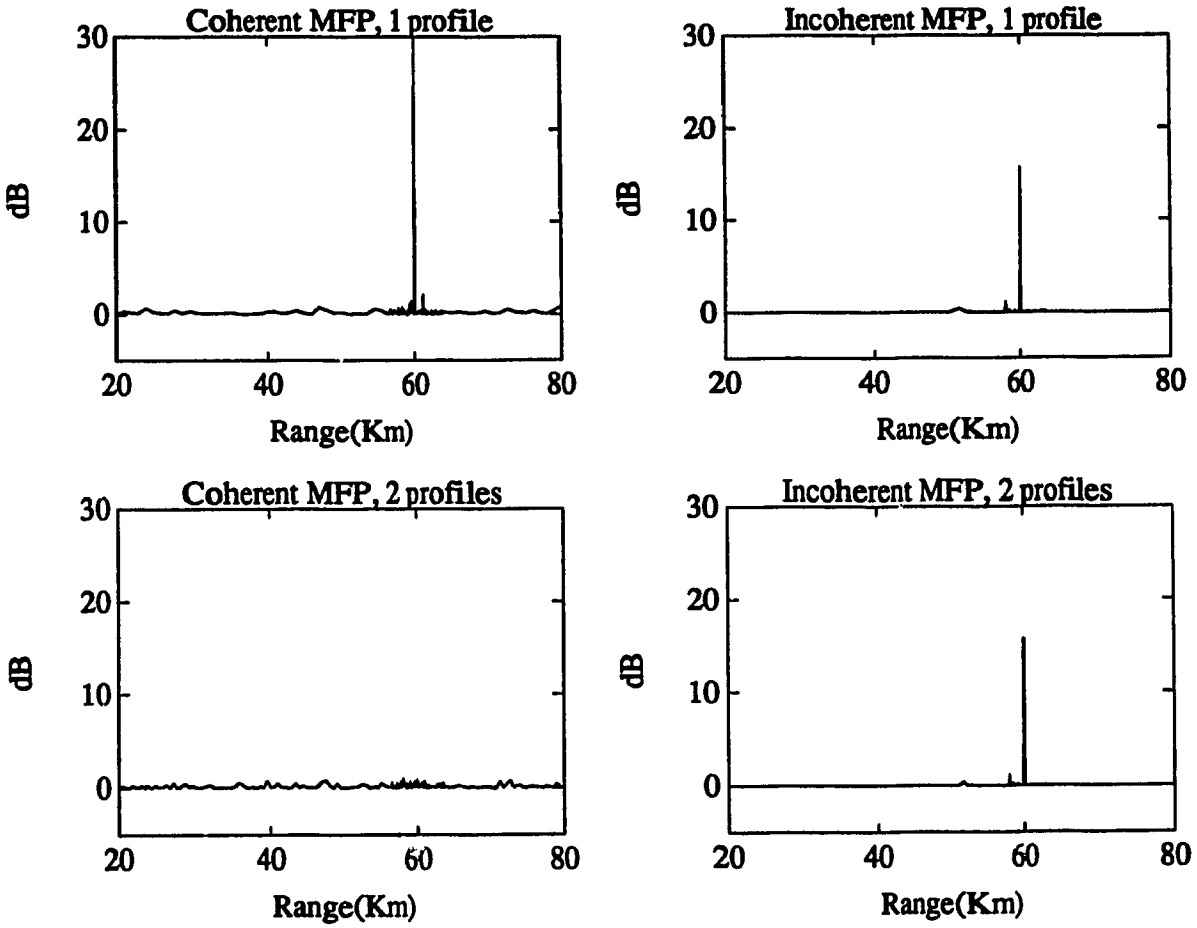

Figure 5.5: Comparison of the Coherent & Incoherent MFP responses

Chapter 6

Conclusion

In a very rapidly evolving field, new approaches to spectral estimation are presented at a tremendous rate, each with their own set of advantages, disadvantages and restrictions. One such method, the Rayleigh family based on original work by Lagunas, was studied in this work. It was motivated by an interesting property of this family of spectral estimates: the resolution is user-controlled. The present work evolves around the investigation of the properties and characteristics of the Rayleigh family of spectral estimates. This family includes as its first three members: the Blackman–Tukey, the Capon Minimum Variance and the Normalized Maximum Likelihood estimators. The output spectrum, the bandwidth used as a measure of resolution and the sensitivity to mismatch are the three main properties investigated in the first section of this work. For loss of generality, the analysis and the resulting derived expressions are order-independent. They could be used with any member of the Rayleigh family. This approach also enables the easy modelling of any member of the Rayleigh's properties on a computer. The different derived expressions are always functions of three parameters: the signal-to-noise ratio, the number of elements in the array and the order of the estimate. A trigonometric approach was used to better visualize the behavior of the different estimators in the spatial domain.

The generalized angle introduced by Cox was used in the various expressions to visualize any discrepancies between the hypothesized and the true direction vector. A closed form expression representing the output spectrum of Rayleigh family was derived. Working within a context of array signal processing and more specifically in the area of source localization, two cases of interest were further investigated: the matched case and the not matched case response. In the matched case response, the results indicate that when the

array is steered in the exact direction of the source, the different members of the Rayleigh family have the same output level. This peak value is a function of the signal-to-noise ratio and the number of elements in the array. For the not matched case response, the output level is bounded between the peak level and the noise power. An important property of the Rayleigh family observed in this analysis is that any given estimate is a bound for the next higher one. This could be considered as an increase in the measure of resolution and was investigated in further detail.

The resolution of a given estimator is an important criterion. Several definitions and measures exist and the one proposed by Lacoss was chosen for its general acceptance. The resolution of an estimate is given by the width of the main peak at the -3dB point. An expression was first derived for the Rayleigh estimate of order 1 and 2. This was further extended to the Rayleigh family for estimates of arbitrary order. As the order increases, the width of the main peak decreases, indicating an increase in resolution and supporting the bounded nature of the estimate observed in the analysis of the output spectrum. However, this increase is achieved at a high cost.

The sensitivity to mismatch was the third property studied in the Rayleigh family. This mismatch was expressed in terms of the generalized angle to demonstrate the percentage drop in the peak output level for different angular differences between the hypothesized and the true direction vector. The power ratio proposed by Gingras was used to measure the sensitivity and represents the ratio of the matched case response to that of the not matched case. Expressions for the two cases were readily available from the investigation of the output spectrum of the Rayleigh family. Forming and simplifying the ratio resulted in a closed form expression of the sensitivity of the Rayleigh family as a function of the generalized angle. As the order increases, the estimate becomes more sensitive to a small mismatch. This results in a sharp level drop at the output.

In the analysis of the main properties of the Rayleigh family it was assumed that the observation interval was of infinite length. However, in many real life situations shorter data segments are forced. The effect of using shorter data segments in the estimation process was investigated through Monte–Carlo simulations. The degradation observed in the resulting estimate indicates a dependency of the estimate on the size of the data segments. The sharper peaks (i.e. increase in resolution) previously recorded is achieved at the expense of longer data segments. As the segments become shorter, the observed performance degraded rapidly and below a certain threshold level, these results were discarded.

The asymptotic convergence and the effect of the order on the resulting estimate were also investigated. As the order increases and goes to infinity, the smallest eigenvalue of the correlation matrix becomes significant and forms a threshold for the non-matched case response. In the white noise case, this smallest eigenvalue was found to be equal to the noise power. The last property of the Rayleigh family considered was its asymptotic convergence. A matrix based analysis was conducted and properties of the eigenvalues were used. Results indicate that as the size of the correlation matrix goes to infinity, the Rayleigh family results in *true* power spectral density estimates.

Spectral estimation constitutes a basic element in matched-field processing where the plane wave vector is replaced by a vector derived from a propagation model. It explores the complete propagation characteristics of the ocean channel in an attempt to match the predicted field to the actual one. The modelling of the ocean plays an important role in this process. The closer the used model is to the real ocean conditions, the better the results achieved. Prior to the application of the Rayleigh family to matched-field processing, three different acoustic propagation models were considered ranging from the simplest to the most complete and complex.

The isovelocity model was first considered. In this simple model the sound speed is assumed constant in both the vertical and horizontal layer. Closed form expressions for the elevation angle with respect to the horizontal plane and the total travel time were obtained for any ray travelling from the source to the receiver. The second model investigated is the Munk and Wunsh model where the sound speed is expressed by either a bilinear or a quadratic profile resulting in a better modelling of the ocean. In both models mentioned so far, parameters such as the propagation loss and the boundary conditions were not considered. However in a real ocean environment these parameters play an important role. The last propagation model considered was the Multiple–Profile Program from the Wood Hole Oceanographic Institute. This numerical model considered most of the important criteria including multiple sound speed profiles, bottom and surface reflections and transmission losses. However the results were achieved at a high computational load.

With different propagation models at hand, the application of the Rayleigh family in matched-field processing was presented. The MPP program was combined with the Rayleigh estimate of order 1 to investigate its behavior in a real ocean environment. The performance was satisfactory and the source was detected at the correct range. The incoherent matched-field processor developed by Krolik was presented. This processor relies only

on the angle of arrival structure of the rays and is less sensitive to errors in the propagation model. The behavior of both coherent and incoherent processors in a real ocean model followed. When the same information was used to generate the field, and the detection of the source, both methods were capable of detecting the presence of the source at the correct range. Later, a small error was introduced in the model. Using this information, a second field was generated. The first one was used to form the source pressure field and the second field was used for the detection process. The coherent processor behaved poorly while the incoherent method was still capable of detecting the source.

The performance of the Rayleigh family in the presence of non-white noise and multiple sources was not considered in this work. A theoretical investigation of statistical performance of the Rayleigh family can also represent the basis for future work. Expressions for the mean and the variance combined with the Cramer–Rao bound can present a very robust way of bounding the resolution performance of the estimator. Better understanding of the trade-off between the order of the estimate, the bandwidth or resolution and the size of the observation interval will result. The incoherent approach to matched-field processing offers some promises for further development and could be extended to the different members of the Rayleigh family of spectral estimates. Investigation of the 2D (range and depth) or the full 3D (range depth and bearing) case can provide further insight on the behavior of these algorithms with various modelling techniques. Combining the user controlled resolution aspect of the Rayleigh family with new techniques in underwater acoustic modelling and matched field processing, can provide users with new powerful tools for source detection and localization.

Bibliography

[1] A.B. Baggeroer, W.A. Kuperman, and Henrik Schmidt. Matched-field processing: Source localization in correlated noise as an optimum parameter estimation problem. *The Journal of the Acoustical Society of America*, 83(2):571–587, feb 1988.

[2] C.Allan Boyles. *Acoustic Waveguides: Applications to oceanic science.* John Wiley & Sons, Inc., New York, NY, 1984.

[3] Homer P. Bucker. Use of calculated sound fields and matched-field detection to locate sound sources in shallow water. *The Journal of the Acoustical Society of America*, 59(2):368–373, feb 1976.

[4] Kevin M. Buckley. Spatial/spectral filtering with linearly constrained minimum variance beamforers. *IEEE Transactions on Acoustics, Speech, and Signal Processing*, ASSP-35(3):249–266, March 1987.

[5] William S. Burdic. *Underwater Acoustic System Analysis.* Prentice-Hall Signal Processing Series. Prentice-Hall, Inc., Englewood Cliffs, NJ, 1984.

[6] J. Capon. High-resolution frequency-wavenumber spectrum analysis. *Proceedings of The Institute of Electrical and Electronics Engineers*, 57:1408–1418, August 1969.

[7] J. Capon and N.R. Goodman. Probability distribution for estimation of the frequency wavenumber spectrum. *Proceedings of The Institute of Electrical and Electronics Engineers*, 58:1785–1786, October 1970.

[8] Clarence S. Clay and Herman Medwin. *Acoustical Oceanography: Principles and Applications.* Ocean Engineering, a Wiley series. John Wiley & Sons, Inc., New York, NY, 1977.

[9] Henry Cox. Resolving power and sensitivity to mismatch of optimum array processors. *The Journal of the Acoustical Society of America*, 54(3):771–785, 1973.

[10] Donald R. DelBalzo, Christopher Feuillade, and Mary M. Rowe. Effects of water-depth mismatch on matched field processing. *The Journal of the Acoustical Society of America*, 83(6):2180–2185, jun 1988.

[11] Ronald L. Fante. *Signal Analysis and Estimation: An Introduction.* John Wiley & Sons, Inc., New York, NY, 1988.

[12] Donald F. Gingras. Methods of predicting the sensitivity of matched-field processors to mismatch. *The Journal of the Acoustical Society of America*, 86(5):1940–1949, November 1989.

[13] O. Grenander and G. Szëgo. *Toeplitz Forms and Their Applications.* Univ. of California Press, Berkeley, CA, 1958.

[14] Joseph C. Hassab. *Underwater Signal and Data Processing.* CRC Press, Inc., Boca Raton, FL, 1989.

[15] Melvin J. Hinich. Maximum likelihood signal processing for a vertical array. *The Journal of the Acoustical Society of America*, 54(2):499–503, 1973.

[16] Alston S. Householder. *The Theory of Matrices in Numerical Analysis*, chapter 11, pages 483–506. Blaisdell Pub. Co., New-York, NY, first edition, 1964.

[17] D.J. Jeffries and D.R. Farrier. Asymptotic results for eigenvector methods. *Proceedings of the IEE*, 132(7):589–594, December 1985.

[18] Don H. Johnson. The application of spectral estimation methods to bearing estimation problems. *Proceedings of the The Institute of Electrical and Electronics Engineers*, 70(9):1018–1028, 1982.

[19] Steven M. Kay and S. Lawrence Marple, Jr. Spetrum analysis-a modern perspective. In Stanislav B. Kesler, editor, *Modern Spectrum Analysis II*, pages 3–41. IEEE Press, New-York, NY, 1986.

[20] Sami Khoury and Jeffrey Krolik. The resolution-robustness trade-off inherent in rayleigh estimates of power spectrum. In S. Tavares and P.H. Wittke, editors, *Proceedings of the 15th Biennial Symposium on Communications*, pages 73–76. Queen's University, June 1990.

[21] Jeffrey Krolik, Jim Lynch, and David Swingler. A robust incoherent matched field processor for source localization in uncertain multipath fields. In *Proceedings of the 1989 International Conference on Acoustics, Speech and Signal Processing*, pages 2637–2639. The Institute of Electrical and Electronics Engineers, 1989.

[22] R. T. Lacoss. Data adaptive spectral analysis methods. *Geophysics*, 36:661–675, August 1971.

[23] Miguel Lagunas et al. Maximum likelihood filters in spectral estimation problems. *Signal Processing*, 10(1):19–34, January 1986.

[24] Miguel A. Lagunas. High performance sud-like procedure for spectral estimation using rayleigh function estimates. In *Proceedings of the 1988 International Conference on Acoustics, Speech and Signal Processing*, pages 2368–2371. The Institute of Electrical and Electronics Engineers, 1988.

[25] Miguel A. Lagunas-Hernandez and Antoni Gasull-Llampallas. An in ɔroved maximum likelihood method for power spectral density estimation. *IEEE Transactions on Acoustics, Speech, and Signal Processing*, ASSP-32(1):170–173, February 1984.

[26] Verne H. MacDonald and Peter M. Schultheiss. Optimum passive bearing estimation in a spatially incoherent noise environment. *The Journal of the Acoustical Society of America*, 46(1):37–43, 1969.

[27] S. Lawrence Marple, Jr. *Digital Spectral Analysis With Applications*, chapter 12, pages 350–360. Prentice-Hall Signal Processing Series. Prentice-Hall, Inc., Englewood Cliffs, NJ, fourth edition, 1987.

[28] R. N. McDonough. Applications of the maximum likelihood method and the maximum entropy method to array processing. In S. Haykin, editor, *Nonlinear Methods of Spectral Analysis*, Topics in Applied Physics, Vol. 34, chapter 6, pages 181–244. Springer-Verlag, New-York, NY, second edition, 1983.

[29] José M. F. Moura and Maria João D. Rendas. Optimal filtering in the presence of multipath. In C.R. Baker, editor, *Stochastic Processes in Underwater Acoustics*, Lectures Notes in Control and Information Sciences No.85, chapter 3, pages 64–94. Springer-Verlag, New-York, NY, 1985.

[30] Walter Munk and Carl Wunsch. Ocean acoustic tomography: Rays and modes. *Reviews of Geophysics and Space Physics*, 21(4):777–793, May 1983.

[31] Arthur Newhall. *MPP Documentation.* Woods Hole Oceanographic Institute, Wood Hole, MA, June 1987. personal copy.

[32] C.B. Officer. *Introduction to the Theory of Sound Transmission, with Application to the Ocean.* McGraw-Hill series in the geological sciences. McGraw-Hill Book Company, Inc., New York, NY, 1958.

[33] Norman L. Owsley. Sonar array processing. In S. Haykin, editor, *Array Signal Processing*, Prentice-Hall Signal Processing Series, chapter 3, pages 115–193. Prentice-Hall, Inc., Englewood Cliffs, NJ, 1985.

[34] John M. Ozard. Matched-field processing in shallow water for range, depth, and bearing determination; results of experiment and simulation. *The Journal of the Acoustical Society of America*, 86(2):744–753, aug 1989.

[35] S. Pasupathy and A. N. Venetsanopoulos. Optimum active array processing and space-time factorability. *IEEE Transactions on Aerospace and Electronic Systems*, AES-10(6):770–778, November 1974.

[36] John S. Perkins and W. A. Kuperman. Environmental signal processing: Three-dimentional matched-field processing with a vertical array. *The Journal of the Acoustical Society of America*, 87(4):1553–1556, April 1990.

[37] V. F. Pisarenko. On the estimation of spectra by means of non-linear functions of the covariance matrix. *Geophysical Journal of the Royal Astronomical Society*, 28:511–531, 1972.

[38] Michael B. Porter, Ronald L. Dicus, and Richard G. Fizell. Simulations of matched-field processing in a deep-water pacific environment. *IEEE Joural of Oceanic Engineering*, OE-12(1):173–181, jan 1987.

[39] Richard A. Roberts and Clifford T. Mullis. *Digital Signal Processing*, chapter 11, pages 120–124. Addison-Wesley series in electrical engineering. Addison-Wesley Publishing Company, Readings, MA, 1987.

[40] R.O. Schmidt. Multiple emitter location and signal parameter estimation. In *Proceedings of RADC Spectral Estimation Workshop*, pages 243–258, Rome, NY, 1979.

[41] R. W. B. Stephens. The sea as an acoustic medium. In R. W. B. Stephens, editor, *Underwater Acoustics*, chapter 1, pages 1–21. John Wiley & Sons, Inc., 1970.

[42] Gilbert Strang. *Linear Algebra and its Applications*. Harcourt, Brace and Jovanovich, San Diego, CA, third edition, 1988.

[43] I. Tolstoy and C.S. Clay. *Ocean Acoustics, Theory and Experiments in Underwater Sound*. McGraw-Hill Book Company, Inc., New York, NY, 1966.

[44] Robert J. Urick. *Principles of Underwater Sound*. McGraw-Hill Book Company, Inc., New York, NY, second edition, 1975.

[45] Robert J. Urick. *Sound Propagation in the Sea*, section 14, pages 1–8. Peninsula Publishing, Los Altos, CA, 1982.

[46] Harry L. Van Trees. *Detection, Estimation, and Modulation Theory*, chapter 3, pages 174–209. John Wiley & Sons, Inc., New York, NY, 1968.

[47] Barry D. Van Veen and Kevin M. Buckley. Beamforming: A versatile approach to spatial filtering. *IEEE ASSP magazine*, 5(2):4-24, April 1988.